Clinical Pharmacokinetics

A Comprehensive Whole-Body Physiologically Based Pharmacokinetic Drug-Drug-Gene Interaction Model of Metformin and Cimetidine in Healthy Adults and Renally Impaired Individuals

Electronic Supplementary Material (ESM)

Nina Hanke[1], Denise Türk[1], Dominik Selzer[1], Naoki Ishiguro[2], Thomas Ebner[3], Sabrina Wiebe[3,4], Fabian Müller[3,5], Peter Stopfer[3], Valerie Nock[3] and Thorsten Lehr[1]

[1] Clinical Pharmacy, Saarland University, Saarbrücken, Germany
[2] Kobe Pharma Research Institute, Nippon Boehringer Ingelheim Co. Ltd., Kobe, Japan
[3] Boehringer Ingelheim Pharma GmbH & Co. KG, Biberach, Germany
[4] Department of Clinical Pharmacology and Pharmacoepidemiology, Heidelberg University Hospital, Heidelberg, Germany
[5] Institute of Experimental and Clinical Pharmacology and Toxicology, Friedrich-Alexander-Universität Erlangen-Nürnberg, Erlangen, Germany

Funding
This project has received funding from Boehringer Ingelheim Pharma GmbH & Co. KG and from the German Federal Ministry of Education and Research (BMBF) «NanoCare4.0 – Anwendungssichere Materialinnovationen» Program (BMBF Grant 03XP0196).

Conflict of Interest
Naoki Ishiguro, Thomas Ebner, Sabrina Wiebe, Fabian Müller, Peter Stopfer and Valerie Nock are employees of Boehringer Ingelheim Pharma GmbH & Co. KG. Thorsten Lehr has received research grants from Boehringer Ingelheim Pharma GmbH & Co. KG and from the German Federal Ministry of Education and Research. Nina Hanke, Denise Türk and Dominik Selzer declare no conflicts of interest.

Corresponding Author
Prof. Dr. Thorsten Lehr
Clinical Pharmacy, Saarland University, Campus C2 2, 66123 Saarbrücken
ORCID: 0000 0002 8372 1465
Phone: +49 681 302 70255
Email: thorsten.lehr@mx.uni-saarland.de

Contents

1 Physiologically based pharmacokinetic (PBPK) modeling

1.1 PBPK model building

PBPK model building was started with an extensive literature search to collect physicochemical parameters, information on absorption, distribution, metabolism and excretion (ADME) processes, as well as clinical studies of intravenous and oral administration in single- and multiple-dose regimens. In addition to drug plasma concentration-time profiles, further clinical data on fraction excreted to urine or feces, as well as observed tissue concentrations, were integrated whenever available. The concentration-time profiles of the clinical studies were digitized and divided into a training dataset for model building and a test dataset for model evaluation. The studies for the training dataset were selected to include intravenous and oral studies covering the whole published dosing range, as well as information on fraction excreted to urine and feces. If multiple studies of the same dose were available, studies with many participants, modern bioanalytical methods and frequent as well as late sampling were chosen for the training dataset. Model input parameters that could not be informed from literature were optimized by fitting the model simulations of all studies assigned to the training dataset simultaneously to their respective observed data.

1.2 Virtual individuals and virtual populations

Virtual mean individuals were generated for each study according to the published demographic information, with corresponding age, weight, height, sex, ethnicity, hematocrit and GFR, if available. If no information was provided, a default value was substituted (30 years of age, male, European, mean weight, height, hematocrit and GFR characteristics from the PK-Sim® population database). Transporters and metabolizing enzymes relevant to the pharmacokinetics of the modeled drugs were implemented in agreement with current literature, utilizing the PK-Sim® expression database [1] to define their relative expression in the different organs of the body. Details and references on the distribution and localization of the implemented drug transporters and metabolizing enzymes are provided in Section 9.

To cover the variability in a population, virtual populations containing 100 individuals between 20 and 50 years of age were created, with gender composition and ethnicity adapted to each respective study protocol. If no information on sex or ethnicity was available, 100 % male populations of European background were assumed. In the generated virtual populations, system-dependent parameters such as weight, height, organ volumes, blood flow rates, tissue compositions, etc. were varied by an implemented algorithm in PK-Sim® within the limits of the ICRP or NHANES database [2, 3]. The reference concentrations of the implemented enzymes and transporters were distributed according to the variability reported in the PK-Sim® database or the literature. If no information could be found, reference concentrations were set to be log-normally distributed with a moderate variability of 35 % CV (geometric standard deviation of 1.4), see Table S9.0.1.

1.3 PBPK model evaluation

Model performance was evaluated with multiple methods. First, predicted population plasma concentration-time profiles were compared with the data observed in the respective clinical studies. As the clinical data from literature is mostly reported as arithmetic means ± SD, population prediction arithmetic means and 68 % prediction intervals were plotted, that correspond to the range of ± 1 SD around the mean if normal distribution was to be assumed. Furthermore, the predicted plasma concentration values of all studies were plotted against their corresponding observed values in goodness-of-fit plots.

In addition, model performance was evaluated by comparison of predicted to observed AUC and C_{max} values. All AUC values were calculated from the time of drug administration to the time of the last concentration measurement (AUC_{last}). As quantitative measures of model performance, mean relative deviation (MRD) of all predicted and observed plasma concentrations (Equation S1) and geometric mean fold error (GMFE) of all predicted and observed AUC_{last} and C_{max} values (Equation S2) were calculated. MRD and GMFE values ≤ 2 characterize an adequate model performance.

$$MRD = 10^x \text{ with } x = \sqrt{\frac{1}{k}\sum_{i=1}^{k}(\log_{10} c_{\text{predicted},i} - \log_{10} c_{\text{observed},i})^2} \tag{S1}$$

with $c_{\text{predicted},i}$ = predicted plasma concentration, $c_{\text{observed},i}$ = corresponding observed plasma concentration, k = number of observed values.

$$GMFE = 10^x \text{ with } x = \frac{1}{m}\sum_{i=1}^{m}|\log_{10}\left(\frac{\text{predicted PK parameter}_i}{\text{observed PK parameter}_i}\right)| \tag{S2}$$

with predicted PK parameter$_i$ = predicted AUC_{last} or C_{max} value, observed PK parameter$_i$ = corresponding observed AUC_{last} or C_{max} value, m = number of studies.

Furthermore, physiological plausibility of the parameter estimates and the results of sensitivity analyses were assessed.

1.4 PBPK model sensitivity analysis

Sensitivity of the final models to single parameters (local sensitivity analysis) was calculated, measured as relative change of AUC_{0-24}. Sensitivity analysis was carried out using a relative perturbation of 1000 % (variation range 10.0, maximum number of 9 steps). Parameters were included into the analysis if they have been optimized, if they are associated with optimized parameters or if they might have a strong impact due to calculation methods used in the model.

Sensitivity to a parameter was calculated as the ratio of the relative change of the simulated AUC to the relative variation of the parameter around its value used in the final model according to Equation S3.

$$S = \frac{\Delta AUC}{AUC} \cdot \frac{p}{\Delta p} \tag{S3}$$

with S = sensitivity of the AUC to the examined model parameter, ΔAUC = change of the AUC, AUC = simulated AUC with the original parameter value, Δp = change of the examined parameter value, p = original parameter value. A sensitivity of +1.0 signifies that a 10 % increase of the examined parameter value causes a 10 % increase of the simulated AUC.

1.5 DDI modeling – Cimetidine

To model the impact of cimetidine on its victim drugs metformin and midazolam, experimentally determined values were used for all inhibition constants. However, for the development of the cimetidine model no information on human kidney or liver concentrations (other than postmortem measurements) were available, to evaluate the cimetidine concentrations on the DDI sites of action. Therefore, clinical data of the cimetidine-metformin and of the cimetidine-midazolam DDIs were

included into the training dataset used to build the cimetidine model, fixing the interaction parameters to experimentally determined literature values. In addition to the inhibition of OCT2/MATE and CYP3A4, cimetidine is also described as moderate inhibitor of CYP2D6 and as weak inhibitor of CYP1A2 [4]. The DDI performance with CYP2D6 or CYP1A2 victim drugs could not yet be tested, due to the lack of victim drug PBPK models, lack of clinical DDI studies with the CYP1A2 victim drugs caffeine and theophylline and lack of published inhibition parameters for the weaker CYP inhibitions by cimetidine.

1.6 Mathematical implementation of competitive inhibition

Competitive inhibition describes the reversible binding of an inhibitor to the active site of an enzyme or transporter and, as a consequence, the competition of substrate and inhibitor for binding. Competitive inhibition can be overcome by high substrate concentrations (concentration-dependency). In the case of competitive inhibition, the maximum reaction velocity (v_{max}) remains unaffected, while the Michaelis-Menten constant (K_m) is apparently increased by the inhibition ($K_{m,app}$, Equation S4) [5]. The (reduced) reaction velocity (v) during co-administration of substrate and competitive inhibitor is described by Equation S5 [5]:

$$K_{m,app} = K_m \cdot \left(1 + \frac{[I]}{K_i}\right) \tag{S4}$$

$$v = \frac{v_{max} \cdot [S]}{K_{m,app} + [S]} = \frac{k_{cat} \cdot [E] \cdot [S]}{K_{m,app} + [S]} \tag{S5}$$

with $K_{m,app}$ = Michaelis-Menten constant in the presence of inhibitor, K_m = Michaelis-Menten constant, $[I]$ = free inhibitor concentration, K_i = dissociation constant of the inhibitor-enzyme/transporter complex, v = reaction velocity, v_{max} = maximum reaction velocity, $[S]$ = free substrate concentration, k_{cat} = catalytic rate constant, $[E]$ = enzyme or transporter concentration.

2 Metformin

2.1 PBPK model development

Metformin is widely used as first-line treatment of type 2 diabetes. It is highly hydrophilic, positively charged at physiological pH and depends on active transport for its absorption, distribution and excretion. The absorption of metformin is saturable and reported to be restricted to the upper intestine [6]. The excretion of metformin is mainly mediated via the sequential action of OCT2 and MATE in the kidney, with a moderate contribution of renal glomerular filtration (approximately 20 %). Metformin is recommended by the FDA as OCT2/MATE victim drug for the use in clinical DDI studies and drug labeling [4].

The metformin model was established using 39 clinical studies, covering a dosing range from 0.001 to 2550 mg (see Table S2.2.1). The final model applies active transport of metformin by PMAT, OCT1, OCT2 and MATE as well as passive renal glomerular filtration (see Table S2.3.1). The saturable absorption is implemented via PMAT and OCT1 in the small intestine. As late absorption of orally administered metformin is neither consistent with the reported plasma concentration time-profiles nor with the incomplete absorption of metformin, the relative expression of PMAT and OCT1 in the large intestinal mucosa was set to zero. Furthermore, no information regarding active transport processes at the basolateral side of the intestinal mucosa could be obtained. Therefore, the passive permeability from the intracellular to the interstitial space of the small intestinal mucosa was optimized. Details on the distribution of the implemented transporters are listed in the system-dependent parameter table (Table S9.0.1)).

The good descriptive and predictive performance of the metformin model is demonstrated in semilogarithmic (Figures S2.4.1, S2.4.2 and S2.4.6) as well as linear plots (Figures S2.4.3, S2.4.4 and S2.4.8) of population predicted compared to observed concentration-time profiles of all clinical studies. Predicted compared to observed fraction excreted to urine data are shown, whenever available (Figures S2.4.9 and S2.4.10). In addition, a goodness-of-fit plot comparing all predicted to their corresponding observed plasma concentrations of metformin are presented (Figure S2.5.1) and MRD values for each study are given (see Table S2.5.1). Furthermore, correlation plots of predicted versus observed AUC and C_{max} values are shown (Figure S2.5.2), together with a summary of the respective PK parameters, including calculated model GMFE values (Table S2.5.2).

Sensitivity analysis of a simulation of 500 mg metformin, administered as tablet in the fasted state, reveals that the model predictions are sensitive to the values of fraction unbound and lipophilicity (both literature values), followed by the MATE1 and OCT2 transport rate constants (optimized) (see Figure S2.5.3).

2.2 Clinical studies

The clinical studies used for metformin PBPK model building and evaluation are summarized in Table S2.2.1.

Table S2.2.1: Metformin study table

Dose [mg]	Route	n	Men [%]	Age [years]	Weight [kg]	Height [cm]	BMI [kg/m^2]	Dataset	Reference
0.001445	iv, bolus	4	80	41 (37–47)	-	-	-	training	Gormsen et al. 2016 [7]
250	iv, 15 min	4	100	33 (30–36)	70 (64–83)	177 (175–178)	23 (21–26)	training	Tucker et al. 1981 [8]
500	iv, 5 min	3	33	38 (36–39)	60 (58–63)	168 (161–171)	22 (20–23)	test	Pentikäinen et al. 1979 [9]
1000	iv, bolus	5	80	45 (36–60)	72 (64–81)	-	-	training	Sirtori et al. 1978 [10]
0.0008556	po, -, fast	3	80	41 (37–47)	-	-	-	training	Gormsen et al. 2016 [7]
10	po, sol, fast	24	100	34 ± 8 (20–48)	84 ± 11 (63–105)	180 ± 7 (163–195)	26 ± 2 (22–29)	training	Stopfer et al. 2018 [11]
250, qd	po, tab, fed	7	43	(19–23)	(55–78)	-	-	test	Somogyi et al. 1987 [12]
500	po, -, fast	6	100	(21–32)	(53–73)	-	-	test	Wang et al. 2008 [13]
500	po, sol, fast	13	100	38 ± 10 (22–52)	83 ± 11 (64–108)	181 ± 7 (170–191)	25 ± 3 (20–30)	training	Boehringer 2018 [14]
500	po, tab, fed	24	100	27 (21–40)	-	-	-	test	Caillé et al. 1993 [15]
500	po, tab, fed	14	43	37 ± 8	74 ± 14	173 ± 10	-	test	Gusler et al. 2001 [16]
500	po, tab, fast	24	100	23 ± 3 (18–31)	66 ± 8 (52–80)	174 ± 6 (166–184)	-	test	Najib et al. 2002 [17]
500	po, tab, fast	5	40	42 (36–51)	63 (56–80)	168 (153–186)	22 (20–24)	test	Pentikäinen et al. 1979 [9]
500	po, tab, fast	24	100	(21–35)	-	-	-	test	Sambol et al. 1996b [18]
500	po, tab, fast	20	100	36 ± 8 (23–49)	84 ± 9 (68–100)	180 ± 6 (171–188)	26 ± 2 (22–29)	training	Stopfer et al. 2016 [11]
500	po, tab, fed	4	100	33 (30–36)	70 (64–83)	177 (175–178)	23 (21–26)	test	Tucker et al. 1981 [8]
500, bid	po, tab, fed	16	100	35 (22–55)	84 (71–119)	180 (162–202)	-	test	DiCicco et al. 2014 [19]
500, bid[a]	po, tab, fast	20	100	23 ± 3	67 ± 7	174 ± 6	22 ± 2	test	Jang et al. 2016 [20]
500, bid[a]	po, tab, fast	23	100	26 ± 5	71 ± 9	173 ± 5	-	test	Kim et al. 2014 [21]
500, bid	po, tab, fast	18	84	24 (18–37)	76 (53–104)	-	-	test	Manitpisitkul et al. 2014 [22]
500, bid[a]	po, tab, fast	20	100	-	-	-	-	test	Oh et al. 2016 [23]
750, bid[b]	po, tab, fast	16	88	27 ± 4	67 ± 11	172 ± 7	-	test	Cho et al. 2011 [24]
750, bid[b]	po, tab, fast	12	100	27 ± 5	71 ± 4	175 ± 6	-	test	Cho et al. 2014 [25]
750, bid[b]	po, tab, fast	20	100	35	-	-	22 ± 1	test	Ding et al. 2014 [26]
850	po, sol, fast	24	100	(21–35)	-	-	-	training	Sambol et al. 1996b [18]
850	po, tab, fast	14	36	27 ± 7	-	-	-	test	Chen et al. 2009 [27]
850	po, tab, fast	12	50	27 (23–33)	74 (49–101)	176 (160–192)	24 (18–29)	test	Morissey et al. 2016 [28]
850	po, tab, fed	6	67	32 ± 3 (25–46)	-	-	21 ± 1 (17–24)	test	Robert et al. 2003 [29]
850	po, tab, fast	6	-	28 ± 5	-	-	-	test	Sambol et al. 1995 [30]
850	po, tab, fast	9	56	46 ± 3	76 ± 4	-	-	test	Sambol et al. 1996a [31]

-: not given, **bid**: twice daily, **BMI**: body mass index, **iv**: intravenous, **n**: number of individuals studied, **po**: oral, **qd**: once daily, **sol**: solution,
tab: tablet, **test**: test dataset (model evaluation), **tid**: three times daily, **training**: training dataset (model development and parameter optimization)

[a] first dose 750 mg, second dose (500 mg)

[b] first dose 1000 mg, second dose (750 mg)

[c] first dose 1000 mg, second dose (850 mg)

Table S2.2.1: Metformin study table *(continued)*

Dose [mg]	Route	n	Men [%]	Age [years]	Weight [kg]	Height [cm]	BMI [kg/m^2]	Dataset	Reference
850	po, tab, fed	24	100	(21–35)	-	-	-	training	Sambol et al. 1996b [18]
850	po, tab, fed	24	100	(21–35)	-	-	-	training	Sambol et al. 1996b [18]
850, bid[c]	po, tab, fast	12	67	28 (21–40)	-	-	27 (21–37)	test	Hibma et al. 2016 [32]
850, tid	po, tab, fast	9	56	46 ± 3	76 ± 4	-	-	test	Sambol et al. 1996a [31]
1000	po, tab, fast	14	100	31 (20–47)	80 (60–106)	-	26 (20–30)	test	Johansson et al. 2014 [33]
1000, qd	po, tab, fast	27	89	(43–47)	-	-	(24–27)	test	Gan et al. 2016 [34]
1500	po, tab, fed	4	100	33 (30–36)	70 (64–83)	177 (175–178)	23 (21–26)	test	Tucker et al. 1981 [8]
1700	po, tab, fast	9	56	46 ± 3	76 ± 4	-	-	training	Sambol et al. 1996a [31]
2550	po, tab, fast	9	56	46 ± 3	76 ± 4	-	-	training	Sambol et al. 1996a [31]

-: not given, **bid**: twice daily, **BMI**: body mass index, **iv**: intravenous, **n**: number of individuals studied, **po**: oral, **qd**: once daily, **sol**: solution,
tab: tablet, **test**: test dataset (model evaluation), **tid**: three times daily, **training**: training dataset (model development and parameter optimization)

[a] first dose 750 mg, second dose (500 mg)

[b] first dose 1000 mg, second dose (750 mg)

[c] first dose 1000 mg, second dose (850 mg)

2.3 Drug-dependent parameters

The drug-dependent parameters of the final metformin model are summarized in Table S2.3.1 below. The associated system-dependent parameters are listed in Table S9.0.1.

Table S2.3.1: Drug-dependent parameters of the metformin PBPK model

Parameter	Value	Unit	Source	Literature	Reference	Description
MW	129.16	g/mol	Literature	129.16	[35]	Molecular weight
pKa_1 (base)	2.80	-	Literature	2.80	[36]	First acid dissociation constant
pKa_2 (base)	11.50	-	Literature	11.50	[36]	Second acid dissociation constant
Solubility (pH 6.8)	350.90	g/l	Literature	350.90	[36]	Solubility
logP	-1.43	-	Literature	-1.43	[37]	Lipophilicity
fu	100.00	%	Literature	100.00	[8–10]	Fraction unbound
B/P ratio	-	-	-	Time-dependent	[8]	Blood/plasma ratio
PMAT K_m	367.57	µmol/l	Optimized	1320.00	[38]	PMAT Michaelis-Menten constant
PMAT k_{cat}	76.47	1/min	Optimized	-	-	PMAT transport rate constant
PMAT Hill	3.00	-	Literature	2.64	[38]	PMAT Hill coefficient
OCT1 K_m	1180.00	µmol/l	Literature	1180.00	[27]	OCT1 Michaelis-Menten constant
OCT1 k_{cat}	641.19	1/min	Optimized	-	-	OCT1 transport rate constant
OCT2 K_m	810.00	µmol/l	Literature	810.00	[27]	OCT2 Michaelis-Menten constant
OCT2 (SLC22A2 808G) k_{cat}	5.17E+04	1/min	Optimized	-	-	OCT2 transport rate constant
OCT2 (SLC22A2 808T) k_{cat}	1.38E+05	1/min	Optimized	-	-	OCT2 transport rate constant
MATE1 K_m	283.00	µmol/l	Literature	283.00	[39]	MATE1 Michaelis-Menten constant
MATE1 k_{cat}	165.69	1/min	Optimized	-	-	MATE1 transport rate constant
GFR fraction	1.00	-	Assumed	-	-	Fraction of filtered drug in the urine
EHC continuous fraction	1.00	-	Assumed	-	-	Fraction of bile continually released
Partition coefficients	Diverse	-	Calculated	PK-Sim	[40]	Cell to plasma partition coefficients
Cellular permeability	2.30E-04	cm/min	Calculated	CDS norm.	[5]	Permeability into the cellular space
Luminal intestinal perm.	8.49E-07	cm/min	Optimized	1.87E-07	Calculated	Transcellular specific intestinal perm.
Basolat. small int. perm.	1.16E-05	cm/min	Optimized	1.11E-06	Calculated	Basolateral perm. out of the mucosa
Basolat. large int. perm.	0.00	cm/min	Assumed	1.11E-06	Calculated	Basolateral perm. out of the mucosa
Tablet fasted Weibull shape	1.36	-	Literature	Extracted (Fig. 1)	[41]	Dissolution profile shape
Tablet fasted Weibull time	7.90	min	Literature	Extracted (Fig. 1)	[41]	Dissolution time (50% dissolved)
Tablet fed Weibull shape	0.11	-	Optimized	-	[18]	Dissolution profile shape
Tablet fed Weibull time	7.90	min	Optimized	-	[18]	Dissolution time (50% dissolved)

Basolat: basolateral, **CDS norm**: charge-dependent Schmitt normalized to PK-Sim calculation method, **DGI**: drug-gene-interaction, **EHC**: enterohepatic circulation, **GFR**: glomerular filtration rate, **int**: intestinal, **perm**: permeability, **PK-Sim**: PK-Sim Standard calculation method

2.4 Profiles

2.4.1 Semilogarithmic plots – Plasma

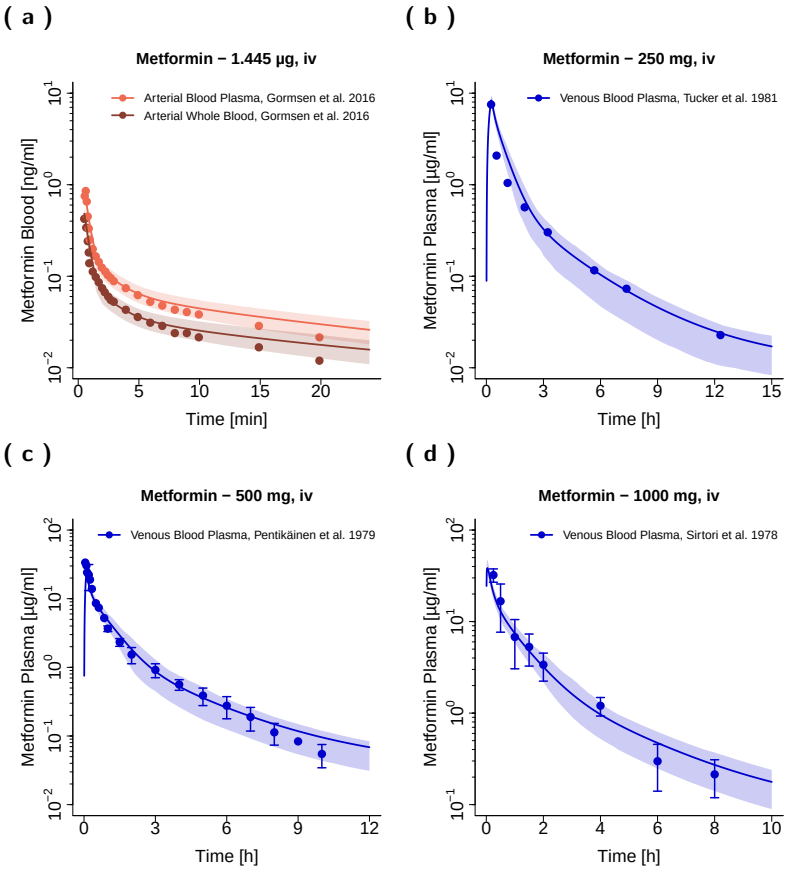

Figure S2.4.1: Metformin venous blood plasma (•, –), arterial blood plasma (•, –) and arterial whole blood (•, –) concentration-time profiles (semilogarithmic) following intravenous administration of metformin. Observed data are shown as dots, if available ± standard deviation (SD). Population simulation arithmetic means are shown as lines; the shaded areas represent the predicted population variation (Q_{16} – Q_{84}).

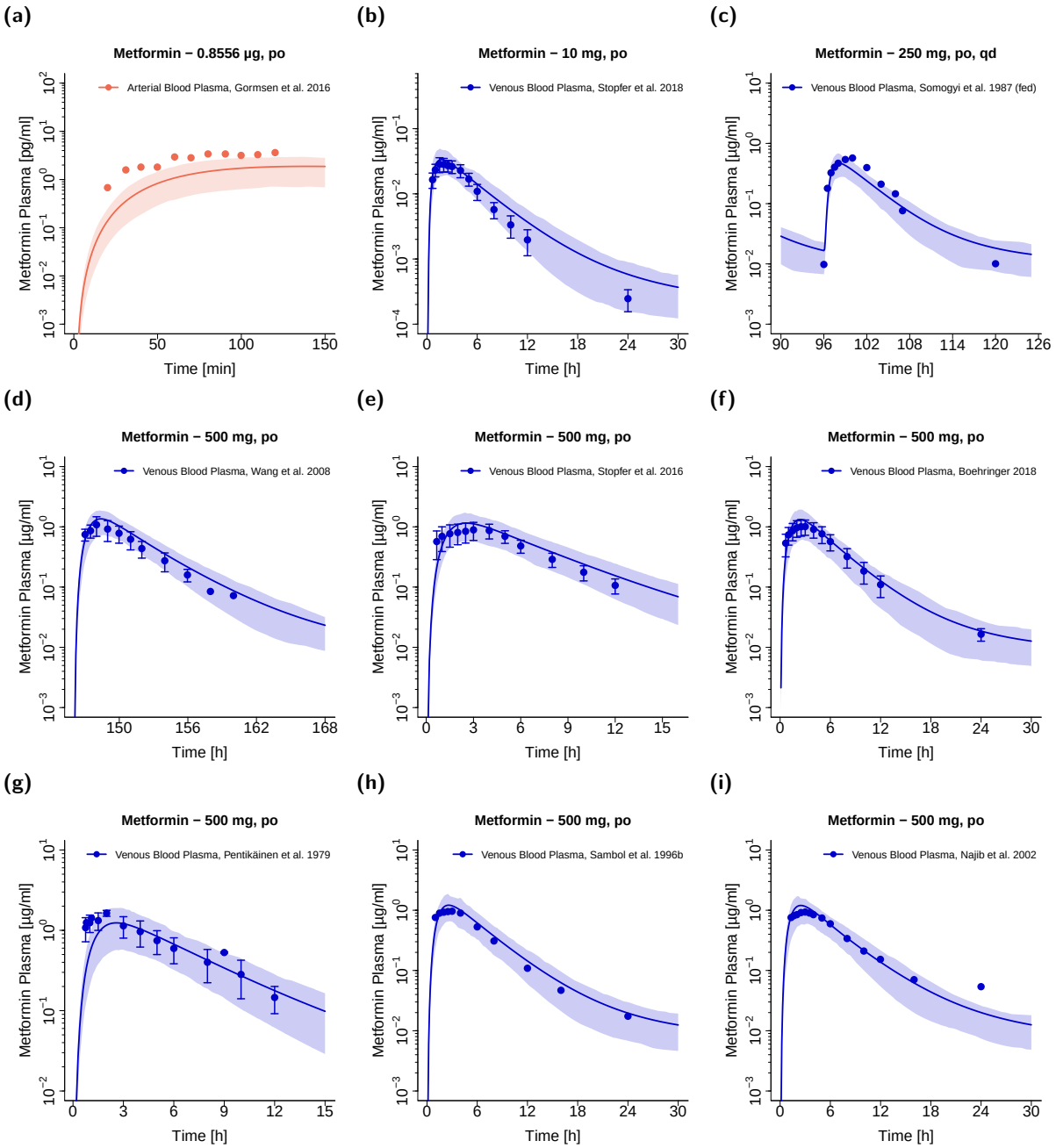

Figure S2.4.2: Metformin venous blood plasma (•, –), arterial blood plasma (•, –) and venous whole blood (•, –) concentration-time profiles (semilogarithmic) following oral administration of metformin. Observed data are shown as dots, if available ± standard deviation (SD). Population simulation arithmetic means are shown as lines; the shaded areas represent the predicted population variation (Q_{16} – Q_{84}).

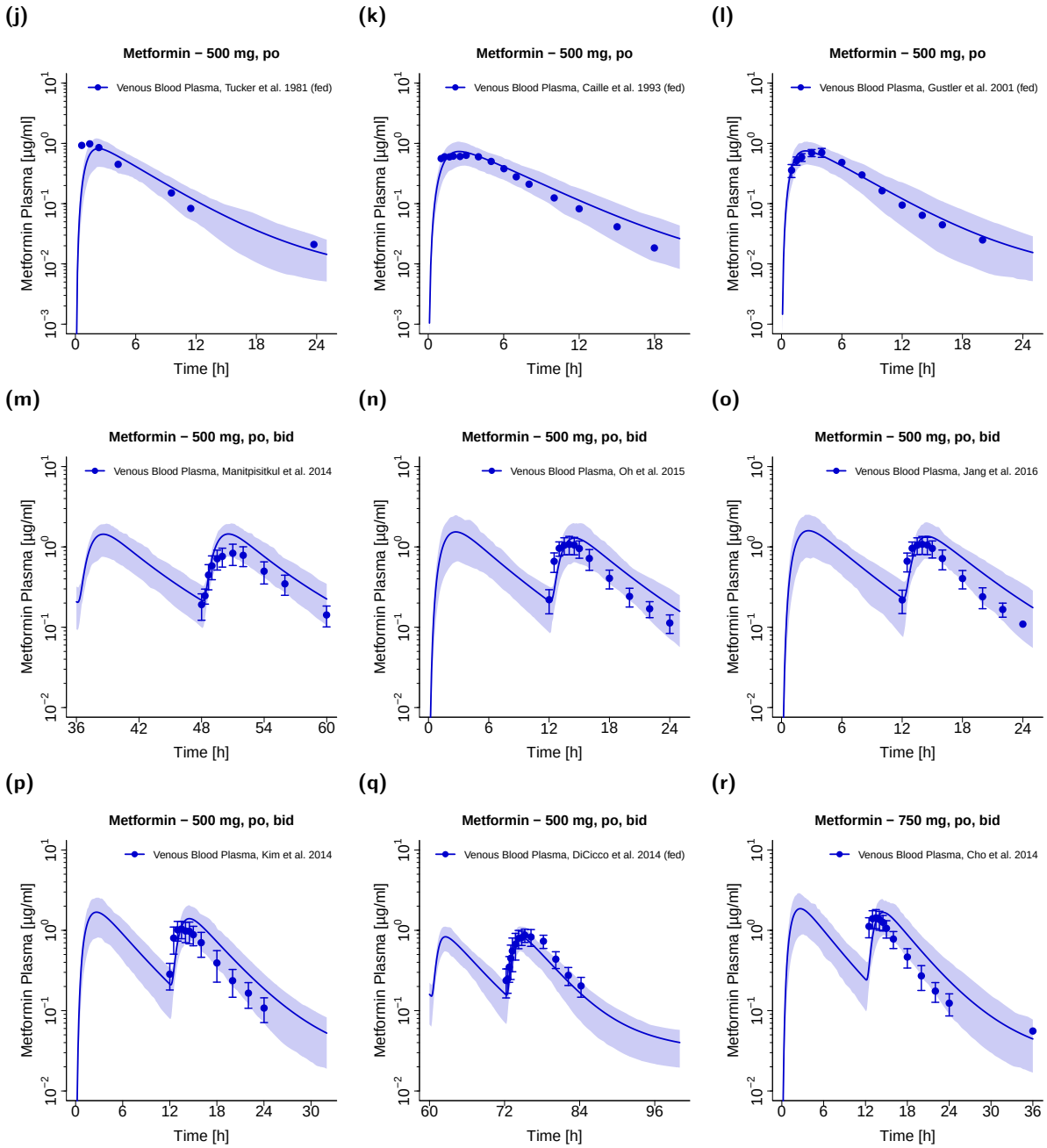

Figure S2.4.2: Metformin venous blood plasma (•, –), arterial blood plasma (•, –) and venous whole blood (•, –) concentration-time profiles (semilogarithmic) following oral administration of metformin. Observed data are shown as dots, if available ± standard deviation (SD). Population simulation arithmetic means are shown as lines; the shaded areas represent the predicted population variation (Q_{16} – Q_{84}). (continued)

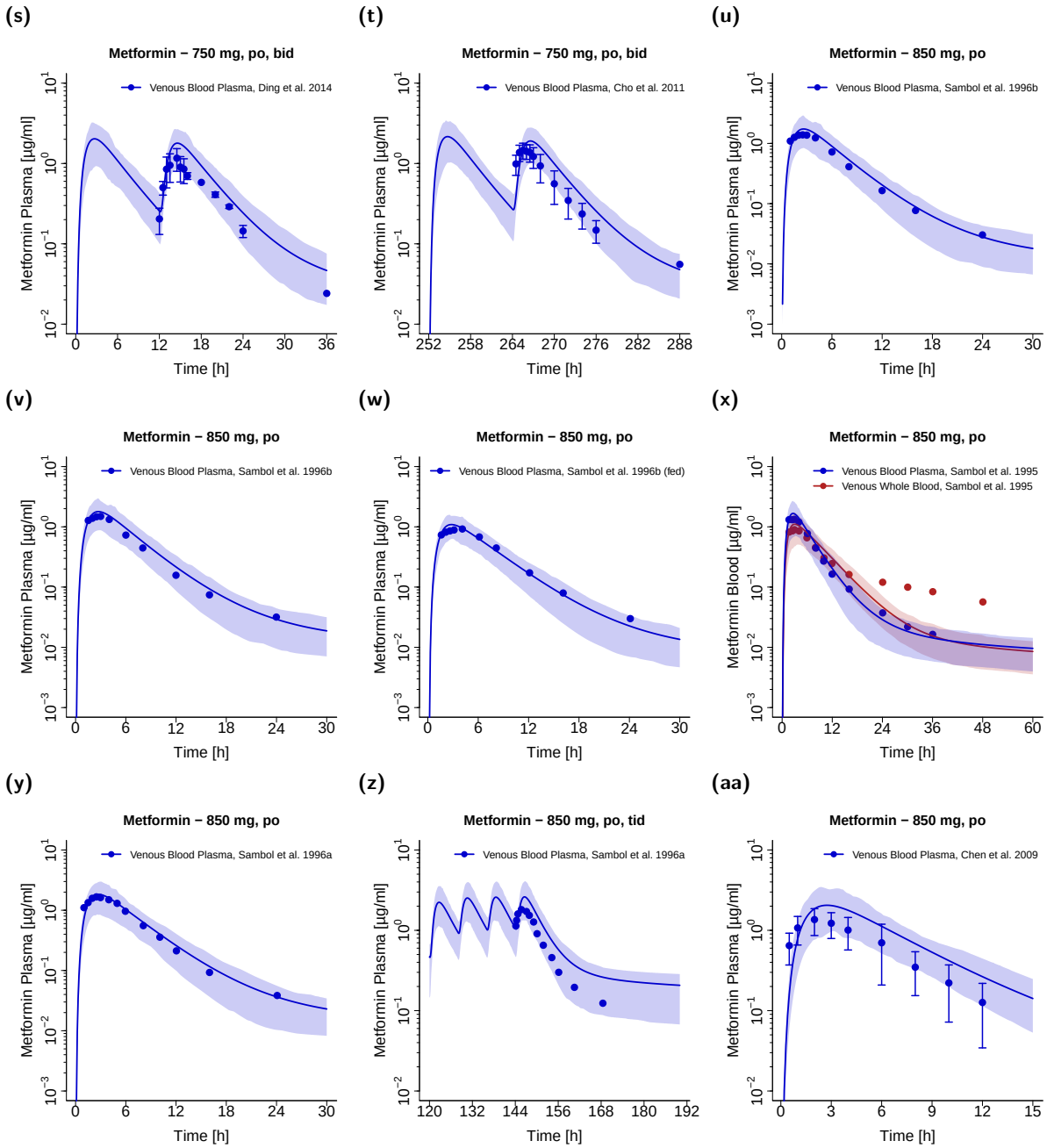

Figure S2.4.2: Metformin venous blood plasma (•, –), arterial blood plasma (•, –) and venous whole blood (•, –) concentration-time profiles (semilogarithmic) following oral administration of metformin. Observed data are shown as dots, if available ± standard deviation (SD). Population simulation arithmetic means are shown as lines; the shaded areas represent the predicted population variation (Q_{16} – Q_{84}). (continued)

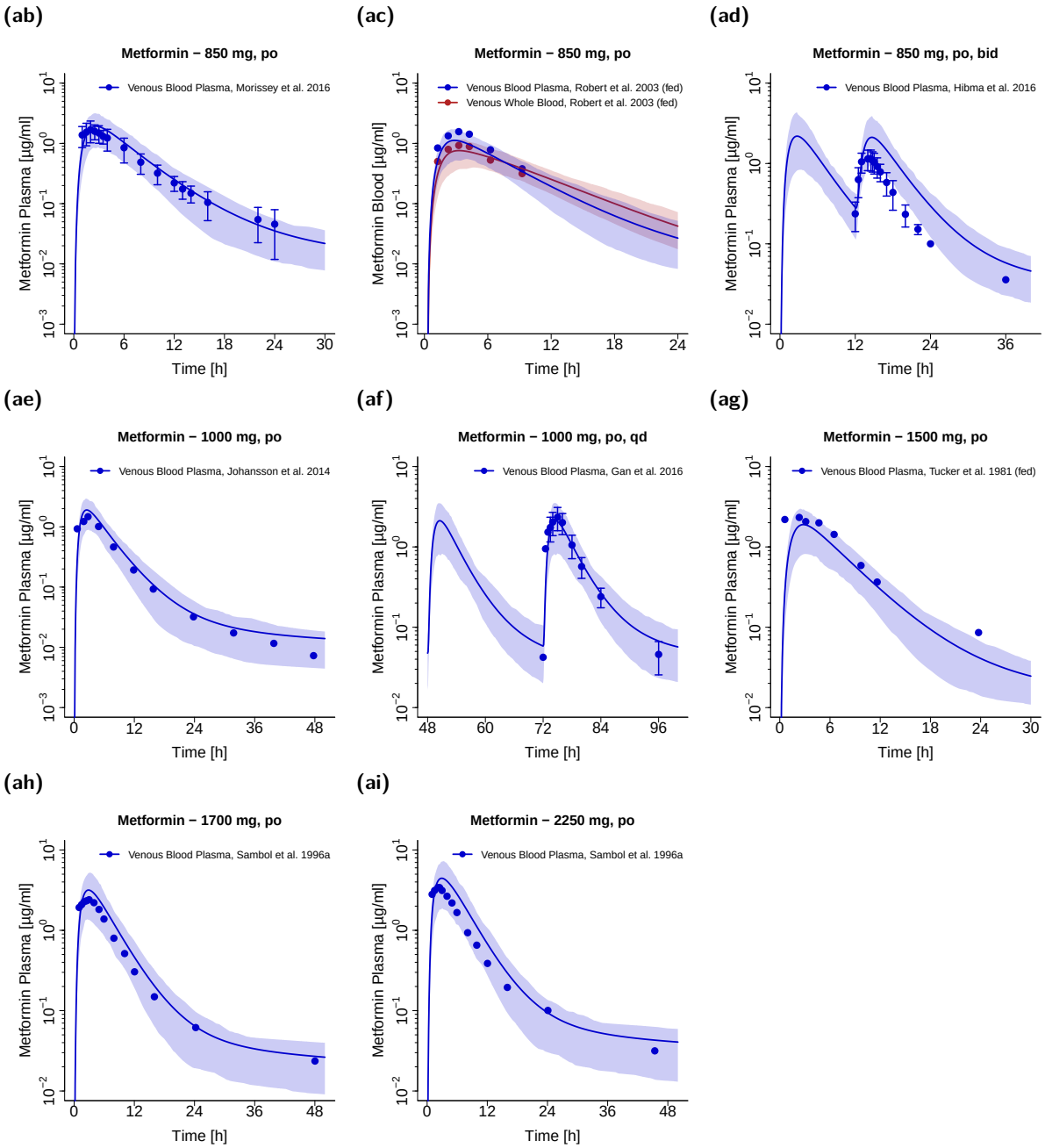

Figure S2.4.2: Metformin venous blood plasma (•, –), arterial blood plasma (•, –) and venous whole blood (•, –) concentration-time profiles (semilogarithmic) following oral administration of metformin. Observed data are shown as dots, if available ± standard deviation (SD). Population simulation arithmetic means are shown as lines; the shaded areas represent the predicted population variation (Q_{16} – Q_{84}). (continued)

2.4.2 Linear plots – Plasma

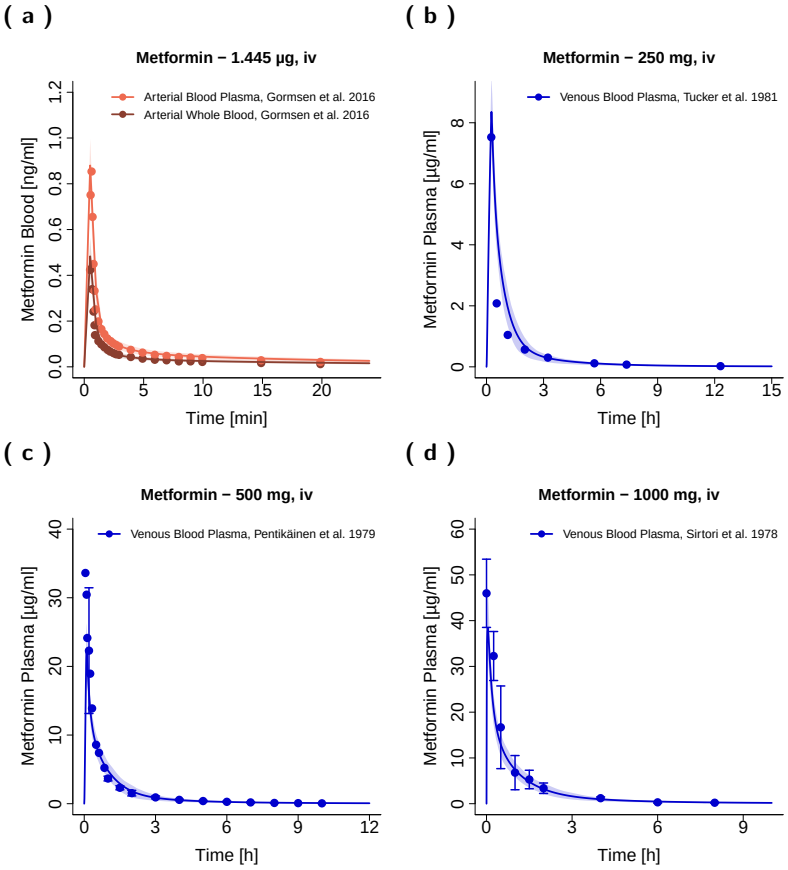

Figure S2.4.3: Metformin venous blood plasma (•, –), arterial blood plasma (•, –) and arterial whole blood (•, –) concentration-time profiles (linear) following intravenous administration of metformin. Observed data are shown as dots, if available ± standard deviation (SD). Population simulation arithmetic means are shown as lines; the shaded areas represent the predicted population variation (Q_{16} – Q_{84}).

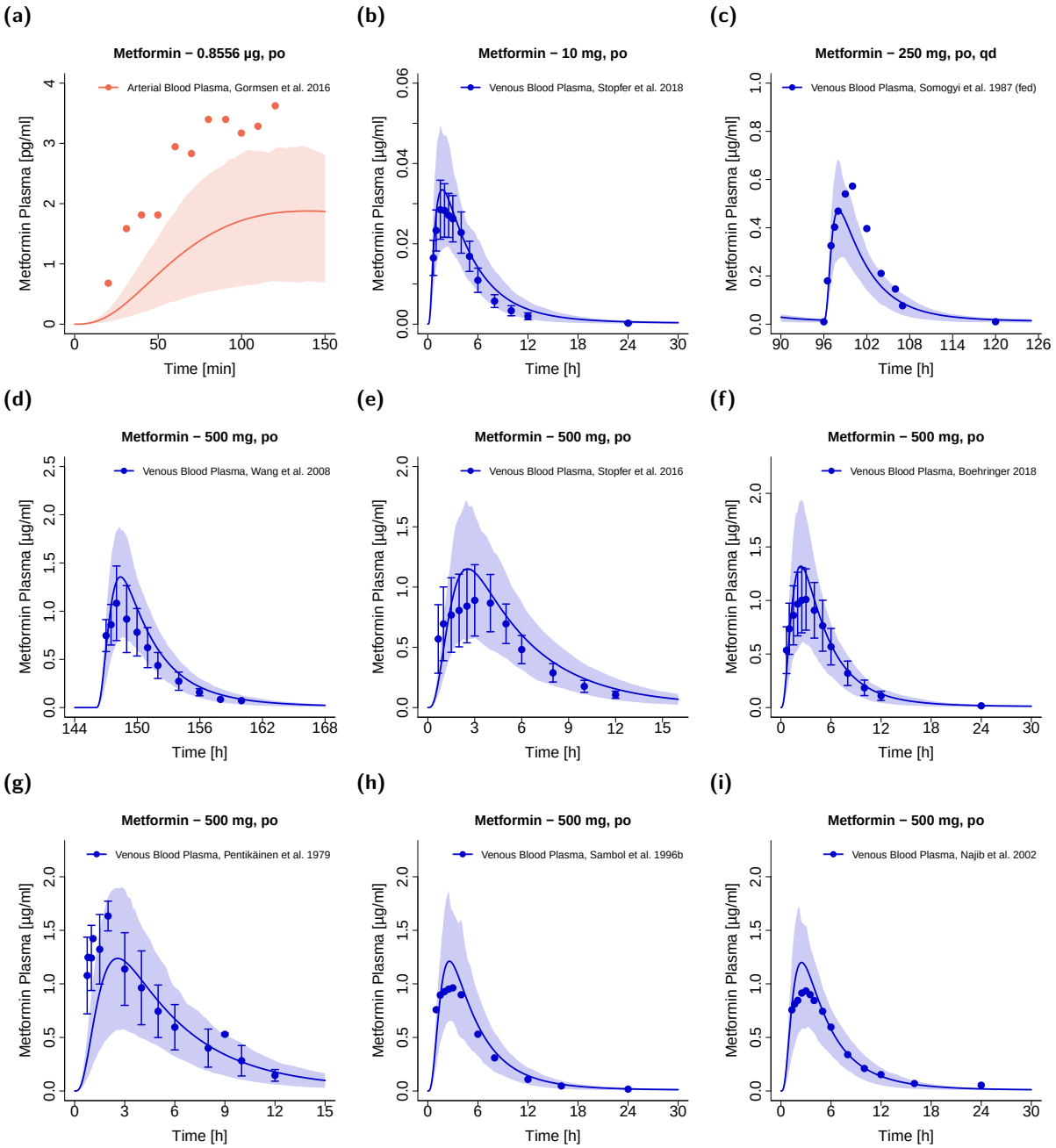

Figure S2.4.4: Metformin venous blood plasma (•, –), arterial blood plasma (•, –) and venous whole blood (•, –) concentration-time profiles (linear) following oral administration of metformin. Observed data are shown as dots, if available ± standard deviation (SD). Population simulation arithmetic means are shown as lines; the shaded areas represent the predicted population variation (Q_{16} – Q_{84}).

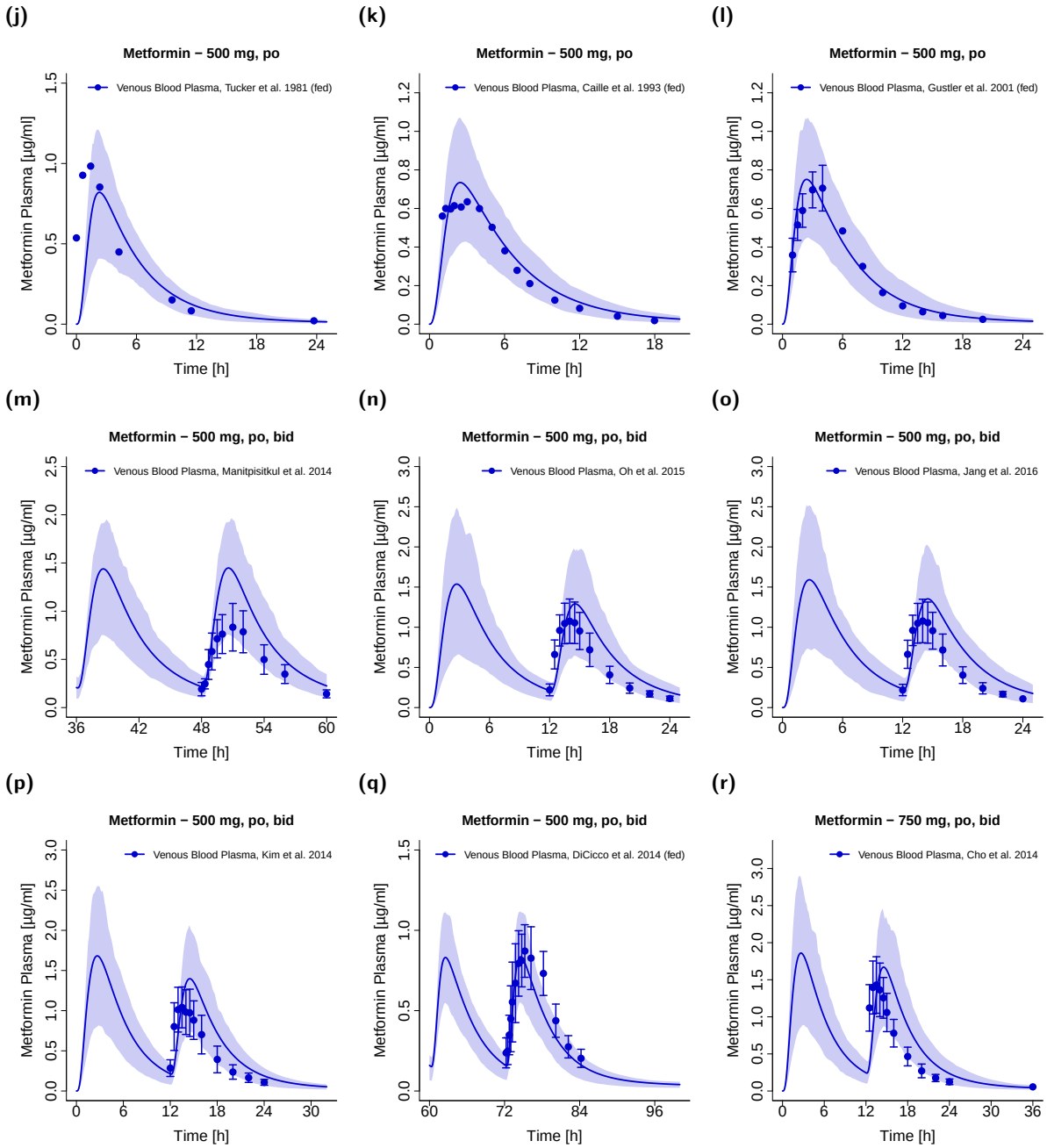

Figure S2.4.4: Metformin venous blood plasma (•, –), arterial blood plasma (•, –) and venous whole blood (•, –) concentration-time profiles (linear) following oral administration of metformin. Observed data are shown as dots, if available ± standard deviation (SD). Population simulation arithmetic means are shown as lines; the shaded areas represent the predicted population variation (Q_{16} – Q_{84}). (continued)

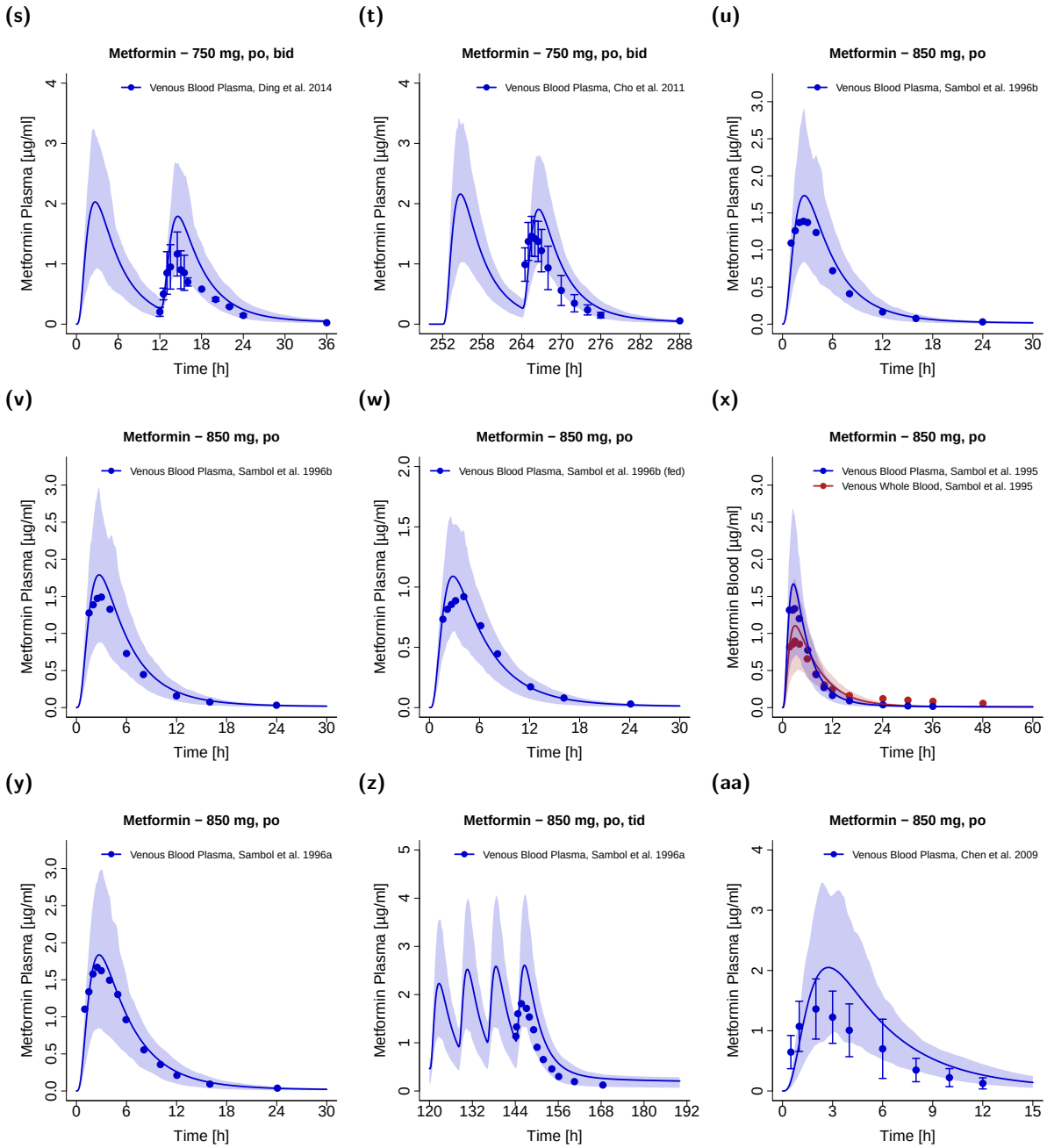

Figure S2.4.4: Metformin venous blood plasma (•, –), arterial blood plasma (•, –) and venous whole blood (•, –) concentration-time profiles (linear) following oral administration of metformin. Observed data are shown as dots, if available ± standard deviation (SD). Population simulation arithmetic means are shown as lines; the shaded areas represent the predicted population variation (Q_{16} – Q_{84}). (continued)

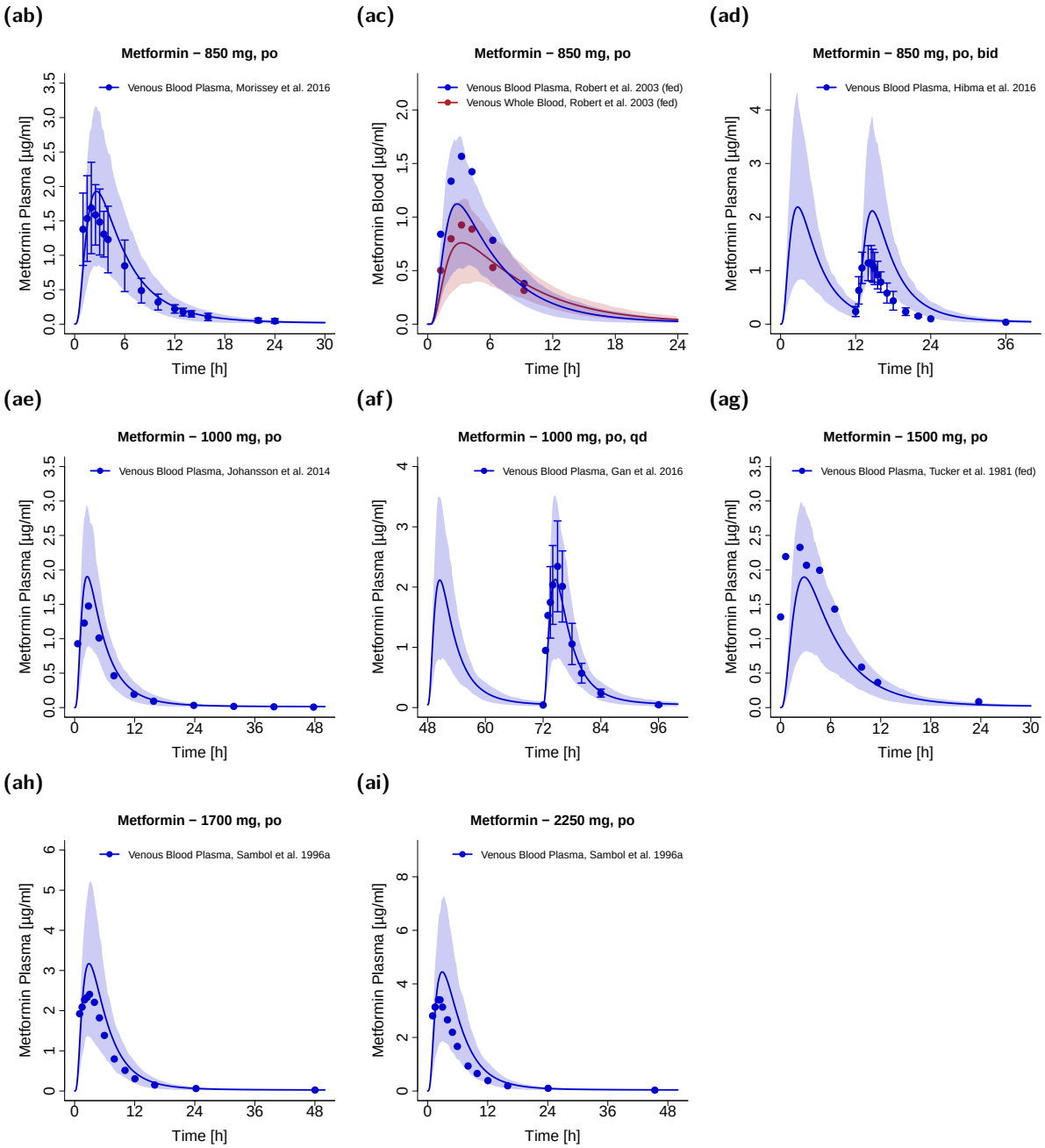

Figure S2.4.4: Metformin venous blood plasma (•, –), arterial blood plasma (•, –) and venous whole blood (•, –) concentration-time profiles (linear) following oral administration of metformin. Observed data are shown as dots, if available ± standard deviation (SD). Population simulation arithmetic means are shown as lines; the shaded areas represent the predicted population variation (Q_{16} – Q_{84}). (continued)

2.4.3 Semilogarithmic plots – Tissue

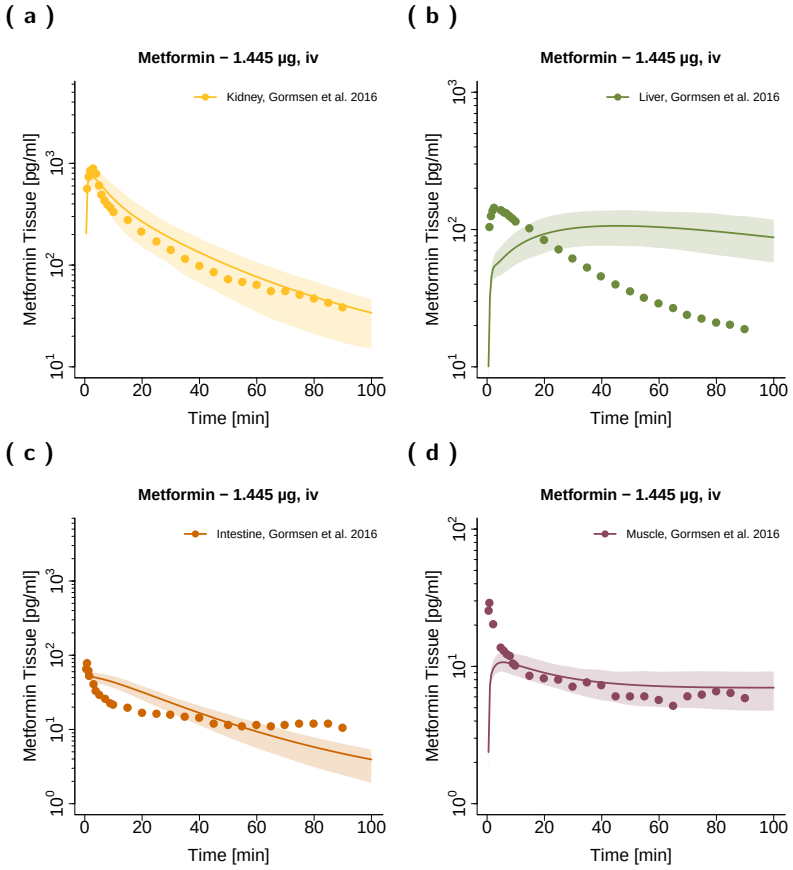

Figure S2.4.5: Metformin kidney (•, –), liver (•, –), intestine (•, –) and muscle (•, –) tissue concentration-time profiles (semilogarithmic) following intravenous administration of metformin. Observed data are shown as dots. Population simulation arithmetic means are shown as lines; the shaded areas represent the predicted population variation (Q_{16} – Q_{84}).

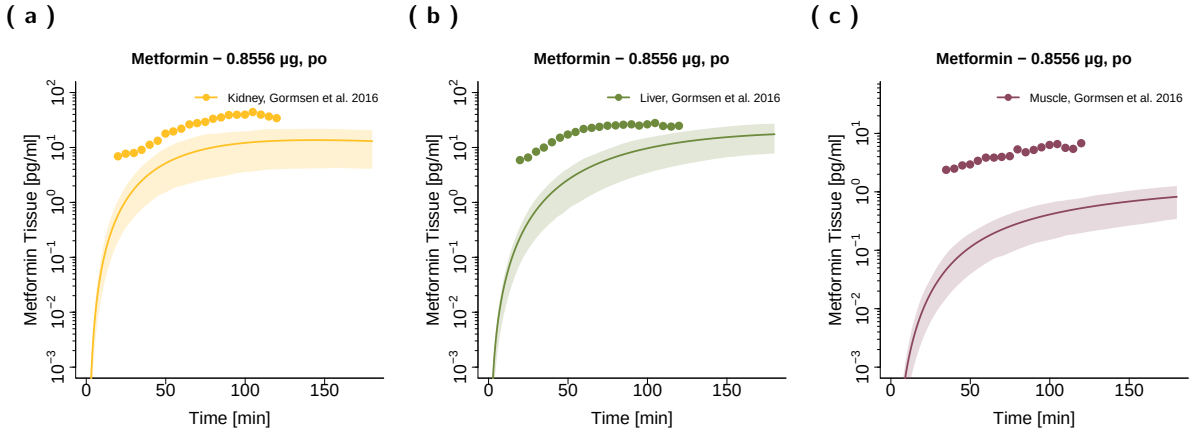

Figure S2.4.6: Metformin kidney (•, –), liver (•, –), intestine (•, –) and muscle (•, –) tissue concentration-time profiles (semilogarithmic) following oral administration of metformin. Observed data are shown as dots. Population simulation arithmetic means are shown as lines; the shaded areas represent the predicted population variation (Q_{16} – Q_{84}).

2.4.4 Linear plots – Tissue

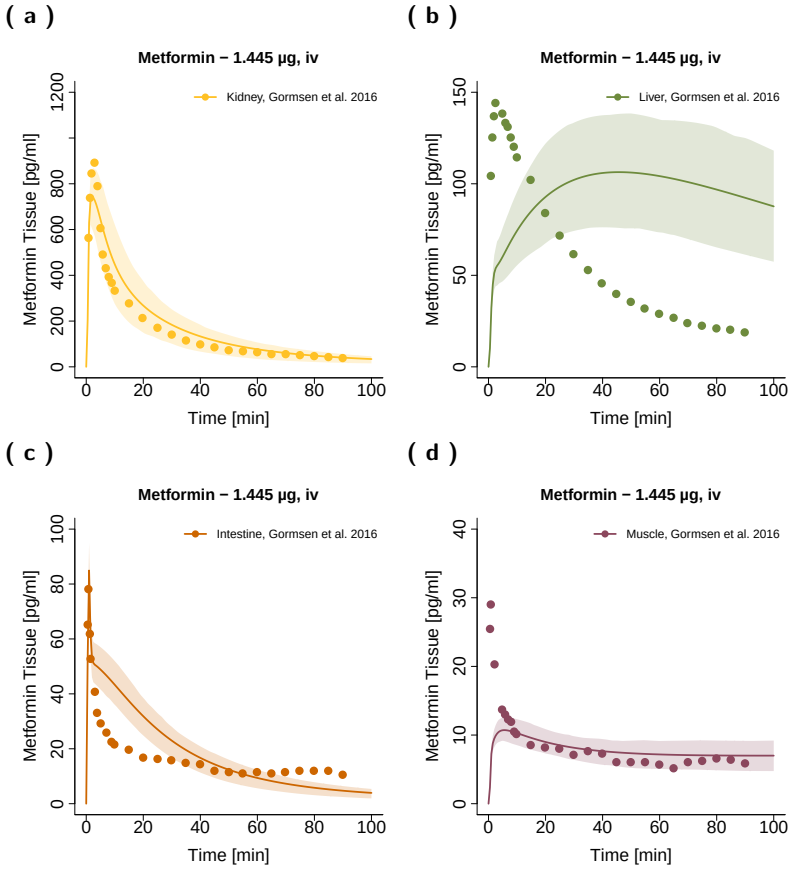

Figure S2.4.7: Metformin kidney (•, –), liver (•, –), intestine (•, –) and muscle (•, –) tissue concentration-time profiles (linear) following intravenous administration of metformin. Observed data are shown as dots. Population simulation arithmetic means are shown as lines; the shaded areas represent the predicted population variation (Q_{16} – Q_{84}).

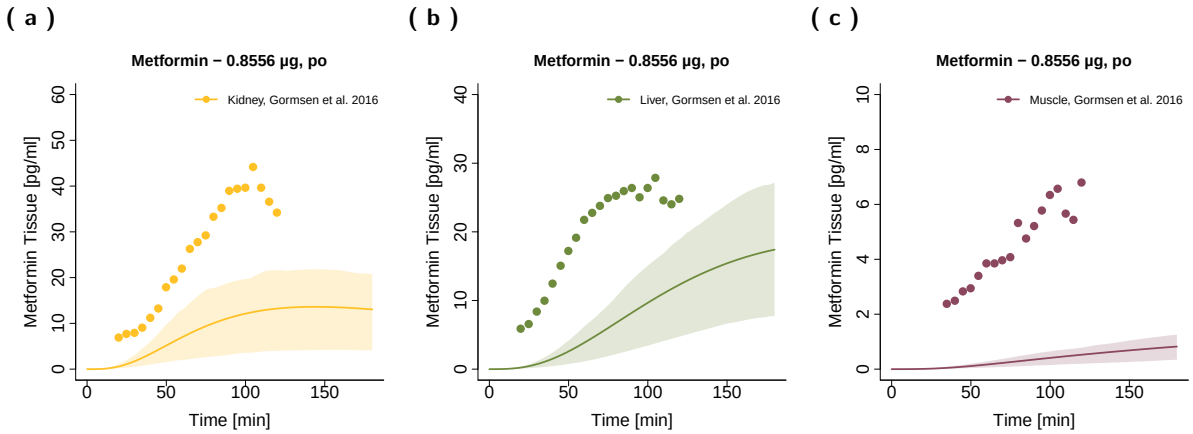

Figure S2.4.8: Metformin kidney (•, –), liver (•, –), intestine (•, –) and muscle (•, –) tissue concentration-time profiles (linear) following oral administration of metformin. Observed data are shown as dots. Population simulation arithmetic means are shown as lines; the shaded areas represent the predicted population variation (Q_{16} – Q_{84}).

2.4.5 Linear plots - Fraction excreted to urine

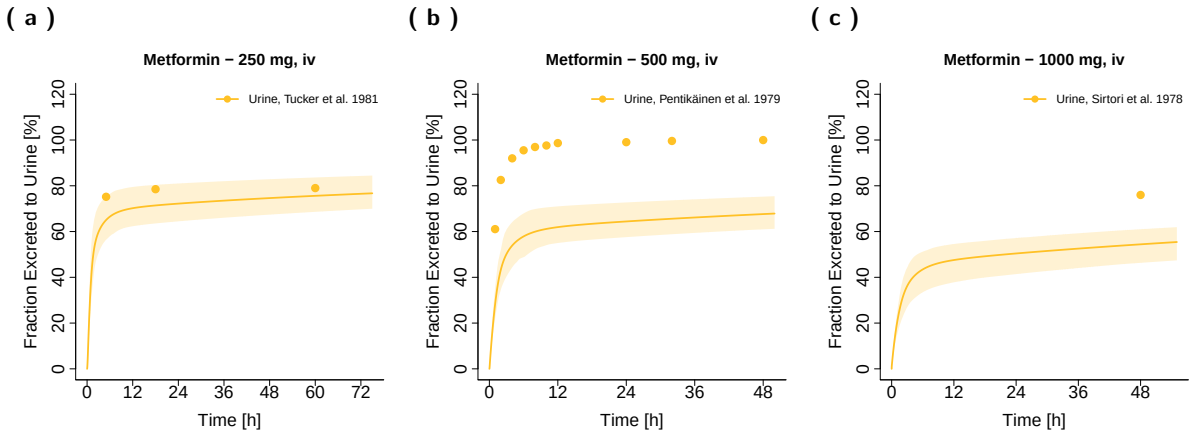

Figure S2.4.9: Metformin fraction excreted to urine (●, –) profiles (linear) following intravenous administration of metformin. Observed data are shown as dots. Population simulation arithmetic means are shown as lines; the shaded areas represent the predicted population variation (Q_{16} – Q_{84}).

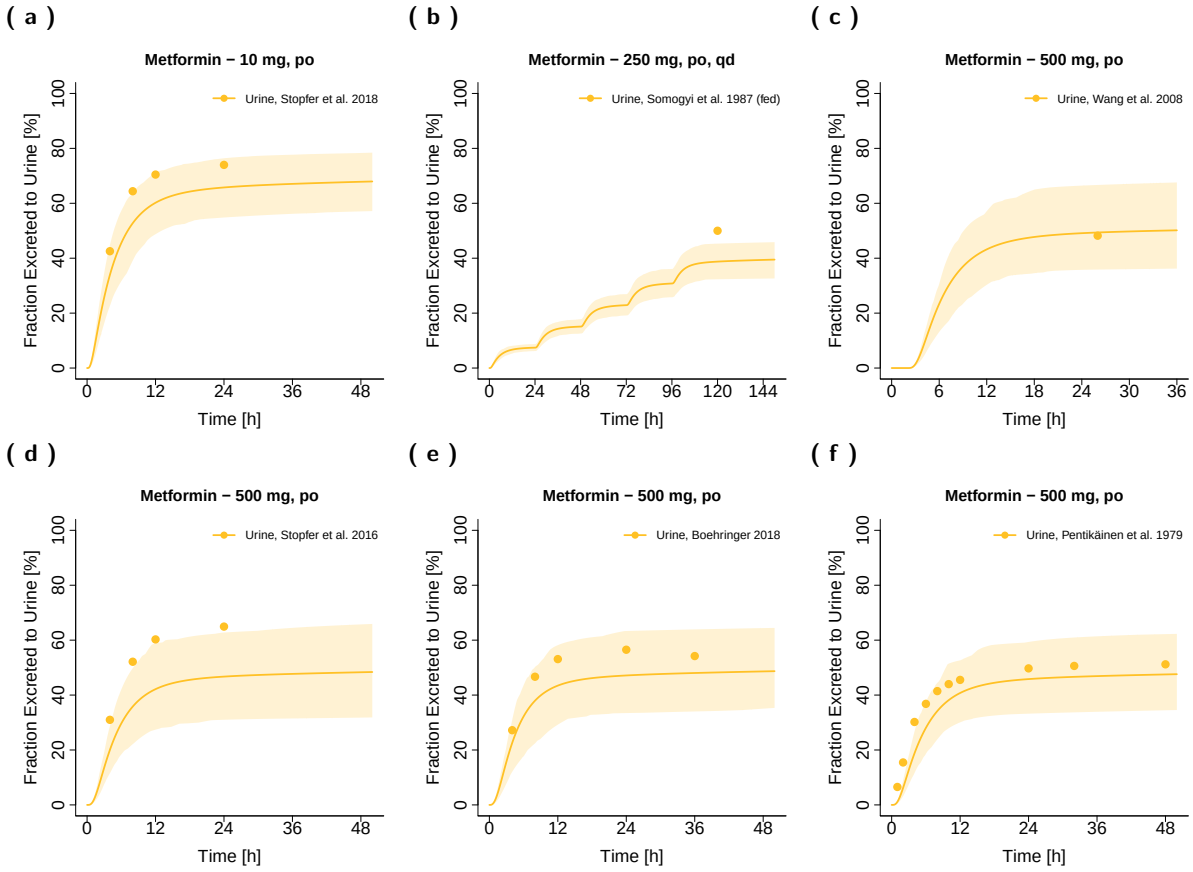

Figure S2.4.10: Metformin fraction excreted to urine (●, –) profiles (linear) following oral administration of metformin. Observed data are shown as dots. Population simulation arithmetic means are shown as lines; the shaded areas represent the predicted population variation (Q_{16} – Q_{84}).

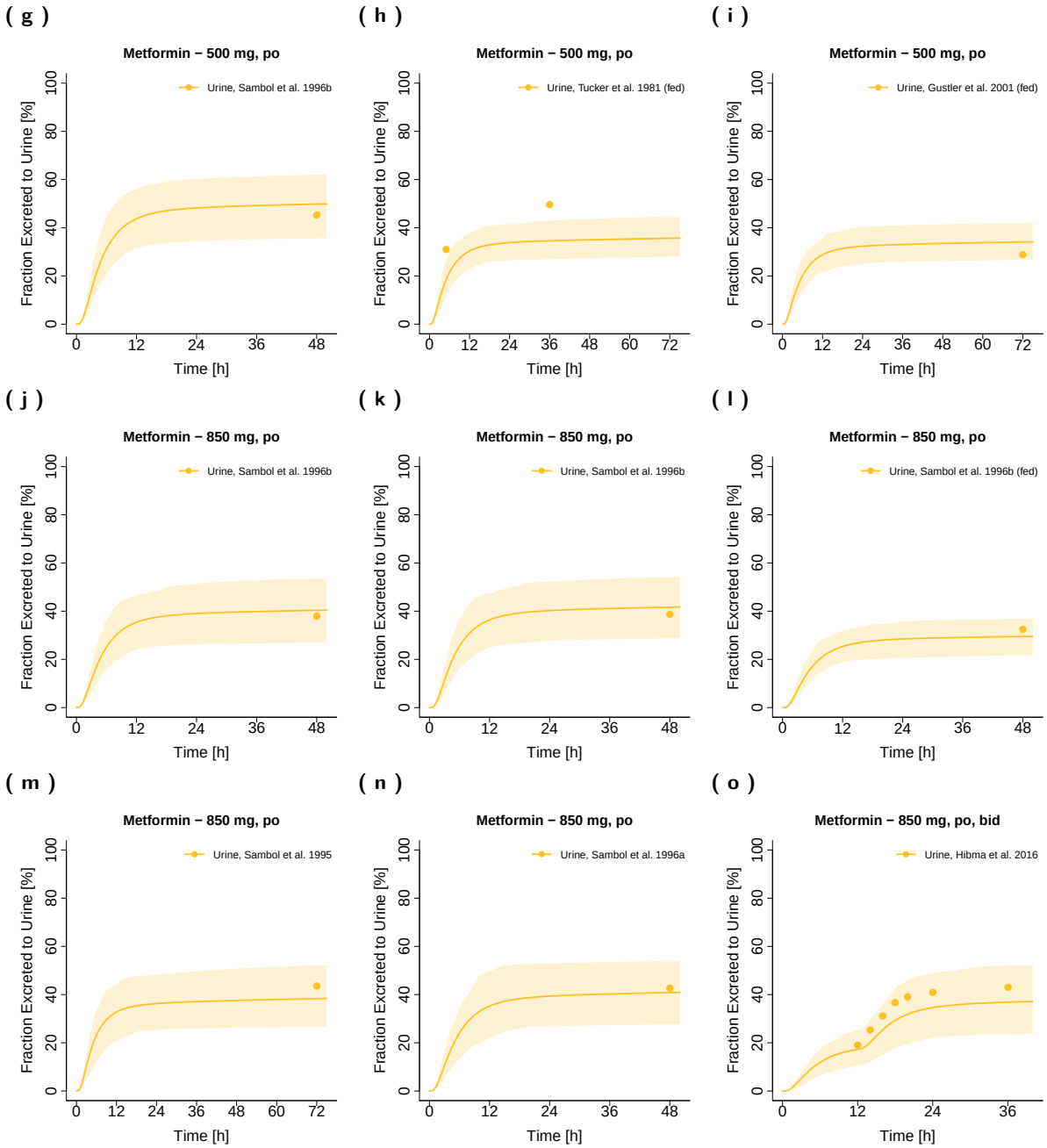

Figure S2.4.10: Metformin fraction excreted to urine (●, –) profiles (linear) following oral administration of metformin. Observed data are shown as dots. Population simulation arithmetic means are shown as lines; the shaded areas represent the predicted population variation (Q_{16} – Q_{84}). (continued)

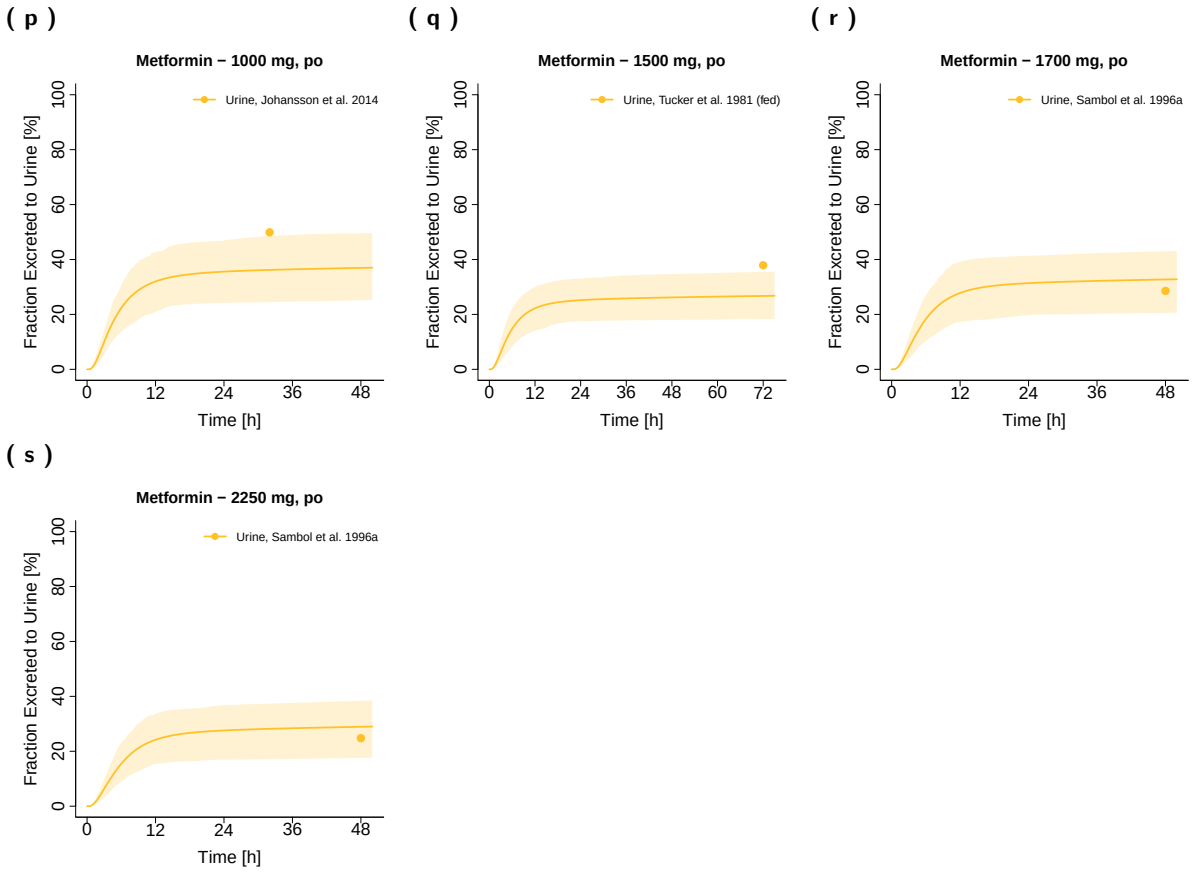

Figure S2.4.10: Metformin fraction excreted to urine (•, –) profiles (linear) following oral administration of metformin. Observed data are shown as dots. Population simulation arithmetic means are shown as lines; the shaded areas represent the predicted population variation (Q_{16} – Q_{84}). (continued)

2.5 Model evaluation

2.5.1 Predicted concentrations versus observed concentrations goodness-of-fit plot

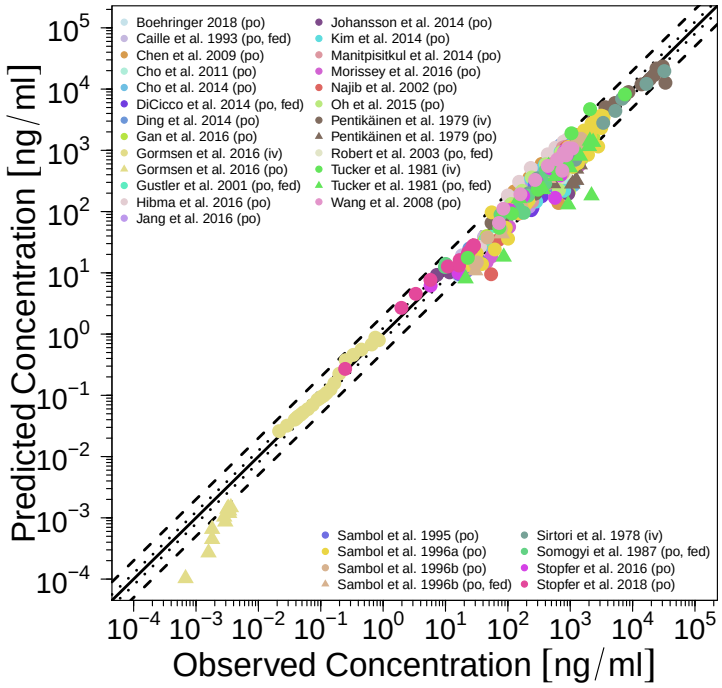

Figure S2.5.1: Predicted versus observed metformin concentrations. The black solid line (——) marks the line of identity. Black dotted lines (·····) indicate 1.25-fold, black dashed lines (- -) indicate 2-fold deviation.

2.5.2 Mean relative deviation of plasma concentration predictions

Table S2.5.1: Mean relative deviation (MRD) values of metformin plasma concentration predictions

Route	Compartment	Dose	MRD	Reference
Intravenous				
iv, bolus	Arterial Blood Plasma	1.45 µg	1.16	Gormsen et al. 2016 [7]
iv, 15 min	Venous Blood Plasma	250.00 mg	1.50	Tucker et al. 1981 [8]
iv, 5 min	Venous Blood Plasma	500.00 mg	1.36	Pentikäinen et al. 1979 [9]
iv, bolus	Venous Blood Plasma	1000.00 mg	1.35	Sirtori et al. 1978 [10]
MRD			**1.32 (1.16–1.50)**	
			4/4 with MRD ≤ 2	
Oral				
oral, solution	Arterial Blood Plasma	0.86 µg	3.39	Gormsen et al. 2016 [7]
oral, solution	Venous Blood Plasma	10.00 mg	1.19	Stopfer et al. 2018 [42]
oral, tablet	Venous Blood Plasma	250.00 mg (qd)	1.32	Somogyi et al. 1987 (fed) [12]
oral, tablet	Venous Blood Plasma	500.00 mg	1.24	Wang et al. 2008 [13]
oral, tablet	Venous Blood Plasma	500.00 mg	1.48	Stopfer et al. 2016 [11]
oral, solution	Venous Blood Plasma	500.00 mg	1.43	Boehringer 2018 [14]
oral, tablet	Venous Blood Plasma	500.00 mg	1.92	Pentikäinen et al. 1979 [9]
oral, tablet	Venous Blood Plasma	500.00 mg	1.30	Sambol et al. 1996b [18]
oral, tablet	Venous Blood Plasma	500.00 mg	1.70	Najib et al. 2002 [17]
oral, tablet	Venous Blood Plasma	500.00 mg	2.39	Tucker et al. 1981 (fed) [8]
oral, tablet	Venous Blood Plasma	500.00 mg	1.17	Caille et al. 1993 (fed) [15]
oral, tablet	Venous Blood Plasma	500.00 mg	1.21	Gustler et al. 2001 (fed) [16]
oral, tablet	Venous Blood Plasma	500.00 mg (bid)	1.35	Manitpisitkul et al. 2014 [22]
oral, tablet	Venous Blood Plasma	500.00 mg (bid)	1.52	Oh et al. 2015 [23]
oral, tablet	Venous Blood Plasma	500.00 mg (bid)	1.56	Jang et al. 2016 [20]
oral, tablet	Venous Blood Plasma	500.00 mg (bid)	1.67	Kim et al. 2014 [21]
oral, tablet	Venous Blood Plasma	500.00 mg (bid)	1.64	DiCicco et al. 2014 (fed) [19]
oral, tablet	Venous Blood Plasma	750.00 mg (bid)	1.85	Cho et al. 2014 [25]
oral, tablet	Venous Blood Plasma	750.00 mg (bid)	1.39	Ding et al. 2014 [26]
oral, tablet	Venous Blood Plasma	750.00 mg	1.68	Cho et al. 2011 [24]
oral, solution	Venous Blood Plasma	850.00 mg	1.36	Sambol et al. 1996b [18]
oral, tablet	Venous Blood Plasma	850.00 mg	1.31	Sambol et al. 1996b [18]
oral, tablet	Venous Blood Plasma	850.00 mg	1.50	Sambol et al. 1996b (fed) [18]
oral, tablet	Venous Blood Plasma	850.00 mg	1.51	Sambol et al. 1995 [30]
oral, tablet	Venous Blood Plasma	850.00 mg	1.54	Sambol et al. 1996a [31]
oral, tablet	Venous Blood Plasma	850.00 mg (tid)	1.44	Sambol et al. 1996a [31]
oral, tablet	Venous Blood Plasma	850.00 mg	1.93	Chen et al. 2009 [27]
oral, tablet	Venous Blood Plasma	850.00 mg	1.68	Morissey et al. 2016 [28]
oral, tablet	Venous Blood Plasma	850.00 mg	1.56	Robert et al. 2003 (fed) [29]
oral, tablet	Venous Blood Plasma	850.00 mg (bid)	1.72	Hibma et al. 2016 [32]
oral, tablet	Venous Blood Plasma	1000.00 mg	1.71	Johansson et al. 2014 [33]
oral, tablet	Venous Blood Plasma	1000.00 mg (qd)	1.75	Gan et al. 2016 [34]
oral, tablet	Venous Blood Plasma	1500.00 mg	3.06	Tucker et al. 1981 (fed) [8]
oral, tablet	Venous Blood Plasma	1700.00 mg	1.49	Sambol et al. 1996a [31]
oral, tablet	Venous Blood Plasma	2550.00 mg	1.52	Sambol et al. 1996a [31]
MRD			**1.65 (1.17–3.39)**	
			32/35 with MRD ≤ 2	
Overall MRD			**1.61 (1.16–3.39)**	
			36/39 with MRD ≤ 2	

bid: twice daily, **iv**: intravenous, **MRD**: mean relative deviation, **qd**: once daily, **tid**: three times daily

2.5.3 AUC and C_{max} goodness-of-fit plots

(a) AUC

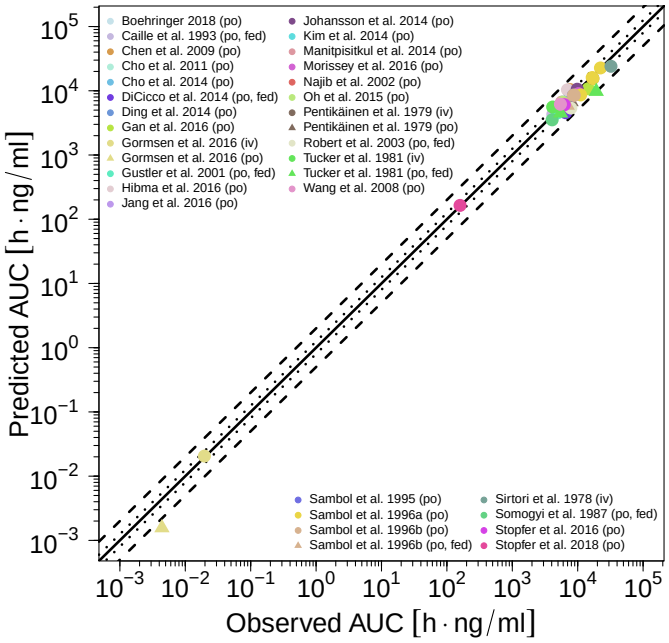

(b) C_{max}

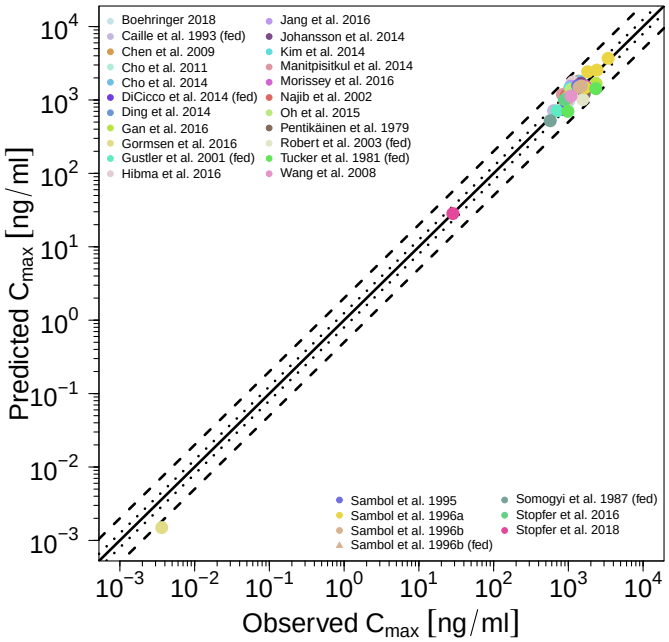

Figure S2.5.2: Predicted versus observed metformin AUC and C_{max} values. Each symbol represents the AUC or C_{max} of a different profile. The black solid line (——) marks the line of identity. Black dotted lines (·····) indicate 1.25-fold, black dashed lines (– –) indicate 2-fold deviation. **AUC**: area under the plasma concentration–time curve from the time of administration to the last data point, **C_{max}**: maximum plasma concentration

2.5.4 Geometric mean fold error of predicted AUC and C_{max} values

Table S2.5.2: Predicted and observed AUC and C_{max} values of metformin plasma concentrations

			AUC			C_{max}			
Route	Compartment	Dose	Pred [h·ng/ml]	Obs [h·ng/ml]	Pred/Obs	Pred [ng/ml]	Obs [ng/ml]	Pred/Obs	Reference
Intravenous									
iv, bolus	Arterial Blood Plasma	1.45 µg	0.021	0.020	1.049	-	-	-	Gormsen et al. 2016 [7]
iv, 15 min	Venous Blood Plasma	250.00 mg	5587.959	4140.891	1.349	-	-	-	Tucker et al. 1981 [8]
iv, 5 min	Venous Blood Plasma	500.00 mg	15744.969	16988.645	0.927	-	-	-	Pentikäinen et al. 1979 [9]
iv, bolus	Venous Blood Plasma	1000.00 mg	24061.360	32245.677	0.746	-	-	-	Sirtori et al. 1978 [10]
GMFE					**1.20 (1.05–1.35)**				
					4/4 with GMFE ≤ 2				
Oral									
oral, solution	Arterial Blood Plasma	0.86 µg	0.002	0.004	0.356	0.001	0.004	0.412	Gormsen et al. 2016 [7]
oral, solution	Venous Blood Plasma	10.00 mg	164.312	158.888	1.034	28.375	28.491	0.996	Stopfer et al. 2018 [42]
oral, tablet	Venous Blood Plasma	250.00 mg (qd)	3530.493	4066.828	0.868	521.870	572.692	0.911	Somogyi et al. 1987 (fed) [12]
oral, tablet	Venous Blood Plasma	500.00 mg	6176.527	5442.724	1.135	1127.770	1082.090	1.042	Wang et al. 2008 [13]
oral, tablet	Venous Blood Plasma	500.00 mg	6056.242	6233.985	0.971	1004.917	889.679	1.130	Stopfer et al. 2016 [11]
oral, solution	Venous Blood Plasma	500.00 mg	5583.679	6751.229	0.827	957.183	1009.165	0.948	Boehringer 2018 [14]
oral, tablet	Venous Blood Plasma	500.00 mg	6740.934	7918.325	0.851	1215.591	1633.658	0.744	Pentikäinen et al. 1979 [9]
oral, tablet	Venous Blood Plasma	500.00 mg	6200.710	6264.348	0.990	1081.878	962.832	1.124	Sambol et al. 1996b [18]
oral, tablet	Venous Blood Plasma	500.00 mg	6099.993	6536.056	0.933	1140.557	933.952	1.221	Najib et al. 2002 [17]
oral, tablet	Venous Blood Plasma	500.00 mg	4488.556	5482.046	0.819	699.898	983.523	0.712	Tucker et al. 1981 (fed) [8]
oral, tablet	Venous Blood Plasma	500.00 mg	4322.651	4168.490	1.037	716.748	634.735	1.129	Caille et al. 1993 (fed) [15]
oral, tablet	Venous Blood Plasma	500.00 mg	4516.587	4882.649	0.925	711.718	705.373	1.009	Gustler et al. 2001 (fed) [16]
oral, tablet	Venous Blood Plasma	500.00 mg (bid)	6677.375	5671.054	1.177	1183.788	833.565	1.420	Manitpisitkul et al. 2014 [22]
oral, tablet	Venous Blood Plasma	500.00 mg (bid)	6648.617	5939.479	1.119	1388.316	1075.310	1.291	Oh et al. 2015 [23]
oral, tablet	Venous Blood Plasma	500.00 mg (bid)	6522.983	5925.074	1.101	1544.315	1078.040	1.433	Jang et al. 2016 [20]
oral, tablet	Venous Blood Plasma	500.00 mg (bid)	6646.019	5838.472	1.138	1442.626	1040.830	1.386	Kim et al. 2014 [21]
oral, tablet	Venous Blood Plasma	500.00 mg (bid)	4560.657	6544.339	0.697	741.019	871.180	0.851	DiCicco et al. 2014 (fed) [19]
oral, tablet	Venous Blood Plasma	750.00 mg (bid)	9456.838	7876.334	1.201	1783.367	1429.550	1.248	Cho et al. 2014 [25]
oral, tablet	Venous Blood Plasma	750.00 mg (bid)	9323.009	7540.401	1.236	1677.773	1164.530	1.441	Ding et al. 2014 [26]
oral, tablet	Venous Blood Plasma	750.00 mg	9589.511	8867.350	1.081	1797.815	1460.504	1.231	Cho et al. 2011 [24]
oral, solution	Venous Blood Plasma	850.00 mg	8564.916	8860.370	0.967	1491.038	1387.106	1.075	Sambol et al. 1996b [18]
oral, tablet	Venous Blood Plasma	850.00 mg	8572.538	8617.807	0.995	1551.791	1489.635	1.042	Sambol et al. 1996b [18]
oral, tablet	Venous Blood Plasma	850.00 mg	6009.868	6895.007	0.872	996.922	920.294	1.083	Sambol et al. 1996b (fed) [18]
oral, tablet	Venous Blood Plasma	850.00 mg	8578.655	8606.521	0.997	1563.728	1333.624	1.173	Sambol et al. 1995 [30]
oral, tablet	Venous Blood Plasma	850.00 mg	8614.909	11072.305	0.778	1471.168	1667.723	0.882	Sambol et al. 1996a [31]
oral, tablet	Venous Blood Plasma	850.00 mg (tid)	16113.605	16672.216	0.966	2425.859	1811.190	1.339	Sambol et al. 1996a [31]
oral, tablet	Venous Blood Plasma	850.00 mg	10445.008	7644.417	1.366	1808.482	1360.878	1.329	Chen et al. 2009 [27]
oral, tablet	Venous Blood Plasma	850.00 mg	9036.179	10307.765	0.877	1546.931	1687.407	0.917	Morissey et al. 2016 [28]
oral, tablet	Venous Blood Plasma	850.00 mg	5380.502	7846.498	0.686	1013.374	1566.437	0.647	Robert et al. 2003 (fed) [29]
oral, tablet	Venous Blood Plasma	850.00 mg (bid)	10362.497	6972.025	1.486	1756.306	1146.000	1.533	Hibma et al. 2016 [32]
Overall GMFE					**1.20 (1.00–2.81)**			**1.24 (1.00–2.43)**	
					38/39 with GMFE ≤ 2			**34/35 with GMFE ≤ 2**	

-: not calculated, **bid**: twice daily, **GMFE**: geometric mean fold error, **iv**: intravenous, **obs**: observed, **pred**: predicted, **qd**: once daily, **tid**: three times daily

Table S2.5.2: Predicted and observed AUC and C_{max} values of metformin plasma concentrations *(continued)*

			AUC			C_{max}			
Route	Compartment	Dose	Pred [h·ng/ml]	Obs [h·ng/ml]	Pred/Obs	Pred [ng/ml]	Obs [ng/ml]	Pred/Obs	Reference
oral, tablet	Venous Blood Plasma	1000.00 mg	10581.824	9832.899	1.076	1691.168	1474.451	1.147	Johansson et al. 2014 [33]
oral, tablet	Venous Blood Plasma	1000.00 mg (qd)	10764.796	14471.488	0.744	1681.405	2343.890	0.717	Gan et al. 2016 [34]
oral, tablet	Venous Blood Plasma	1500.00 mg	9759.984	19215.074	0.508	1431.310	2327.089	0.615	Tucker et al. 1981 (fed) [8]
oral, tablet	Venous Blood Plasma	1700.00 mg	15501.142	17118.050	0.906	2551.992	2405.000	1.061	Sambol et al. 1996a [31]
oral, tablet	Venous Blood Plasma	2550.00 mg	22690.348	22268.997	1.019	3690.435	3403.992	1.084	Sambol et al. 1996a [31]
GMFE					**1.20 (1.00–2.81)**			**1.24 (1.00–2.43)**	
					34/35 with GMFE ≤ 2			**34/35 with GMFE ≤ 2**	
Overall GMFE					**1.20 (1.00–2.81)**			**1.24 (1.00–2.43)**	
					38/39 with GMFE ≤ 2			**34/35 with GMFE ≤ 2**	

-: not calculated, **bid**: twice daily, **GMFE**: geometric mean fold error, **iv**: intravenous, **obs**: observed, **pred**: predicted, **qd**: once daily, **tid**: three times daily

2.5.5 Sensitivity analysis

Sensitivity of the final metformin model to single parameters (local sensitivity analysis) was calculated, measured as the relative change of the $AUC_{0\text{-}24}$ of a 500 mg single dose of metformin administered as tablet in the fasted state. Sensitivity analysis was carried out using a relative parameter perturbation of 1000 % (variation range 10.0, maximum number of 9 steps). Parameters were included into the analysis if they were optimized (PMAT K_m, PMAT k_{cat}, OCT1 k_{cat}, OCT2 k_{cat}, MATE1 k_{cat}, luminal intestinal permeability, basolateral intestinal permeability), if they are associated with optimized parameters (OCT1 K_m, OCT2 K_m, MATE1 K_m) or if they might have a strong impact due to calculation methods used in the model (solubility, lipophilicity, fraction unbound in plasma, blood/plasma concentration ratio, GFR fraction).

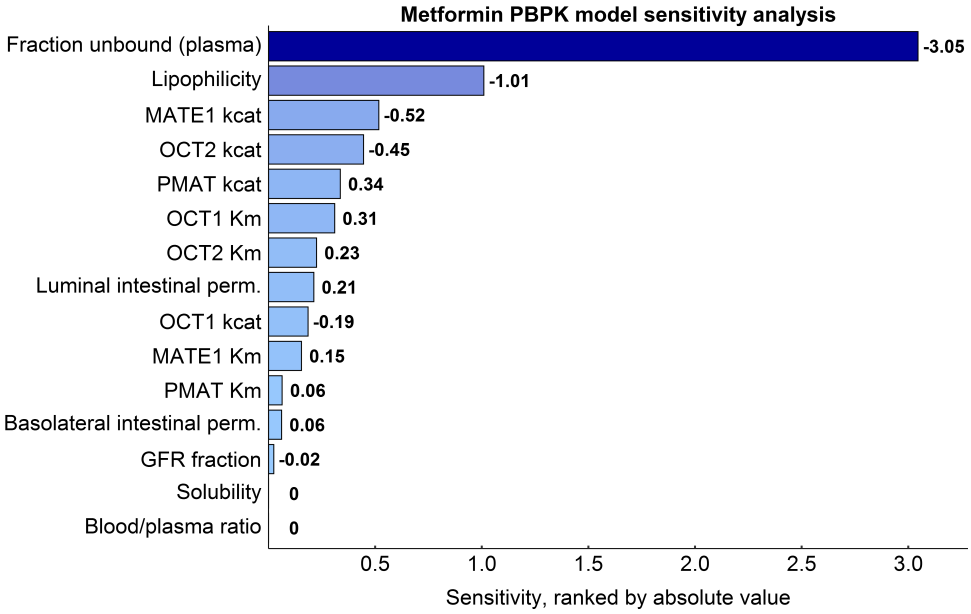

Figure S2.5.3: Metformin PBPK model sensitivity analysis. Sensitivity to single parameters, measured as change of the simulated $AUC_{0\text{-}24}$ of a 500 mg single oral dose. **GFR**: glomerular filtration rate, **kcat**: transport rate constant (turnover number), **Km**: Michaelis-Menten constant, **perm**: permeability

3 Cimetidine population pharmacokinetic (PopPK) analysis

3.1 Background

Cimetidine PBPK model building was supported by a Population Pharmacokinetic (PopPK) analysis to understand and reproduce the double peaks of the cimetidine plasma concentration-time profiles observed after administration in the fasted state. While the plasma profiles of cimetidine exhibit a single, smooth peak after administration with food, most DDI studies are conducted in the fasted state. These double peaks following administration in the fasted state are very prominent, even in mean profiles of larger cohorts, and are explained by the release of cimetidine from the stomach in two portions caused by the phasic gastric emptying activity of the stomach in the fasted state.

3.2 Objective

The objective of this analysis was the development of a PopPK model of cimetidine based on data from intravenous studies and oral studies in the fasted state. The model should focus on the description of the double peak phenomenon and support the PBPK model development.

3.3 Methods

3.3.1 Dataset

For model development 25 studies were utilized in total, including nine studies of intravenous administration as well as 16 studies of fasted oral administration. Study details are summarized in Table S3.3.1. In brief, administered doses ranged from 100 to 800 mg and subjects were between 19 and 80 years old. Average cimetidine concentration-time profiles were used for model building, together with 3 individual profiles that were published as representative examples of larger study populations.

Table S3.3.1: Cimetidine studies used for PopPK modeling

Dose [mg]	Route	n	Age [years]	Reference
100	iv, 5 min	3	(22–25)	Grahnen et al. 1979 [43]
200	iv, -	9	52 (27–66)	Larsson et al. 1982 [44]
200	iv, -	6	(20–54)	Mihaly et al. 1984 [45]
200	iv, bolus	10	40 (19–71)	Bodemar et al. 1981 [46]
200	iv, 5 min	6	(20–54)	Morgan et al. 1983 [47]
200	iv, 30 min	4	(20–54)	Morgan et al. 1983 [47]
300	iv, 2 min	1	(21–35)	Lebert et al. 1981 [48]
300	iv, 2 min	12	-	Walkenstein et al. 1978 [49]
400	iv, 5 min	19	(43–80)	Jönsson et al. 1982 [50]
200	po, -, fasted	10	40 (19–71)	Bodemar et al. 1981 [46]
200	po, -, fasted	8	21 (20–23)	Kanto et al. 1981 [51]
200	po, -, fasted	6	(20–54)	Mihaly et al. 1984 [45]
200	po, sol, fasted	1	(21–46)	Burland et al. 1975 [52]
200	po, caps, fasted	1	(21–46)	Burland et al. 1975 [52]
200	po, tab, fasted	10	56 (33–66)	Bodemar et al. 1979 [53]
200	po, tab, fasted	8	50 (25–71)	Bodemar et al. 1979 [53]
200	po, tab, fasted	10	55 (37–67)	Bodemar et al. 1979 [53]
300	po, sol, fasted	24	-	Walkenstein et al. 1978 [49]
300	po, tab, fasted	6	(27–42)	D'Angio et al. 1986 [54]
300	po, tab, fasted	12	-	Walkenstein et al. 1978 [49]

-: not given, **caps**: capsule, **iv**: intravenous, **n**: number of individuals studied, **po**: oral, **qd**: once daily, **sol**: solution, **tab**: tablet

Table S3.3.1: Cimetidine studies used for PopPK modeling *(continued)*

Dose [mg]	Route	n	Age [years]	Reference
400	po, -, fasted	9	46 (26–59)	Bodemar et al. 1981 [46]
400	po, tab, fasted	10	56 (33–66)	Bodemar et al. 1979 [53]
400	po, tab, fasted	3	(22–25)	Grahnen et al. 1979 [43]
800	po, -, fasted	9	46 (26–59)	Bodemar et al. 1981 [46]
800, qd	po, tab, fasted	18	29 (19–42)	Tiseo et al. 1998 [55]

-: not given, **caps**: capsule, **iv**: intravenous, **n**: number of individuals studied, **po**: oral, **qd**: once daily, **sol**: solution, **tab**: tablet

3.3.2 Model building and evaluation

Population pharmacokinetic analysis was performed using non-linear mixed-effects modeling techniques implemented in NONMEM (version 7.3). These allow estimation of population medians for pharmacokinetic model parameters with simultaneous quantification of interindividual variability which is, due to the usage of averaged concentration-time profiles in this particular analysis, considered as interstudy variability (ISV) and residual (unexplained) variability. Model selection was based on the objective function value (OFV) provided by NONMEM, visual inspection of goodness-of-fit plots and the precision of parameter estimates. A nested model was considered superior to another when the OFV was reduced by 3.84 units (χ^2-test statistic, $p < 0.05$, 1 degree of freedom).

The First-Order Conditional Estimation with Interaction (FOCE-I) method was applied and models were coded in the ADVAN6 subroutine. The structural base model building was performed for the intravenous studies first: one-, two- and three-compartment models were tested with first-order and saturated elimination (Michaelis-Menten) kinetics. Afterwards, the oral data was joined and different absorption models, such as zero-order, first-order and mixed parallel zero- and first-order absorption processes as well as split doses were evaluated. Saturable processes on absorption rates were tested using Michaelis-Menten kinetics. Based on the structural base model, ISVs were modeled exponentially and evaluated univariately. ISVs were added to the model if they improved the model in a statistically significant manner and if the parameter estimates of the model remained stable.

3.4 Results

The pharmacokinetics of cimetidine were best described by a two-compartment model with first-order elimination from the central compartment. To describe the double-peak phenomenon appropriately, the total cimetidine dose (TCD) was split into a first (Dose 1) and a second dose (Dose 2), where the fraction of the second dose (VF2) was estimated and the first dose was calculated as TCD*(1-VF2). Both doses were absorbed with the same absorption rate constant (KA), but the absorption of the second dose was delayed by a lag time (ALAG). A schematic representation of the model is illustrated in Figure S3.4.1.

Parameter estimates of the final model are presented in Table S3.4.1 and the final NONMEM model code is provided in Section 3.5. All parameters were estimated precisely with relative standard errors (RSE) <30%. Interstudy variability was incorporated on the fraction of dose attributed to the second dose (VF2), the lag time of the second dose (ALAG), the clearance (CL) and the central volume of distribution (V3). Diagnostic goodness-of-fit plots (Figure S3.4.2) and plots of predicted concentration-time profiles in logarithmic and linear presentation (Figures S3.4.3 to S3.4.16) demonstrate that the data is very well described.

The final model accurately captures the observed double-peak phenomenon in the fasted oral studies

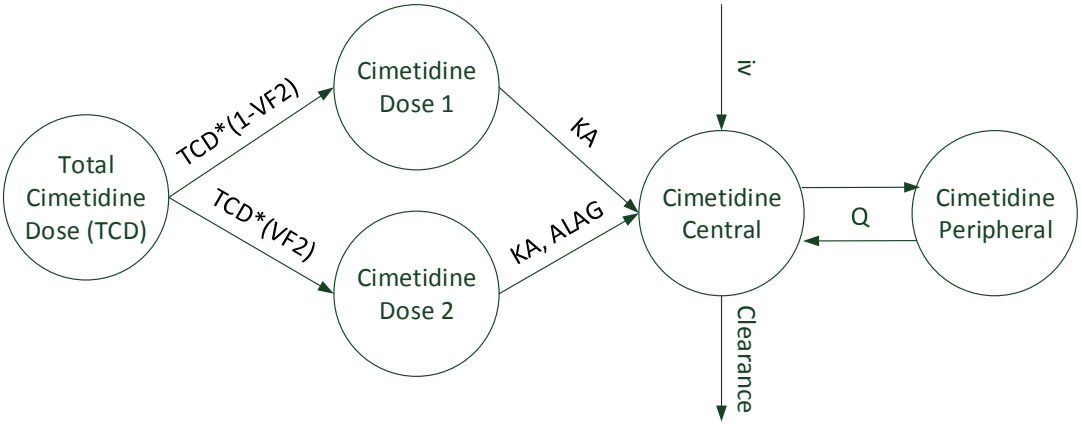

Figure S3.4.1: Schematic representation of the final cimetidine PopPK model

very well. It was estimated that in median 71.2% of the total dose are assigned to the first dose, being absorbed directly without a lag time. The remaining 28.8% of the dose were assigned to the second dose with an estimated median lag time of 1.54 h. Due to the interstudy variability on the dose distribution (VF2) and the lag time (ALAG), individual parameters were estimated for each study and are presented in Table S3.4.2. These estimated splitted doses and lag times were used as input parameters for the cimetidine PBPK model development.

Table S3.4.1: Parameter estimates of the final cimetidine PopPK model

Parameter	Unit	Value	RSE [%]	Description
KA	1/h	0.753	5.1	Absorption rate constant
FTOT	%	90.2	6.3	Absolute bioavailability
VF2	-	0.288	19.4	Fraction of total dose attributed to 2nd dose
ALAG	h	1.54	0	Lag time 2nd dose
CL	L/h	41.2	6	Clearance
V3	L	32.6	11.8	Central volume of distribution
Q	L/h	45.4	7.3	Intercompartmental clearance
V4	L	46	4.8	Peripheral volume of distribution
ISV VF2	%CV	84.8	28.8	Interstudy variability VF2
ISV ALAG	%CV	20.5	18	Interstudy variability ALAG
ISV CL	%CV	21.6	20.9	Interstudy variability CL
ISV V3	%CV	38.7	15.7	Interstudy variability V3
Prop RE	%	12.2	7.8	Proportional residual error
Add RE	±	1.8	fixed	Additive residual error

RSE: Relative standard error

Table S3.4.2: Estimated dose splitting for oral cimetidine doses

Dose [mg]	Route	Fraction (VF2)	Lag time (ALAG)	Reference
200	po, -, fasted	0.426	1.68 h	Bodemar et al. 1981 [46]
200	po, -, fasted	0.276	2.46 h	Kanto et al. 1981 [51]
200	po, -, fasted	0.496	1.39 h	Mihaly et al. 1984 [45]
200	po, sol, fasted	0.147	1.97 h	Burland et al. 1975 [52]
200	po, caps, fasted	0.078	1.32 h	Burland et al. 1975 [52]
200	po, tab, fasted	0.400	1.94 h	Bodemar et al. 1979 [53]
200	po, tab, fasted	0.402	1.37 h	Bodemar et al. 1979 [53]
200	po, tab, fasted	0.308	1.97 h	Bodemar et al. 1979 [53]
300	po, sol, fasted	0.148	1.64 h	Walkenstein et al. 1978 [49]
300	po, tab, fasted	0.233	1.93 h	D'Angio et al. 1986 [54]
300	po, tab, fasted	0.282	1.66 h	Walkenstein et al. 1978 [49]
400	po, -, fasted	0.481	1.41 h	Bodemar et al. 1981 [46]
400	po, tab, fasted	0.364	1.93 h	Bodemar et al. 1979 [53]
400	po, tab, fasted	0.133	1.53 h	Grahnen et al. 1979 [43]
800	po, -, fasted	0.393	1.64 h	Bodemar et al. 1981 [46]
800, qd	po, tab, fasted	0.623	1.24 h	Tiseo et al. 1998 [55]

-: not given, **caps**: capsule, **po**: oral, **qd**: once daily, **sol**: solution, **tab**: tablet

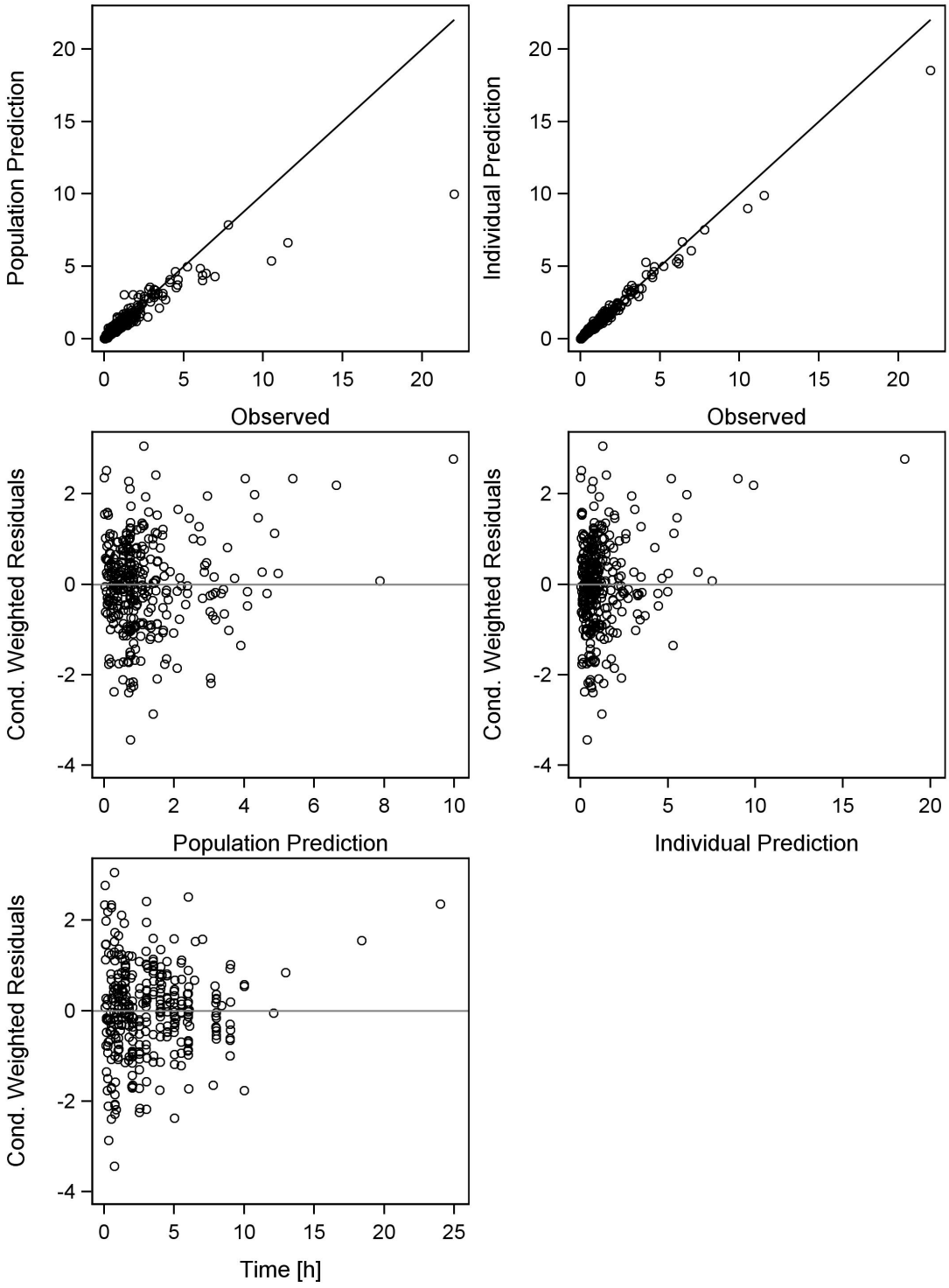

Figure S3.4.2: Goodness-of-fit plots of the final cimetidine model. Upper panel: population (left) and individual (right) predictions versus observed concentrations. Solid line indicates line of identity. Middle panel: conditional weighted residuals versus population (left) and individual (right) predictions. Lower panel: conditional weighted residuals versus time (left).

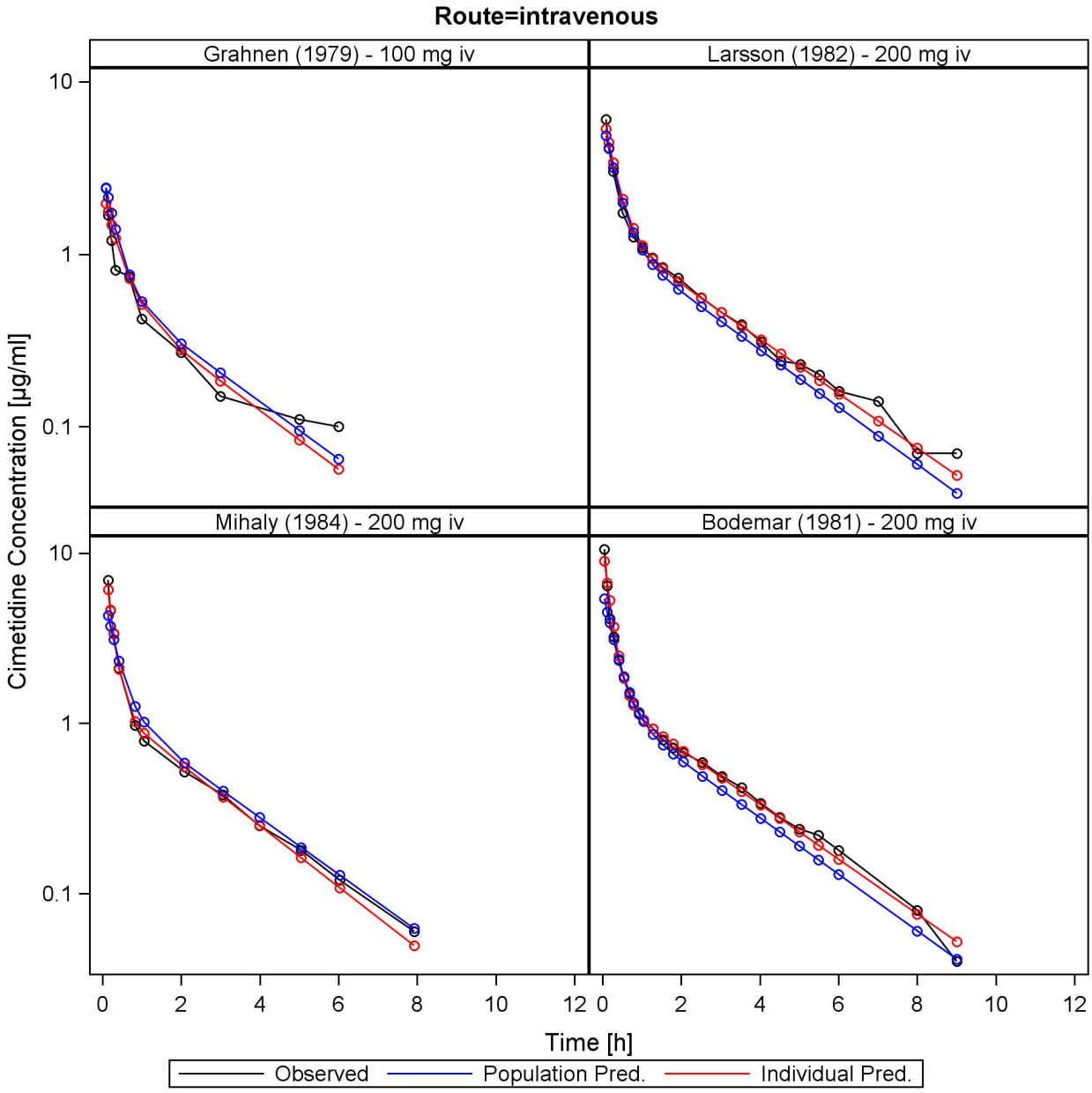

Figure S3.4.3: Concentration-time profiles (observed, population and individual predictions) from the final PopPK model of the studies Grahnen (1979), Larsson (1982), Mihaly (1984) and Bodemar (1981) presented on a logarithmic Y-axis.

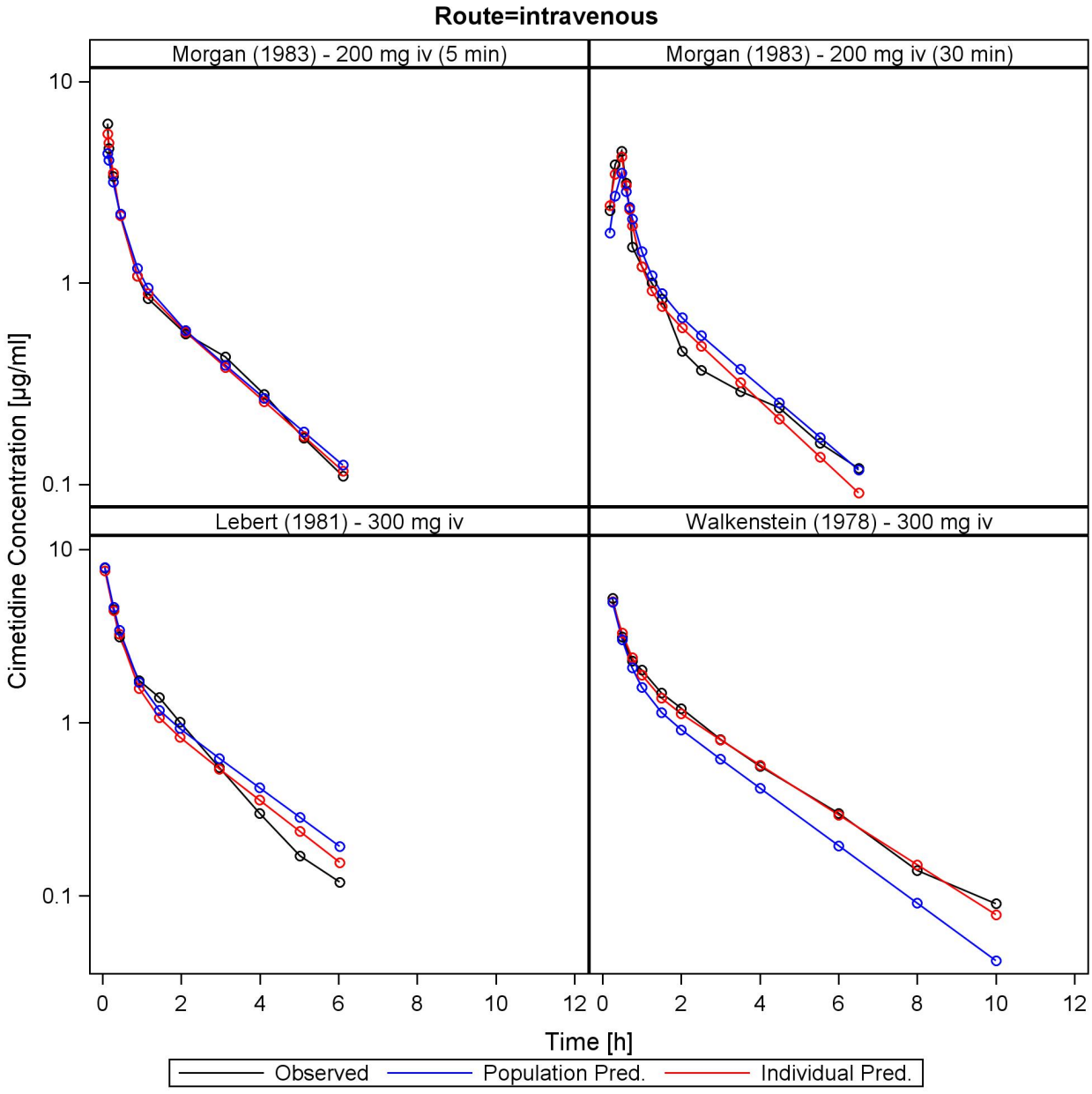

Figure S3.4.4: Concentration-time profiles (observed, population and individual predictions) from the final PopPK model of the studies Morgan (1983), Lebert (1981) and Walkenstein (1978) presented on a logarithmic Y-axis.

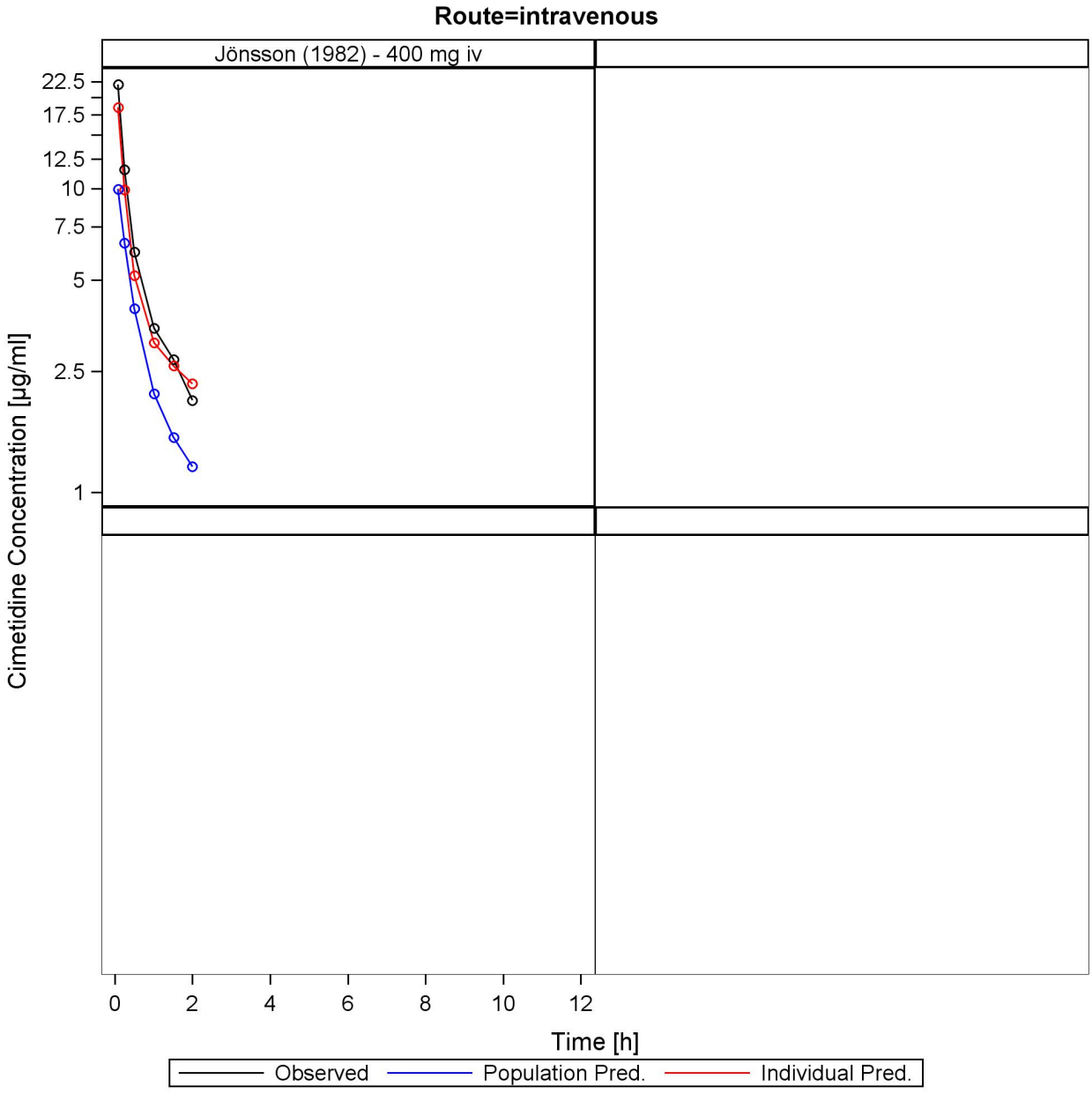

Figure S3.4.5: Concentration-time profiles (observed, population and individual predictions) from the final PopPK model of the study by Jönsson (1982) presented on a logarithmic Y-axis.

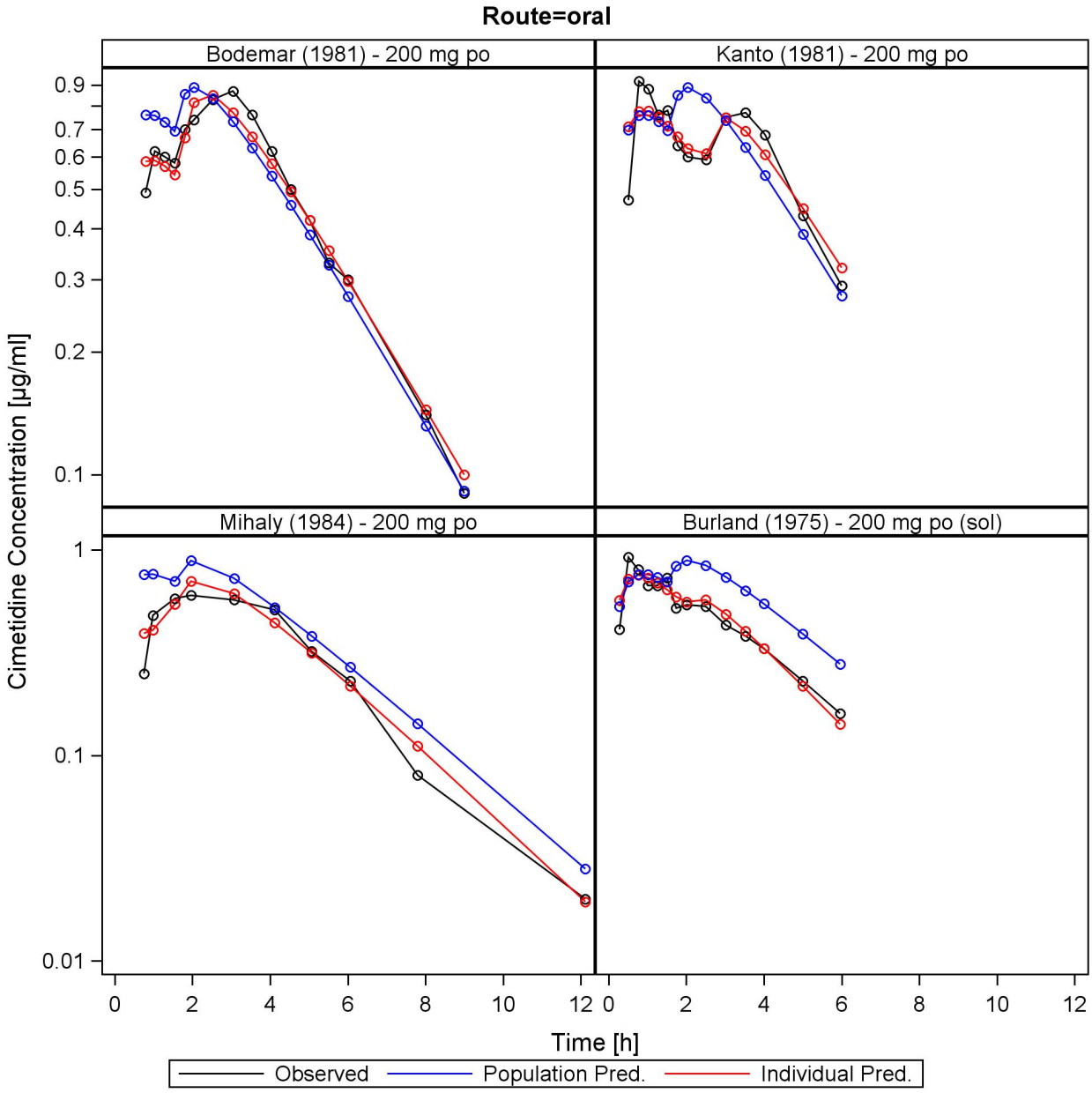

Figure S3.4.6: Concentration-time profiles (observed, population and individual predictions) from the final PopPK model of the studies Bodemar (1981), Kanto (1981), Mihaly (1984) and Burland (1975) presented on a logarithmic Y-axis.

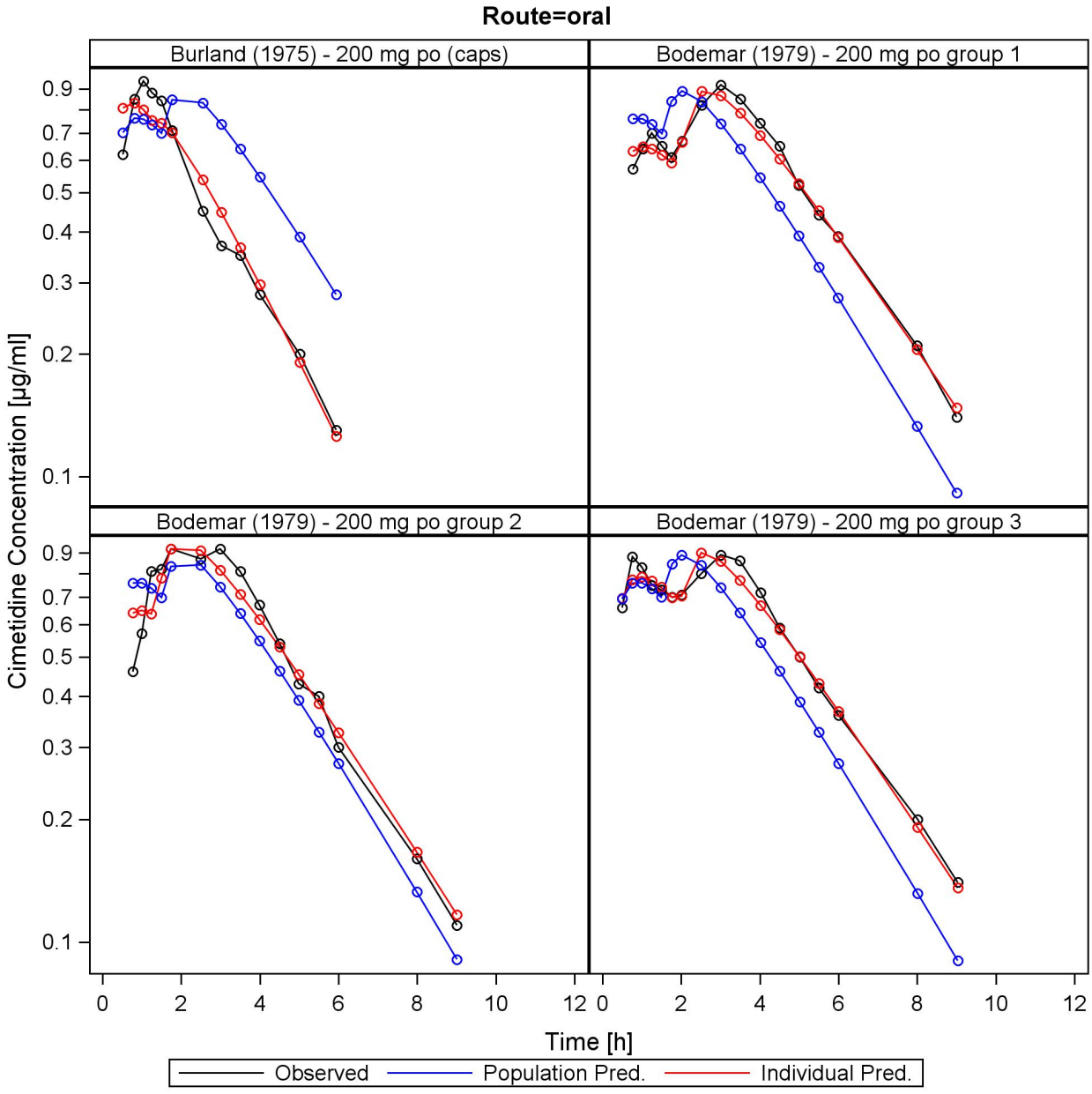

Figure S3.4.7: Concentration-time profiles (observed, population and individual predictions) from the final PopPK model of the studies Burland (1975) and Bodemar (1979) groups 1 to 3 presented on a logarithmic Y-axis.

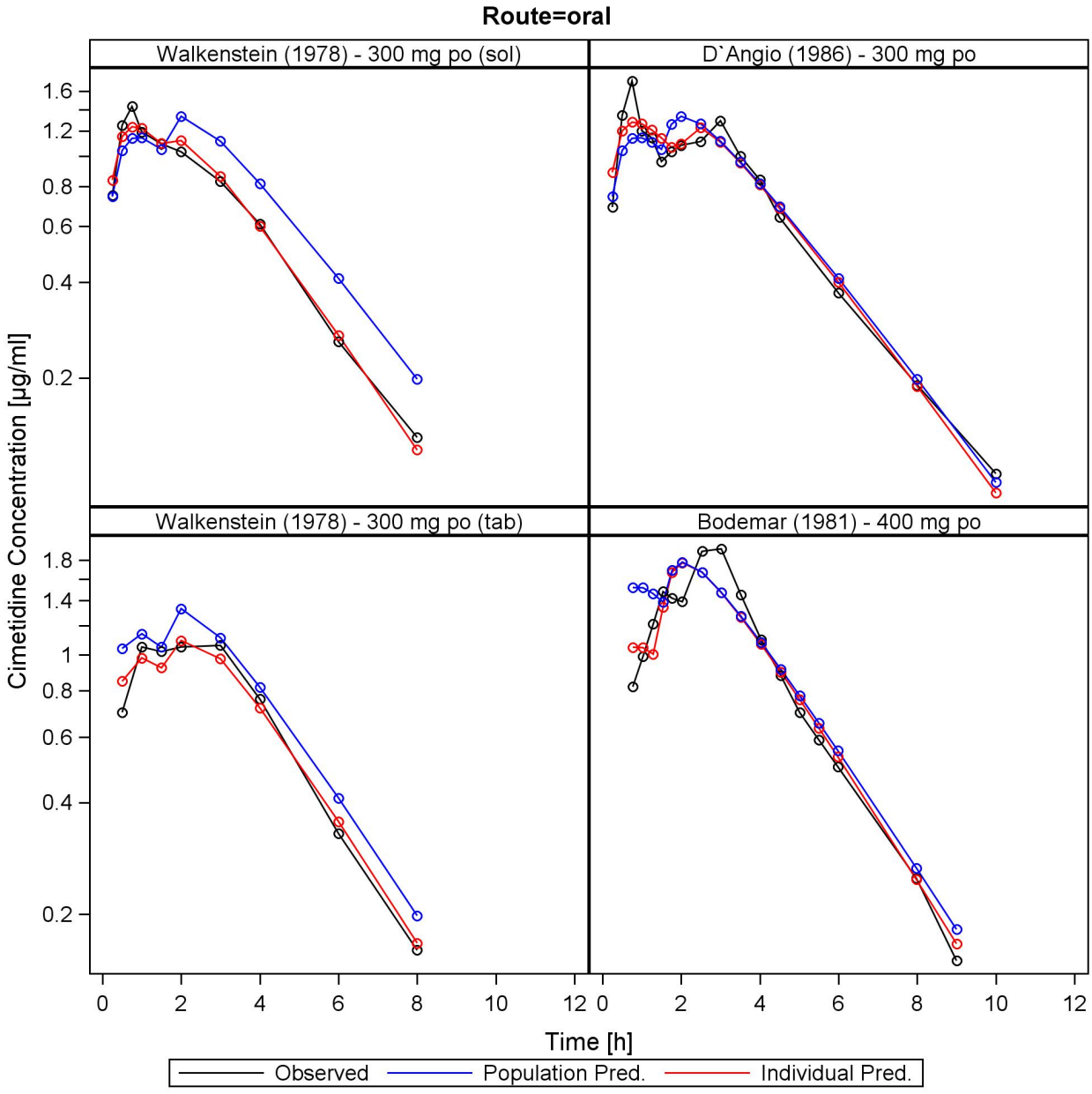

Figure S3.4.8: Concentration-time profiles (observed, population and individual predictions) from the final PopPK model of the studies Walkenstein (1978), D'Angio (1986) and Bodemar (1981) presented on a logarithmic Y-axis.

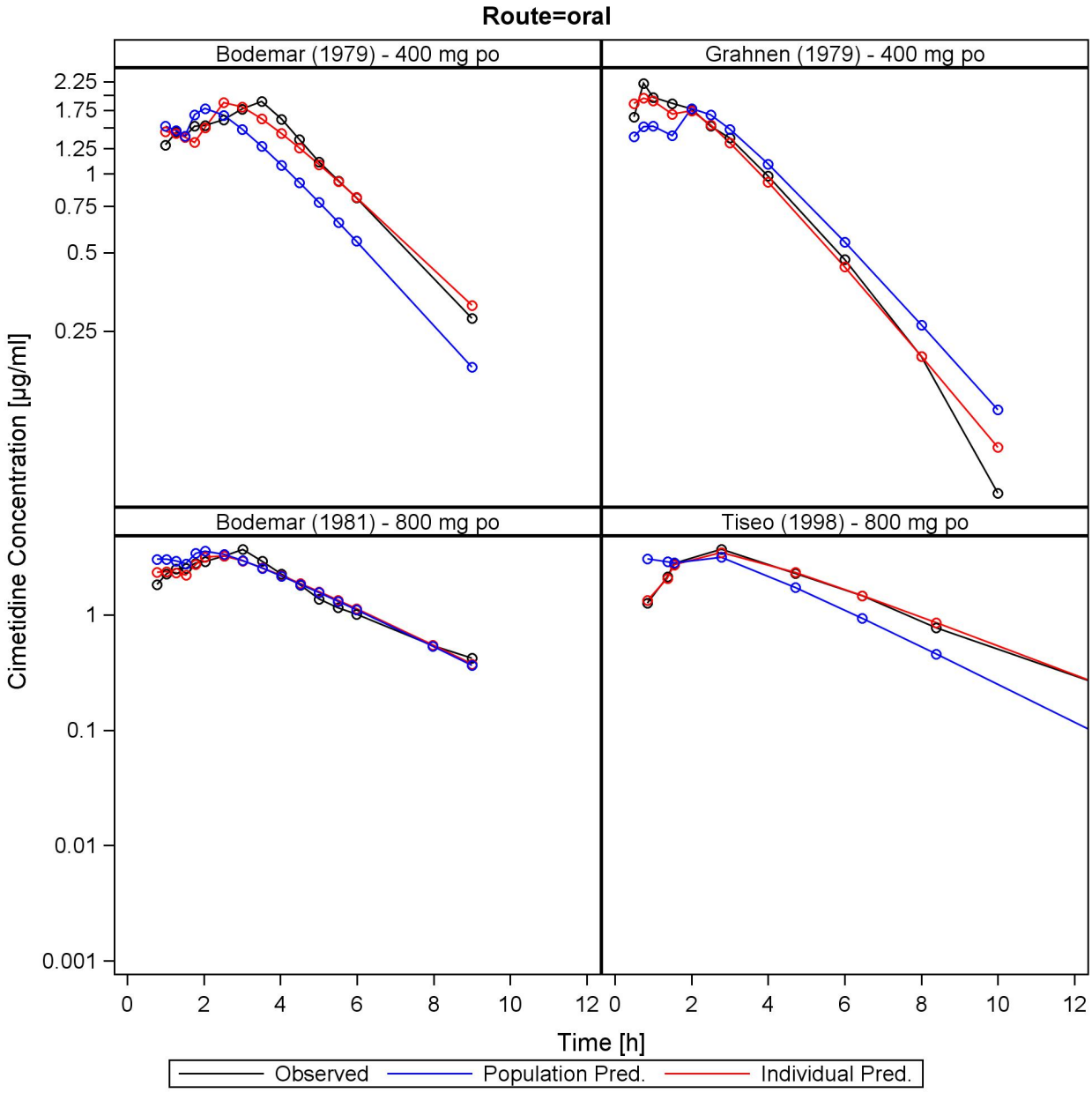

Figure S3.4.9: Concentration-time profiles (observed, population and individual predictions) from the final PopPK model of the studies Bodemar (1979), Grahnen (1979), Bodemar (1981) and Tiseo (1998) presented on a logarithmic Y-axis.

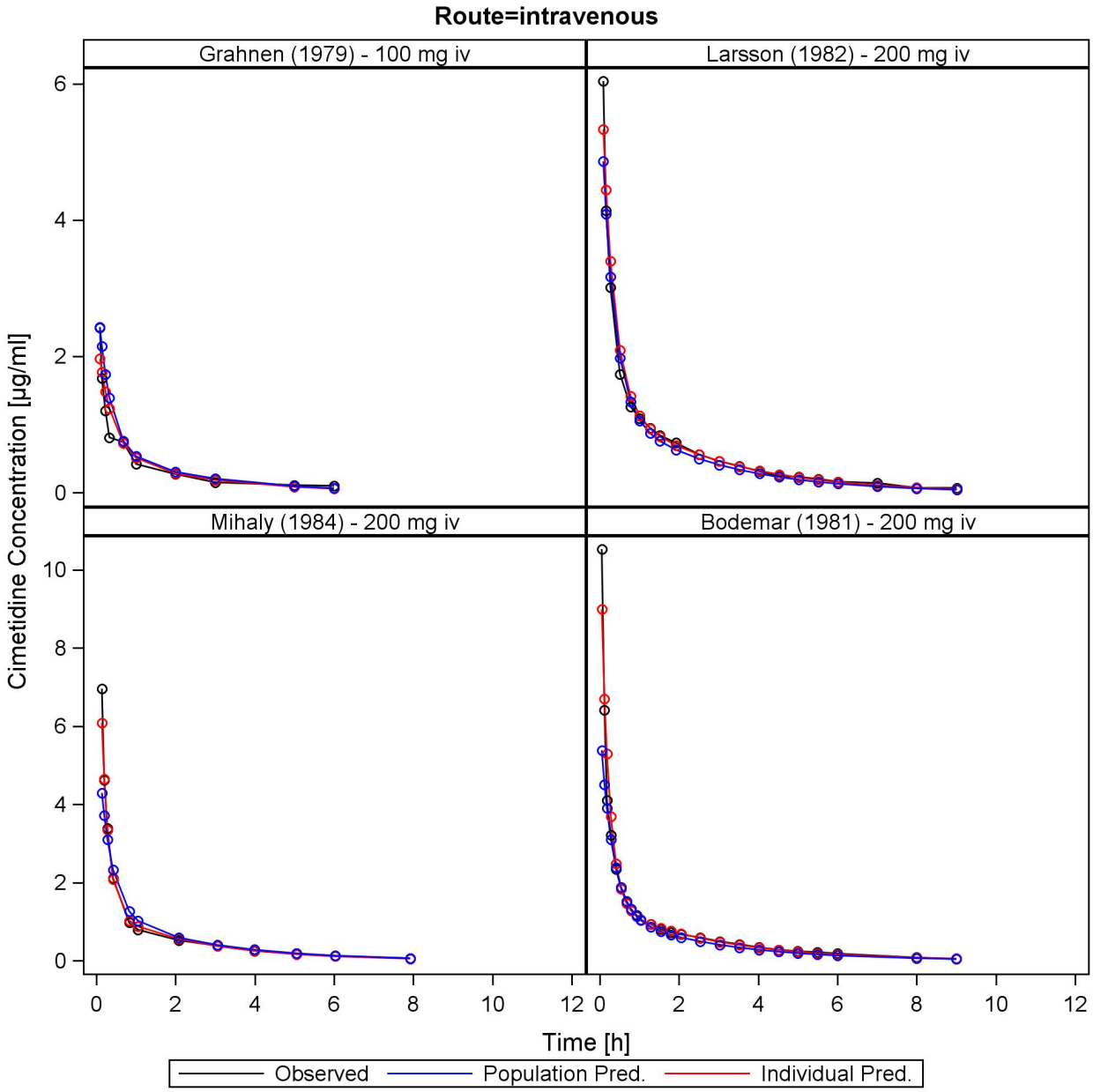

Figure S3.4.10: Concentration-time profiles (observed, population and individual predictions) from the final PopPK model of the studies Grahnen (1979), Larsson (1982), Mihaly (1984) and Bodemar (1981) presented on a linear Y-axis.

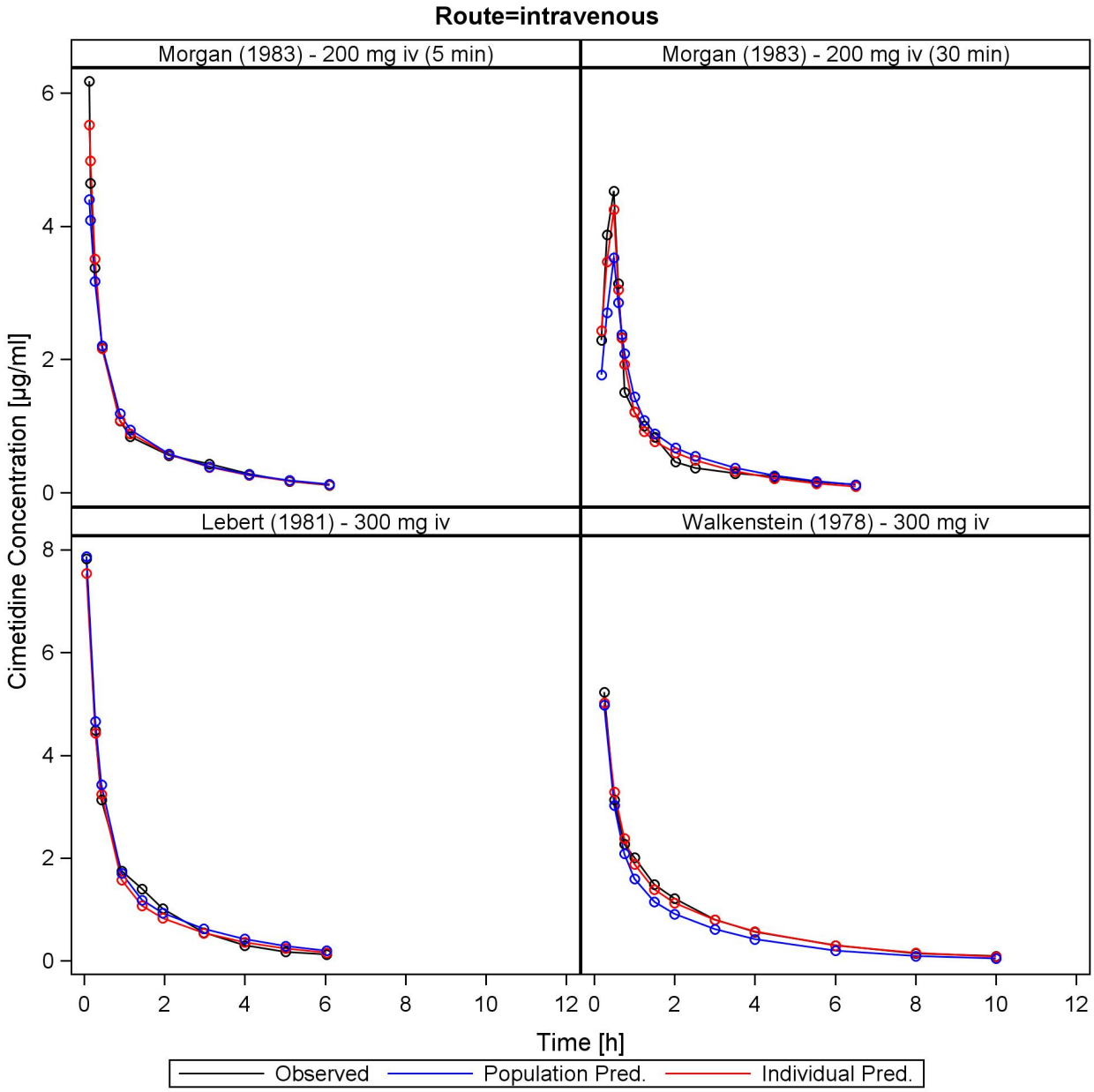

Figure S3.4.11: Concentration-time profiles (observed, population and individual predictions) from the final PopPK model of the studies Morgan (1983), Lebert (1981) and Walkenstein (1978) presented on a linear Y-axis.

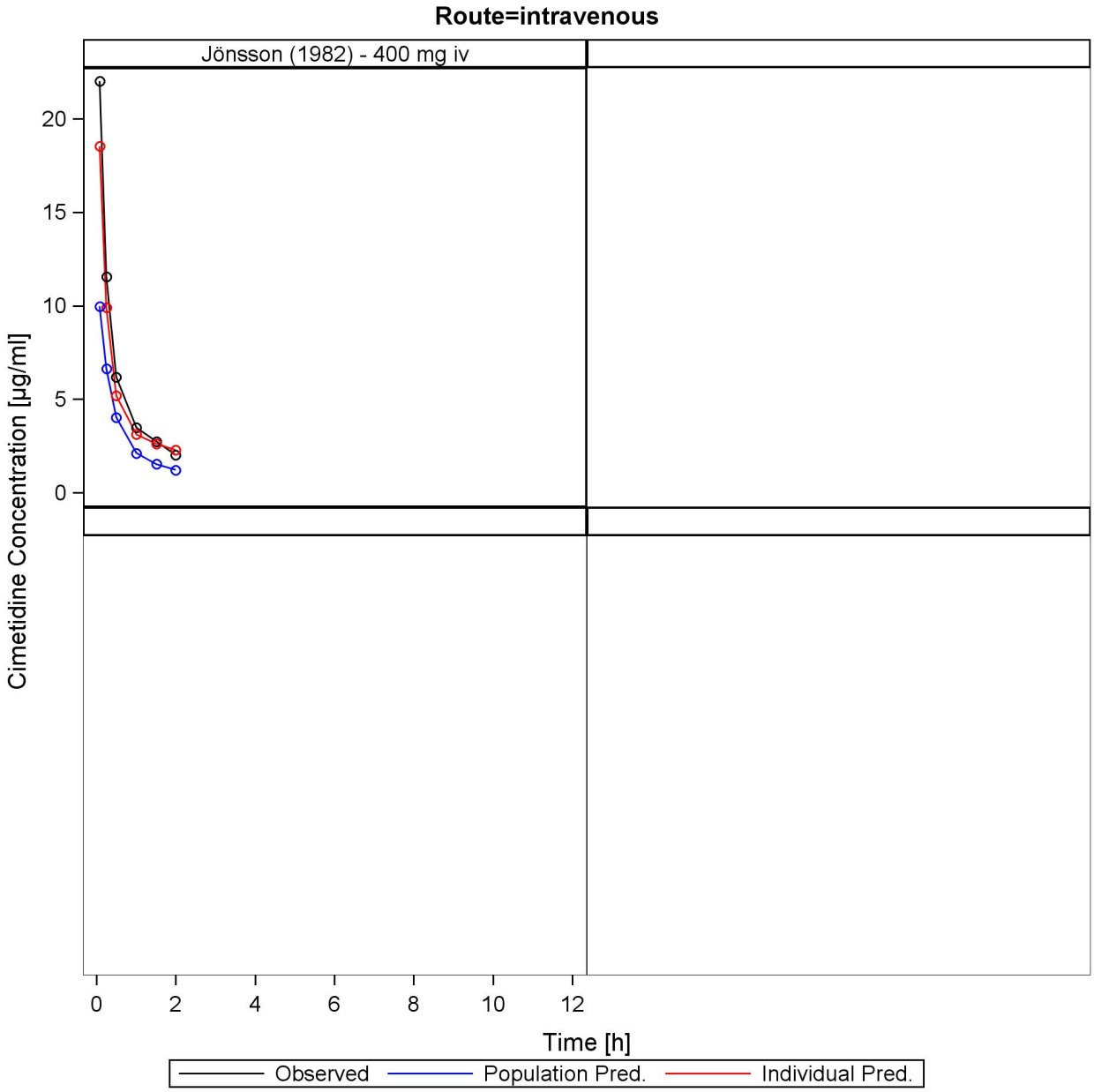

Figure S3.4.12: Concentration-time profiles (observed, population and individual predictions) from the final PopPK model of the study by Jönsson (1982) presented on a linear Y-axis.

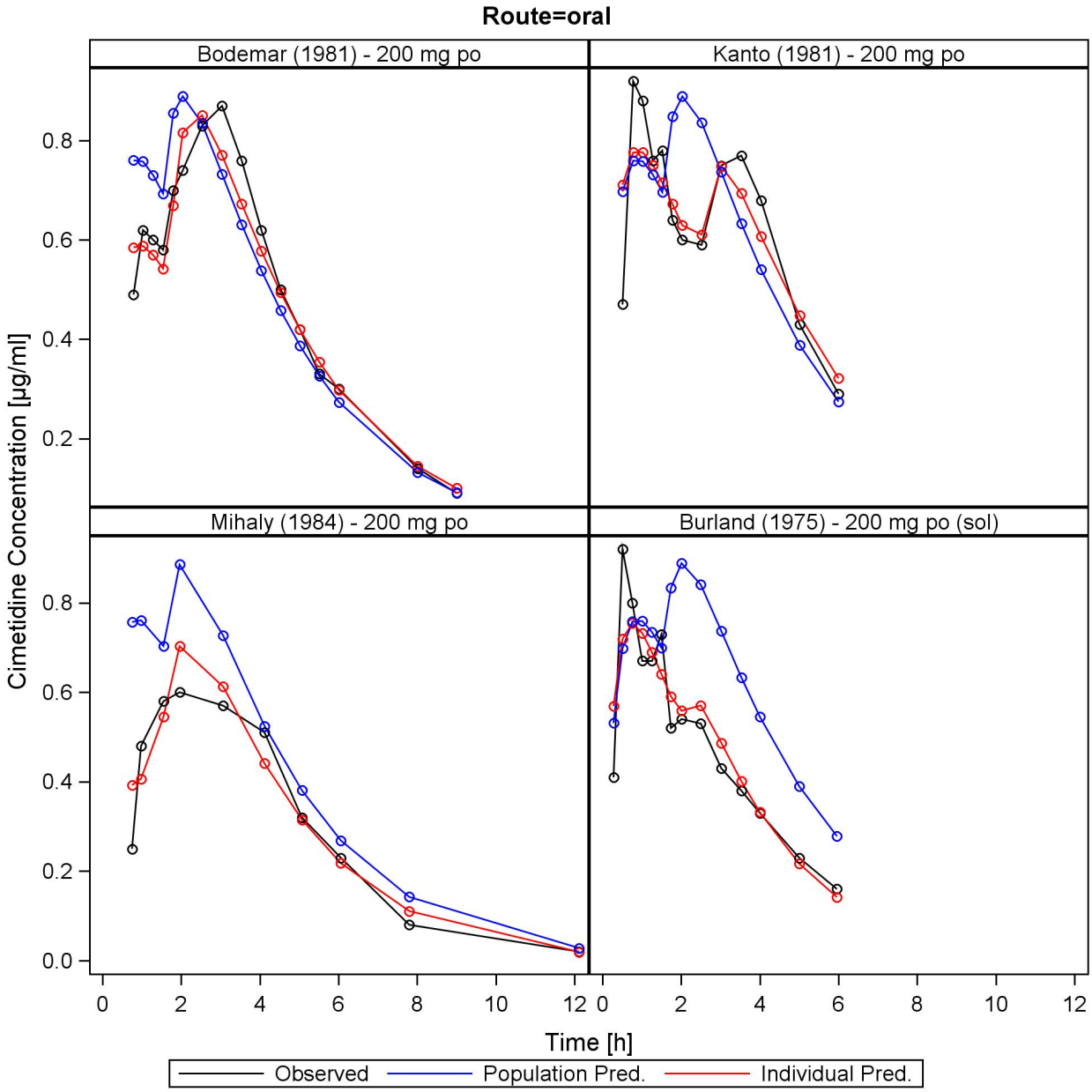

Figure S3.4.13: Concentration-time profiles (observed, population and individual predictions) from the final PopPK model of the studies Bodemar (1981), Kanto (1981), Mihaly (1984) and Burland (1975) presented on a linear Y-axis.

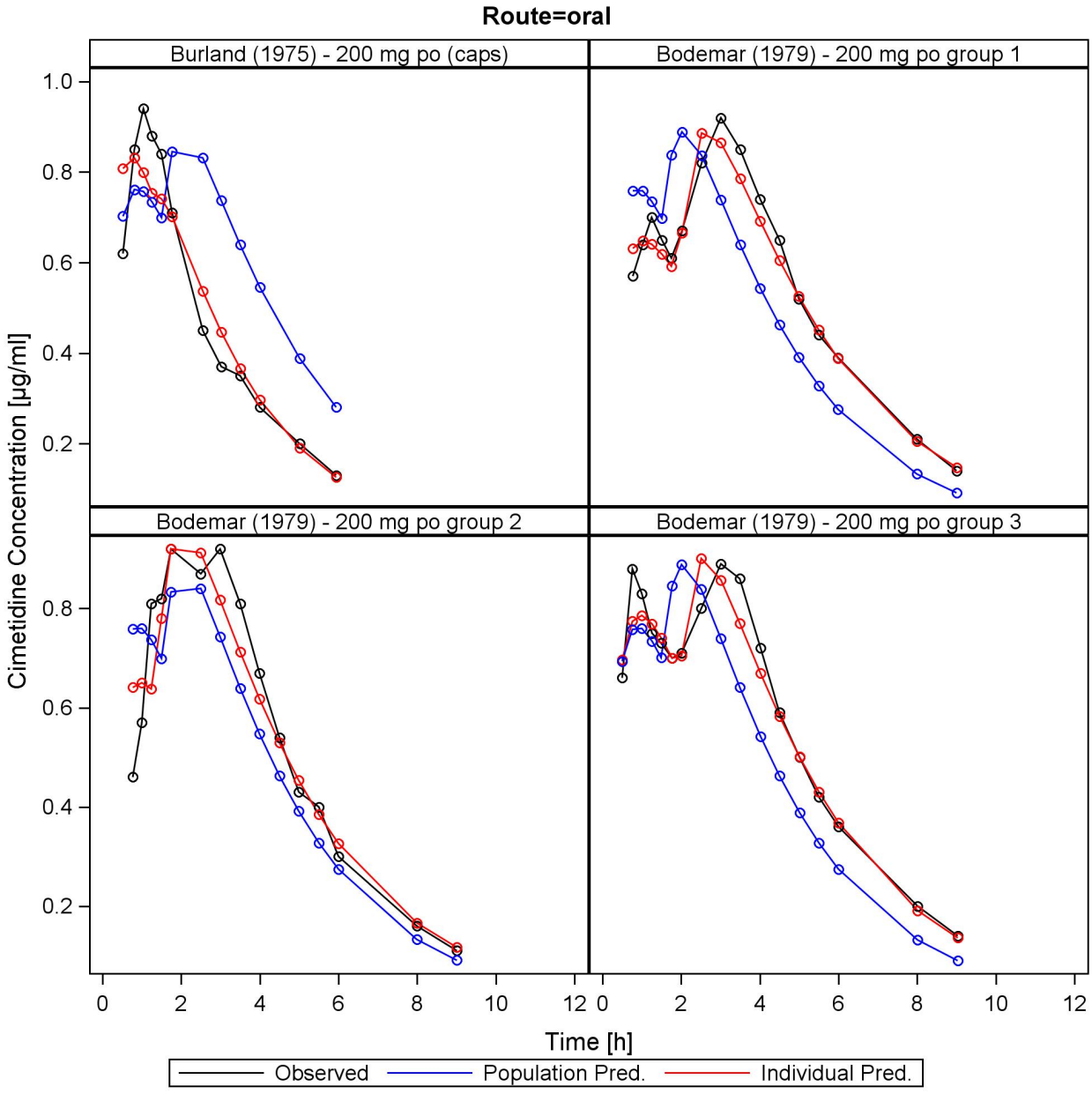

Figure S3.4.14: Concentration-time profiles (observed, population and individual predictions) from the final PopPK model of the studies Burland (1975) and Bodemar (1979) groups 1 to 3 presented on a linear Y-axis.

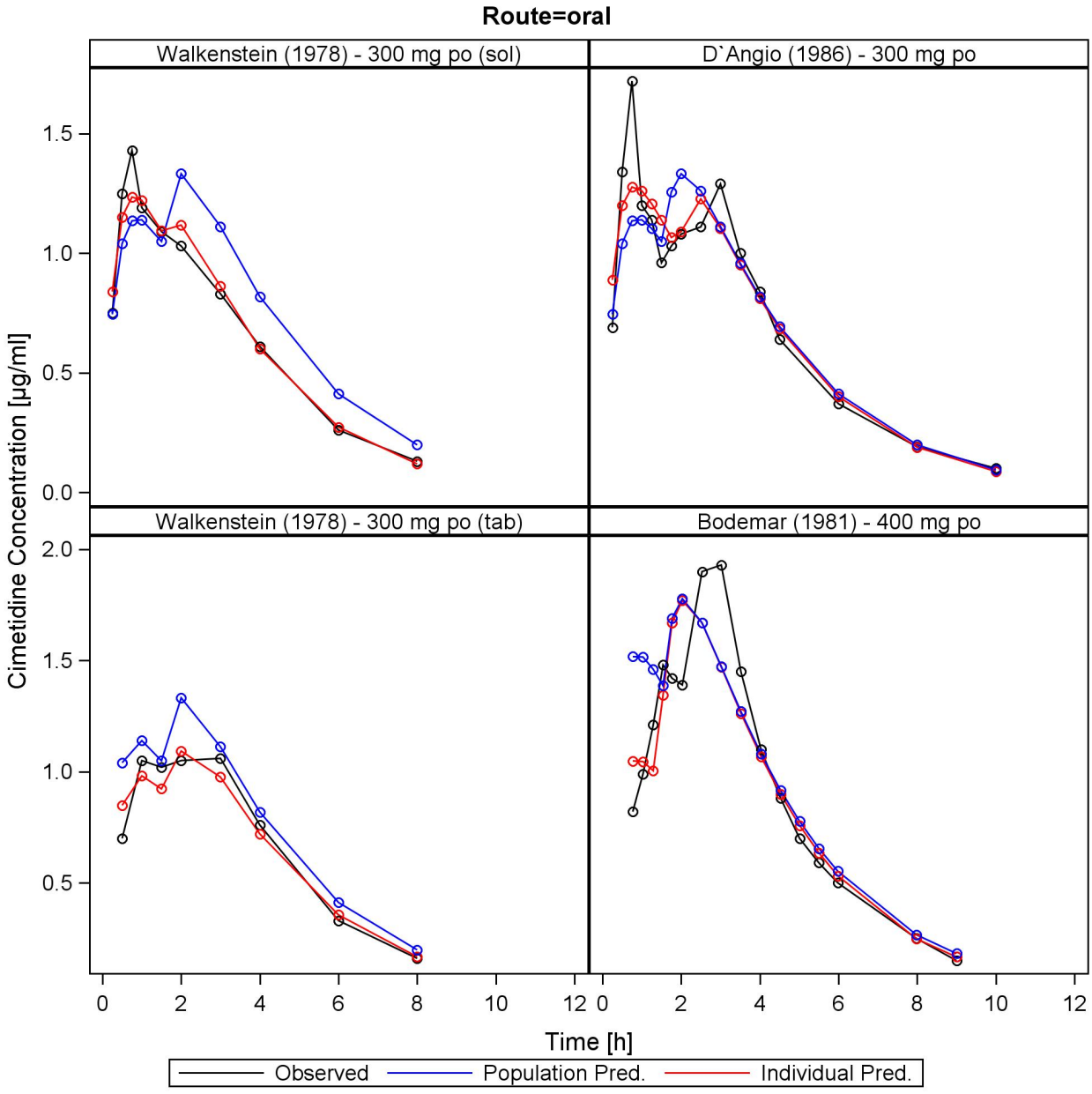

Figure S3.4.15: Concentration-time profiles (observed, population and individual predictions) from the final PopPK model of the studies Walkenstein (1978), D'Angio (1986) and Bodemar (1981) presented on a linear Y-axis.

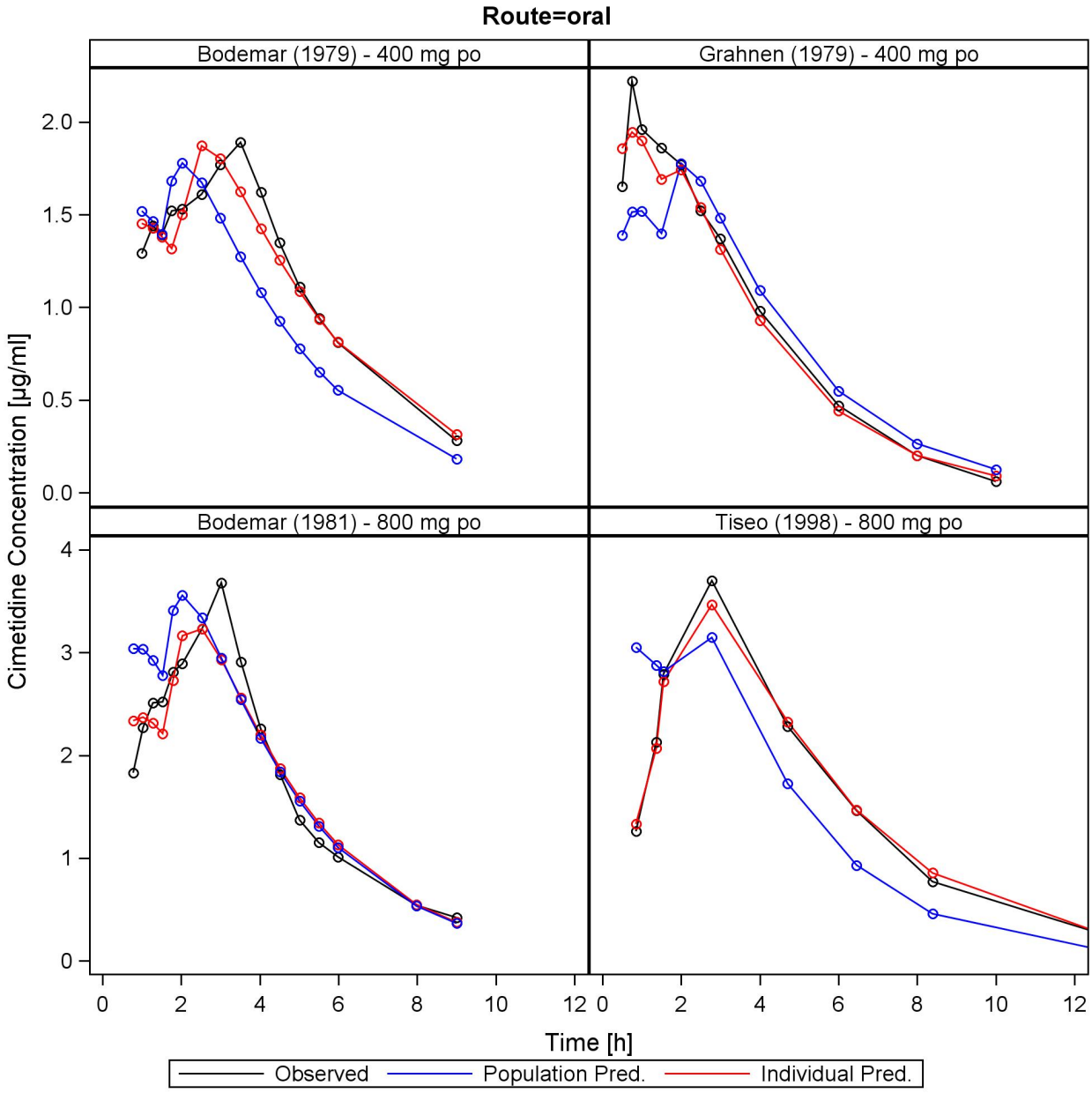

Figure S3.4.16: Concentration-time profiles (observed, population and individual predictions) from the final PopPK model of the studies Bodemar (1979), Grahnen (1979), Bodemar (1981) and Tiseo (1998) presented on a linear Y-axis.

3.5 NONMEM code of the final population pharmacokinetic model

```
$PROBLEM CIMETIDINE

$INPUT ID TIME TAD AMT RATE DOSE DV CMT MDV EVID

$DATA DATASET_CIMETIDINE_V02.csv IGNORE=@
$SUBROUTINES ADVAN6 TOL=6

$MODEL
NCOMPARTMENTS = 4
COMP     = (DEPOT1)
COMP     = (DEPOT2)
COMP     = (CENTRAL, DEFOBS)
COMP     = (PERIPH1)

$PK
KA1      = THETA(1)
ALAG2    = THETA(2) * EXP(ETA(4))
CL       = THETA(3) * EXP(ETA(2))
V3       = THETA(4) * EXP(ETA(3))
Q        = THETA(5)
V4       = THETA(6)
S3       = V3

FTOT     = THETA(7)
VF2      = THETA(8)

PHI_2    = LOG(VF2/(1-VF2))
VF2_2    = EXP(PHI_2 + ETA(1)) / (1+EXP(PHI_2 + ETA(1)))
F2       = VF2_2 * FTOT

VF1      = (1-VF2_2)
F1       = VF1 * FTOT
FTOT     = F1 + F2

$DES
K30      = CL/V3
K34      = Q/V3
K43      = Q/V4

DADT(1) = - KA1*A(1)
DADT(2) = - KA1*A(2)
DADT(3) =   KA1*A(1) + KA1*A(2) - K30*A(3) - K34*A(3) + K43*A(4)
DADT(4) =                                    K34*A(3) - K43*A(4)

$ERROR
IPRED    = F
DEL      = 0
IF(IPRED.EQ.0) DEL = 0.0001
W        = F
IRES     = DV - IPRED
IWRES    = IRES/(W+DEL)
Y        = IPRED + W*EPS(1) + EPS(2)

$THETA
(0, 0.722)     ; KA1
(0, 1.35)      ; ALAG2
(0, 40.7)      ; CL
(0, 30.6)      ; V3
(0, 46.4)      ; Q
(0, 46.1)      ; V4
(0, 0.906)     ; FTOT
(0, 0.248)     ; VF2

$OMEGA
 0.579         ; IIV VF2
 0.042         ; IIV CL
 0.142         ; IIV V3
 0.104         ; IIV ALAG2

$SIGMA
 0.0152        ; Prop RE
 0.000323 FIX  ; Add RE

$EST METHOD=1 INTER MAXEVAL=9999 NOABORT PRINT=1 SIG=3 POSTHOC
$COV
$TABLE ID TIME DV IWRES CWRES NOPRINT ONEHEADER FILE=sdtab0020
```

4 Cimetidine

4.1 PBPK model development

Cimetidine is a histamine H2 receptor antagonist that inhibits gastric acid production. It is mainly used as an antacid for the treatment of gastric and duodenal ulcers, Zollinger-Ellison syndrome and esophageal reflux. Cimetidine is highly water soluble and rapidly absorbed, with an oral bioavailability of 50–70 %. The volume of distribution is approximately 1 l/kg and elimination is rapid with an elimination half-life of about 2 h. Cimetidine is mainly excreted unchanged via the kidneys (40–80 % of the dose) with a high renal clearance of 400 ml/min. Metabolism is reported to account for 25–40 % of of the total elimination of cimetidine, with less than 2 % of the dose excreted unchanged with the bile [56]. Cimetidine inhibits several transporters and CYP enzymes and it is recommended by the FDA as strong inhibitor of OCT2/MATE and as moderate inhibitor of CYP3A4 and CYP2D6 for the use in clinical DDI studies and drug labeling [4].

The cimetidine model was established using 27 clinical studies, covering a dosing range from 100 to 800 mg (Table S4.2.1). The final model applies active uptake of cimetidine into the liver by OCT1, uptake into the kidney by OAT3 and secretion from the kidney into the urine by MATE1, as well as an unspecific hepatic clearance and passive renal glomerular filtration (Table S4.2.1). Details on the distribution of the implemented transporters are listed in the system-dependent parameter table (Table S9.0.1)). Oral administration of cimetidine in the fasted state frequently produces two plasma concentrations peaks. These double peaks are probably caused by the phasic gastrointestinal motility that controls gastric emptying in the fasted state. To describe the very different shapes of the observed mean cimetidine plasma profiles, split dose administration protocols for all studies of cimetidine administered orally in the fasted state were optimized in a NONMEM analysis (see Section 3).The resulting split dose administration protocols (Table S3.4.2) were then implemented and used for the PBPK modeling of the respective cimetidine studies.

To apply the cimetidine PBPK model with the split dose approach for cimetidine studies that are not included in the presented NONMEM analysis, there are two options:

1. If cimetidine concentration-time profiles are available, the NONMEM model can be used (`MAXEVAL=0`) to estimate the study specific Empirical Bayesian Estimates (EBE) for the split dose parameters.

2. If no cimetidine concentration-time profiles are available, the population estimates of the final PopPK model can be applied (see Table S3.4.1).

The good descriptive and predictive performance of the cimetidine model is demonstrated in semilogarithmic (Figures S4.4.1 and S4.4.2) as well as linear plots (Figures S4.4.3 and S4.4.4) of population predicted compared to observed plasma concentration-time profiles of all clinical studies. Predicted compared to observed fraction excreted to urine data are shown, whenever available (Figures S4.4.5 and S4.4.6). In addition, a goodness-of-fit plot comparing all predicted to their corresponding observed plasma concentrations of cimetidine is presented (Figure S4.5.1) and MRD values for each study are given (Table S4.5.1). Furthermore, correlation plots of predicted versus observed AUC and C_{max} values are shown (Figure S4.5.2), together with a summary of the respective PK parameters, including calculated model GMFE values (Table S4.5.2).

Sensitivity analysis of a simulation of 400 mg cimetidine, administered as tablet in the fasted state, reveals that the model predictions are sensitive to the value of fraction unbound (literature value), followed by total hepatic clearance and the MATE1 transport rate constant (both optimized) (see Figure S4.5.3).

4.2 Clinical studies

The clinical studies used for cimetidine PBPK model building and evaluation are summarized in Table S4.2.1.

Table S4.2.1: Cimetidine study table

Dose [mg]	Route	n	Men [%]	Age [years]	Weight [kg]	Height [cm]	BMI [kg/m^2]	Dataset	Reference
100	iv, 5 min	3	-	(22–25)	(54–76)	-	-	test[a]	Grahnen et al. 1979 [43]
200	iv, -	9	67	52 (27–66)	-	-	-	test[b]	Larsson et al. 1982 [44]
200	iv, -	6	83	(20-54)	(59-81)	-	-	test[b]	Mihaly et al. 1984 [45]
200	iv, bolus	10	60	40 (19–71)	72 (58–93)	-	-	training[b]	Bodemar et al. 1981 [46]
200	iv, 5 min	6	-	(20-54)	(59–81)	-	-	training[b]	Morgan et al. 1983 [47]
200	iv, 30 min	4	-	(20-54)	(59–81)	-	-	test[b]	Morgan et al. 1983 [47]
300	iv, 2 min	1	100	(21-35)	(50–90)	-	-	test	Lebert et al. 1981 [48]
300	iv, 2 min	12	-	-	-	-	-	test	Walkenstein et al. 1978 [49]
200	po, -, fast	10	60	40 (19–71)	72 (58–93)	-	-	training[b]	Bodemar et al. 1981 [46]
200	po, -, fast	8	-	21 (20–23)	61 (53–80)	-	-	test[a]	Kanto et al. 1981 [51]
200	po, -, fast	6	83	(20–54)	(59–81)	-	-	test[b]	Mihaly et al. 1984 [45]
200	po, sol, fast	1	100	(21–46)	-	-	-	test[a]	Burland et al. 1975 [52]
200	po, caps, fast	1	100	(21–46)	-	-	-	test[a]	Burland et al. 1975 [52]
200	po, tab, fast	10	70	56 (33–66)	-	-	-	test[b]	Bodemar et al. 1979 [53]
200	po, tab, fast	8	100	50 (25–71)	-	-	-	test[b]	Bodemar et al. 1979 [53]
200	po, tab, fast	10	70	55 (37–67)	-	-	-	training[b]	Bodemar et al. 1979 [53]
200/400, qid	po, -, fast	10	60	45 (29–58)	72 (40–93)	-	-	test	Bodemar et al. 1981 [46]
300	po, sol, fast	24	-	-	-	-	-	training	Walkenstein et al. 1978 [49]
300	po, tab, fast	6	100	(27–42)	-	-	-	training[a]	D'Angio et al. 1986 [54]
300	po, tab, fast	12	-	-	-	-	-	test	Walkenstein et al. 1978 [49]
300, qid	po, tab, fast	18	100	27 (19–40)	76 (60–95)	179 (170–193)	-	test[a]	Barbhaiya et al. 1995 [57]
400	po, -, fast	9	100	46 (26–59)	76 (50-101)	-	-	training[b]	Bodemar et al. 1981 [46]
400	po, tab, fast	10	70	56 (33–66)	-	-	-	test[b]	Bodemar et al. 1979 [53]
400	po, tab, fast	3	-	(22–25)	(54–76)	-	-	test[a]	Grahnen et al. 1979 [43]
400	po, tab, fast	8	50	25 (22–35)	65 (52–95)	-	-	test[a]	Somogyi et al. 1981 [58]
800	po, -, fast	9	100	46 (26–59)	76 (50–101)	-	-	training[b]	Bodemar et al. 1981 [46]
800, qd	po, tab, fast	18	100	29 (19–42)	76 (64–85)	179 (170–190)	-	test[a]	Tiseo et al. 1998 [55]

-: not given, **BMI**: body mass index, **caps**: capsule, **iv**: intravenous, **n**: number of individuals studied, **po**: oral, **qd**: once daily, **qid**: four times daily, **sol**: solution, **tab**: tablet, **test**: test dataset (model evaluation), **training**: training dataset (model development and parameter optimization)

[a] healthy volunteers

[b] peptic ulcer patients

4.3 Drug-dependent parameters

The drug-dependent parameters of the final cimetidine model are summarized in Table S4.3.1 below. The associated system-dependent parameters are listed in Table S9.0.1.

Table S4.3.1: Drug-dependent parameters of the cimetidine PBPK model

Parameter	Value	Unit	Source	Literature	Reference	Description
MW	252.34	g/mol	Literature	252.34	[35]	Molecular weight
pKa1 (base)	6.93	-	Literature	6.93	[59]	First acid dissociation constant
pKa2 (acid)	13.38	-	Literature	13.38	[35]	Second acid dissociation constant
Solubility (pH 6.8)	24.00	g/l	Literature	24.00	[59]	Solubility
logP	1.66	-	Calculated from B/P ratio	0.48	[59]	Lipophilicity
fu	78.00	%	Literature	78.00	[60]	Fraction unbound
B/P ratio	0.98	-	Literature	0.98[a]	[56]	Blood/plasma ratio
OCT1 K_m	2600.00	µmol/l	Literature	2600.00	[61]	OCT1 Michaelis-Menten constant
OCT1 k_{cat}	8.66E+04	1/min	Optimized	-	-	OCT1 transport rate constant
CL_{hep}	0.16	1/min	Optimized	-	[56]	Hepatic metabolic clearance
OAT3 K_m	149.00	µmol/l	Literature	149.00	[62]	OAT3 Michaelis-Menten constant
OAT3 k_{cat}	5.75E+07	1/min	Optimized	-	-	OAT3 transport rate constant
MATE1 K_m	8.00	µmol/l	Literature	8.00	[63]	MATE1 Michaelis-Menten constant
MATE1 k_{cat}	32.37	1/min	Optimized	-	-	MATE1 transport rate constant
GFR fraction	1.00	-	Assumed	-	-	Fraction of filtered drug in the urine
EHC continuous fraction	1.00	-	Assumed	-	-	Fraction of bile continually released
OCT1 K_i	104.00	µmol/l	Literature	104.00	[64]	Conc. for half-maximal inhibition
OCT2 K_i	124.00	µmol/l	Literature	124.00	[64]	Conc. for half-maximal inhibition
MATE1 K_i	3.80	µmol/l	Literature	3.80	[64]	Conc. for half-maximal inhibition
CYP3A4 K_i	268.00	µmol/l	Literature	268.00	[65]	Conc. for half-maximal inhibition
Partition coefficients	Diverse	-	Calculated	R&R	[66, 67]	Cell to plasma partition coefficients
Cellular permeability	5.04E-03	cm/min	Calculated	PK-Sim	[5]	Permeability into the cellular space
Luminal intestinal perm. Tablet fasted[b]	8.72E-07	cm/min	Optimized	1.12E-05	Calculated	Transcellular specific intestinal perm.

conc: concentration, **EHC**: enterohepatic circulation, **GFR**: glomerular filtration rate, **perm**: permeability,

PK-Sim: PK-Sim standard calculation method, **R&R**: Rodgers and Rowland calculation method

[a] in patients

[b] Split dose administration, with the fraction of dose and lag time for the second gastric emptying optimized for each study of oral administration in the fasted state using a NONMEM approach (see Table S3.4.2)

4.4 Profiles

4.4.1 Semilogarithmic plots – Plasma

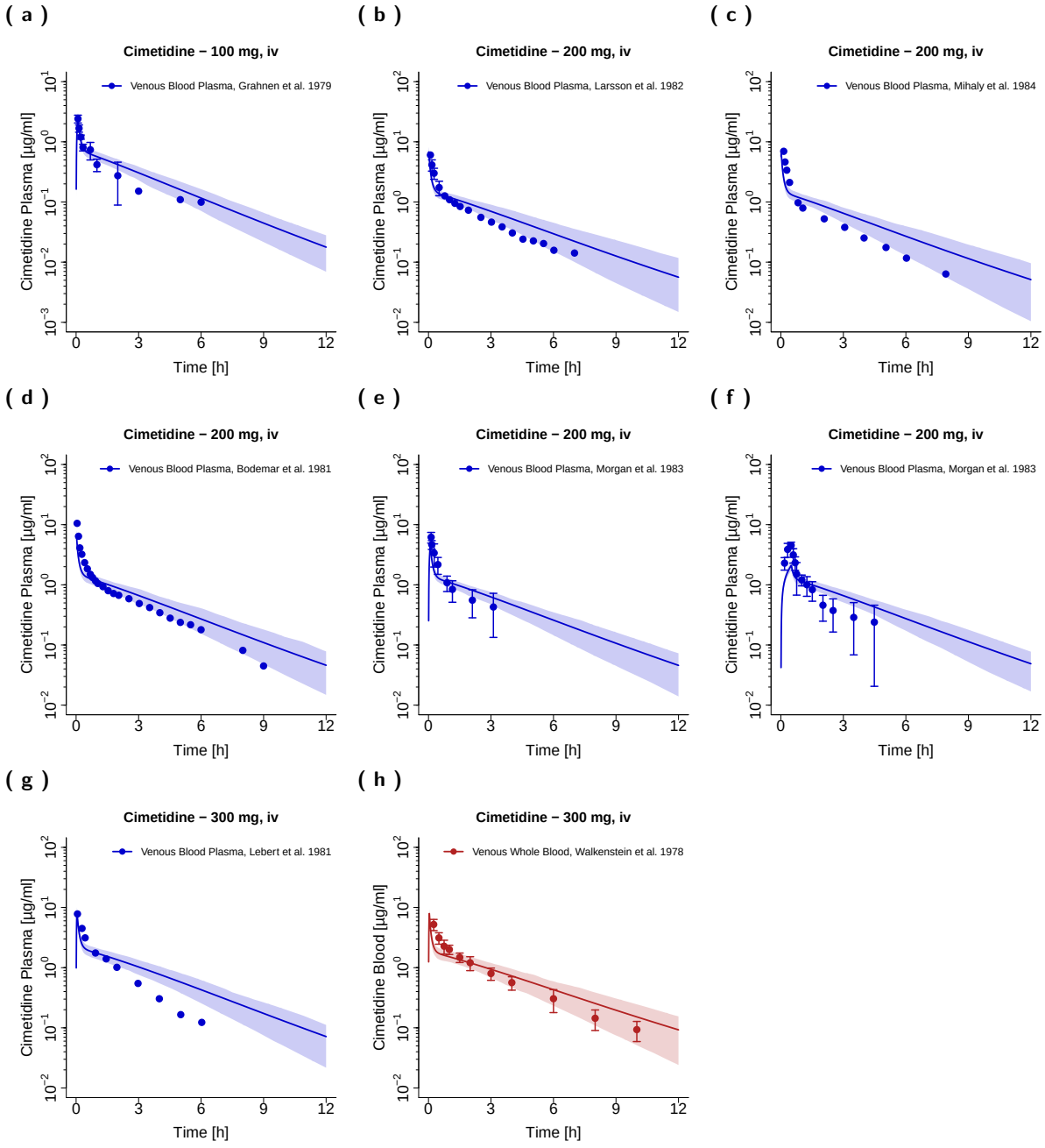

Figure S4.4.1: Cimetidine venous blood plasma (•, –) and venous whole blood (•, –) concentration-time profiles (semilogarithmic) following intravenous administration of cimetidine. Observed data are shown as dots, if available ± standard deviation (SD). Population simulation arithmetic means are shown as lines; the shaded areas represent the predicted population variation (Q_{16} – Q_{84}).

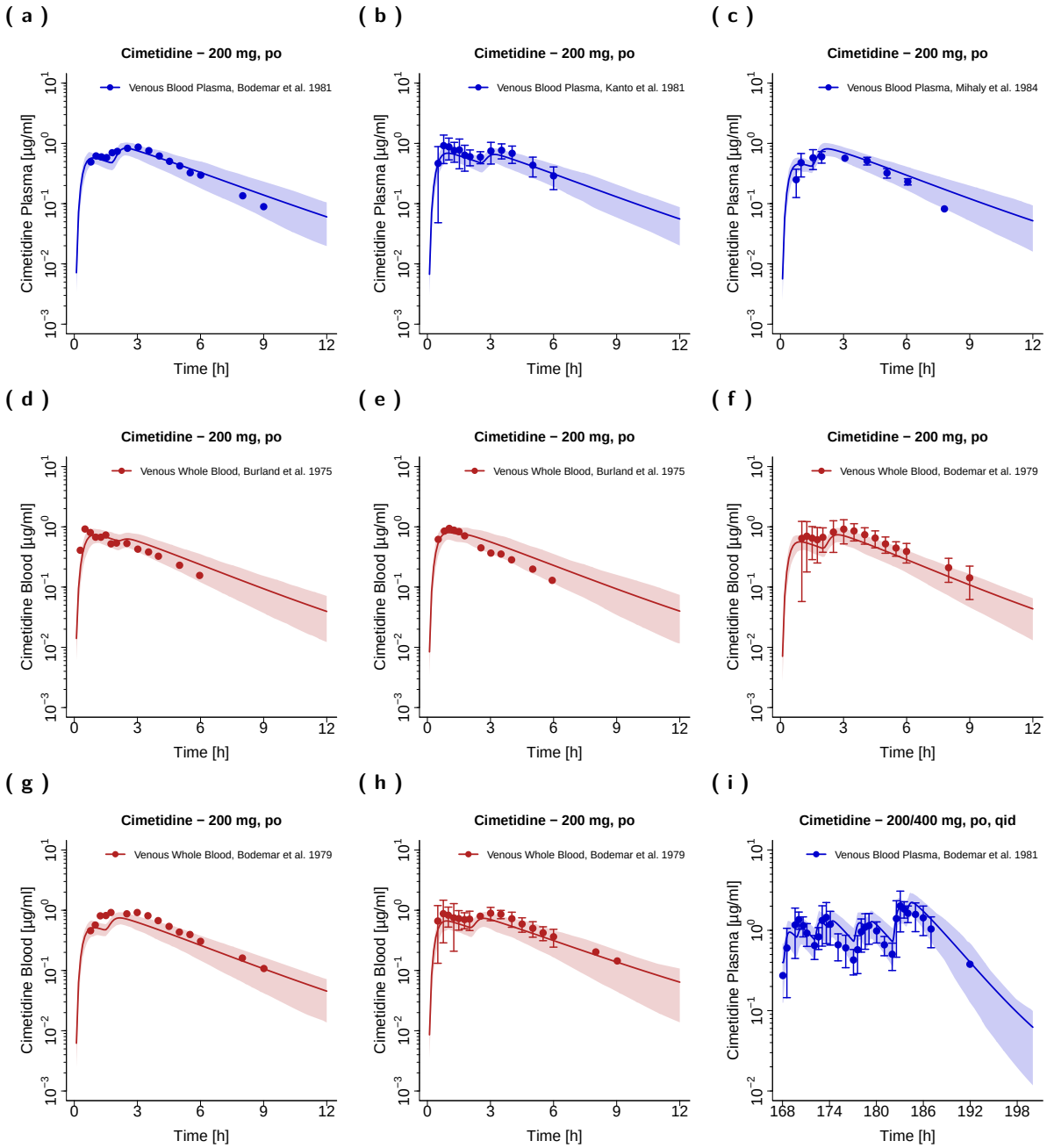

Figure S4.4.2: Cimetidine venous blood plasma (●, –) and venous whole blood (●, –) concentration-time profiles (semilogarithmic) following oral administration of cimetidine. Observed data are shown as dots, if available ± standard deviation (SD). Population simulation arithmetic means are shown as lines; the shaded areas represent the predicted population variation (Q_{16} – Q_{84}).

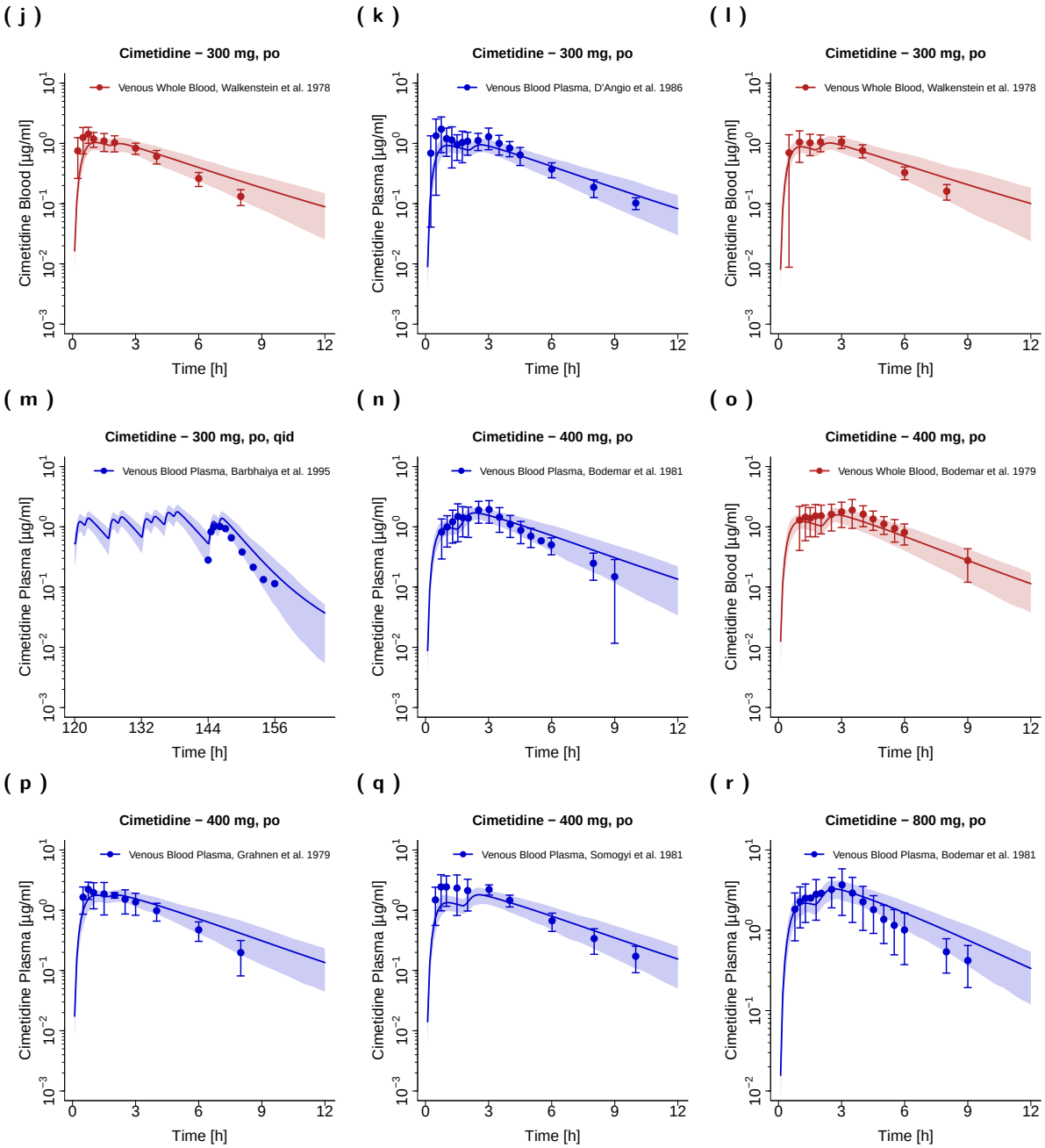

Figure S4.4.2: Cimetidine venous blood plasma (●, –) and venous whole blood (●, –) concentration-time profiles (semilogarithmic) following oral administration of cimetidine. Observed data are shown as dots, if available ± standard deviation (SD). Population simulation arithmetic means are shown as lines; the shaded areas represent the predicted population variation (Q_{16} – Q_{84}). (continued)

(s)

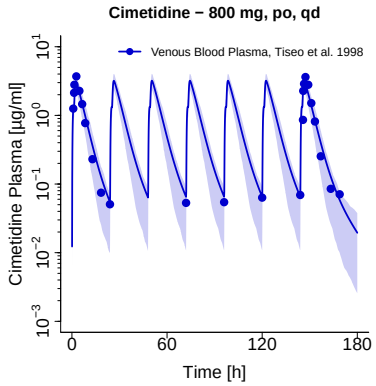

Figure S4.4.2: Cimetidine venous blood plasma (•, –) and venous whole blood (•, –) concentration-time profiles (semilogarithmic) following oral administration of cimetidine. Observed data are shown as dots, if available ± standard deviation (SD). Population simulation arithmetic means are shown as lines; the shaded areas represent the predicted population variation (Q_{16} – Q_{84}). (continued)

4.4.2 Linear plots – Plasma

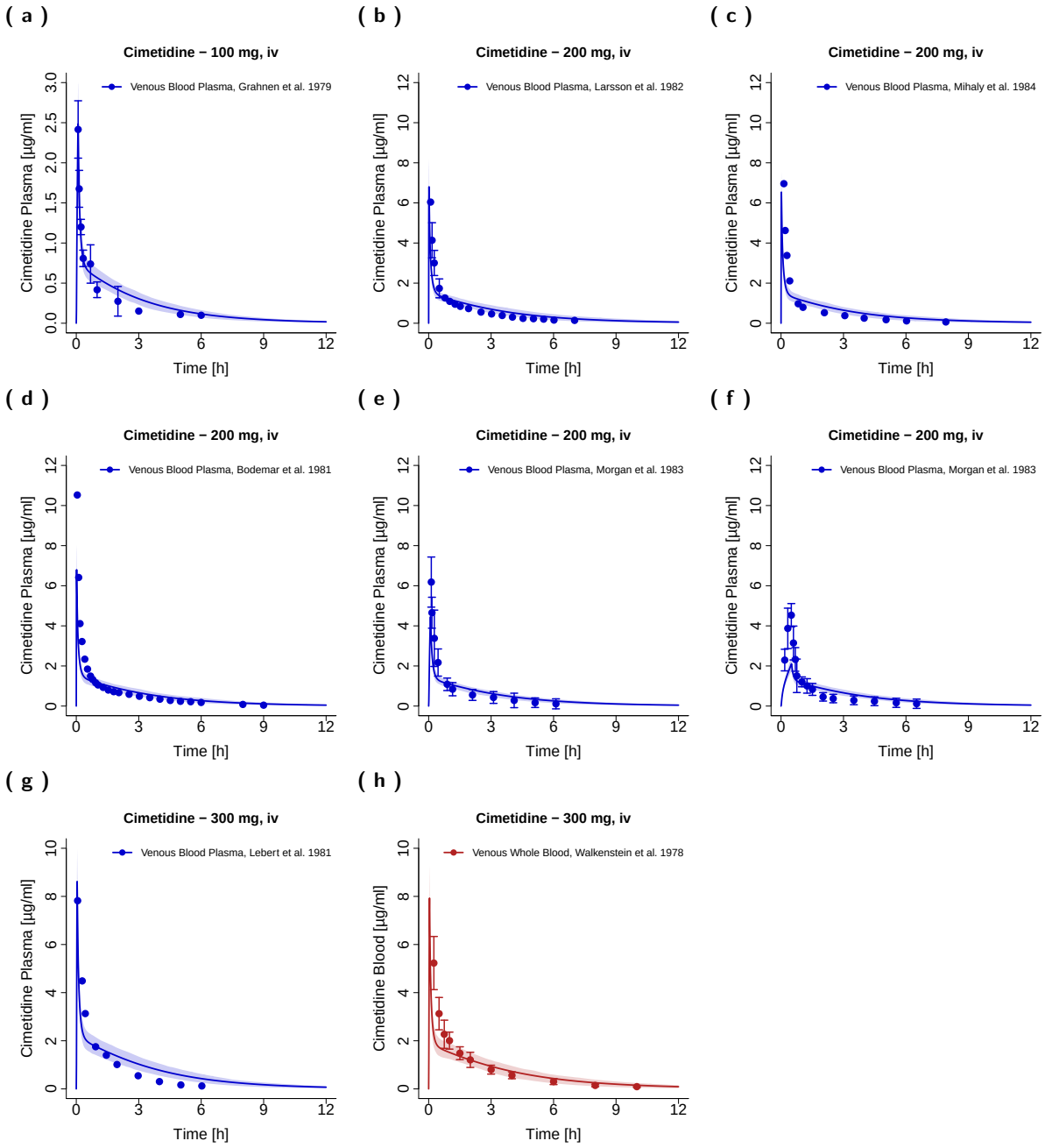

Figure S4.4.3: Cimetidine venous blood plasma (•, –) and venous whole blood (•, –) concentration-time profiles (linear) following intravenous administration of cimetidine. Observed data are shown as dots, if available ± standard deviation (SD). Population simulation arithmetic means are shown as lines; the shaded areas represent the predicted population variation (Q_{16} – Q_{84}).

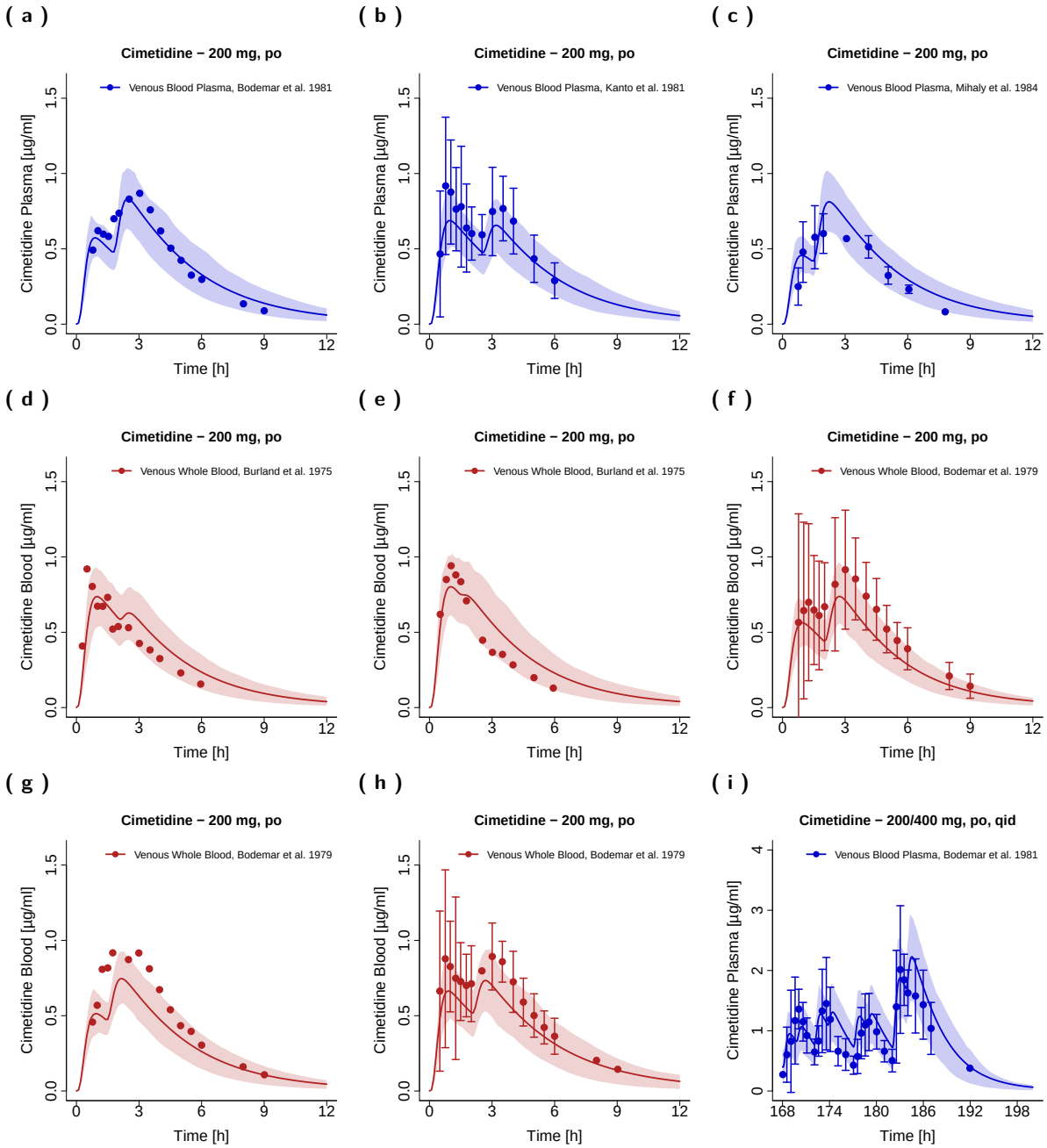

Figure S4.4.4: Cimetidine venous blood plasma (●, –) and venous whole blood (●, –) concentration-time profiles (linear) following oral administration of cimetidine. Observed data are shown as dots, if available ± standard deviation (SD). Population simulation arithmetic means are shown as lines; the shaded areas represent the predicted population variation (Q_{16} – Q_{84}).

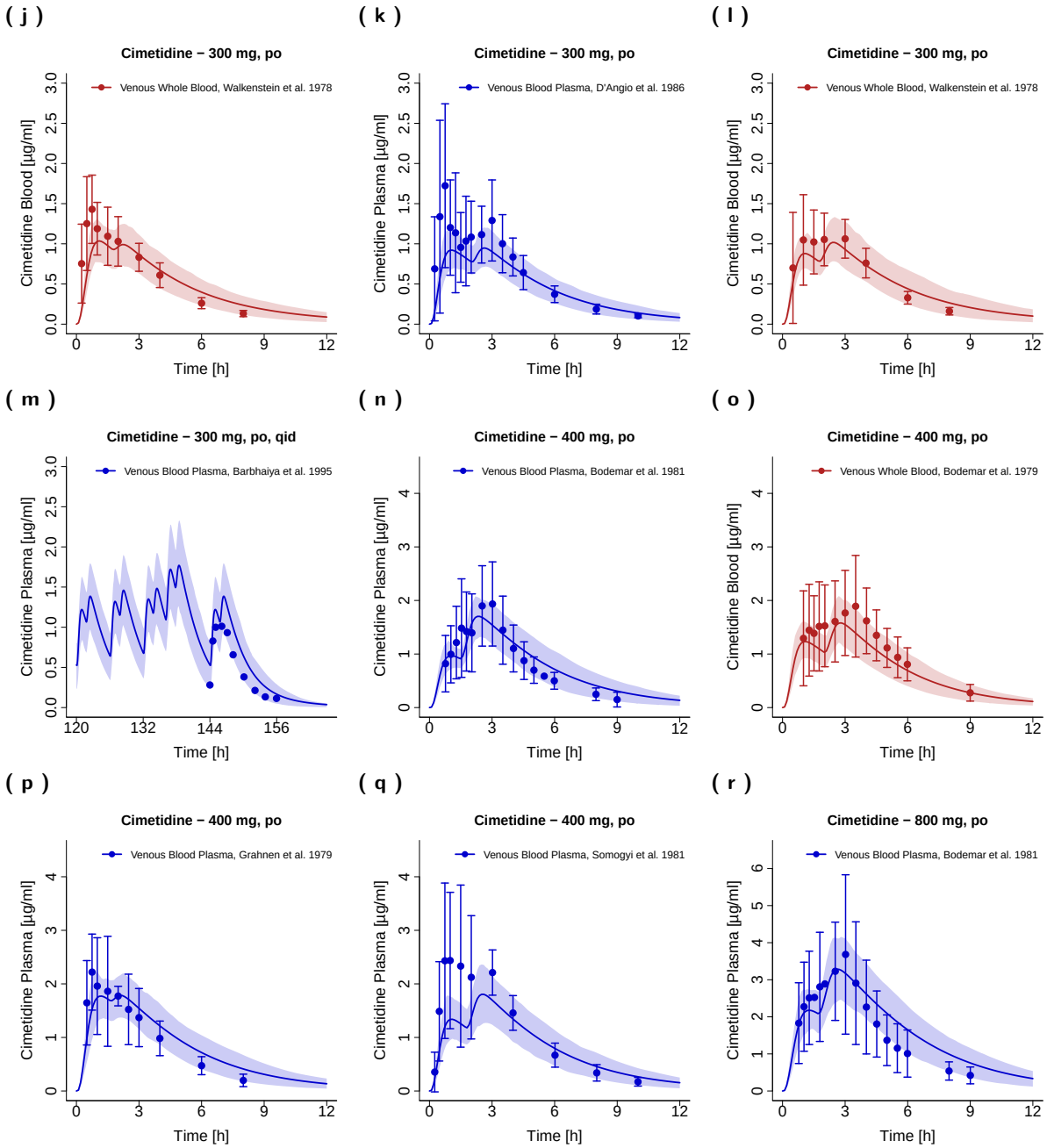

Figure S4.4.4: Cimetidine venous blood plasma (●, –) and venous whole blood (●, –) concentration-time profiles (linear) following oral administration of cimetidine. Observed data are shown as dots, if available ± standard deviation (SD). Population simulation arithmetic means are shown as lines; the shaded areas represent the predicted population variation (Q_{16} – Q_{84}). (continued)

(s)

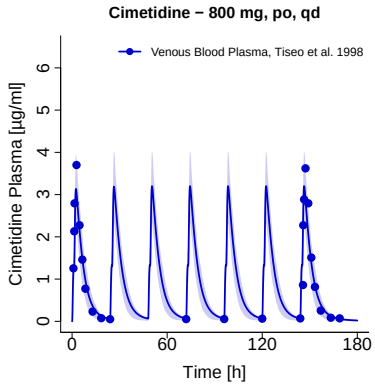

Figure S4.4.4: Cimetidine venous blood plasma (•, –) and venous whole blood (•, –) concentration-time profiles (linear) following oral administration of cimetidine. Observed data are shown as dots, if available ± standard deviation (SD). Population simulation arithmetic means are shown as lines; the shaded areas represent the predicted population variation (Q_{16} – Q_{84}). (continued)

4.4.3 Linear plots - Fraction excreted to urine

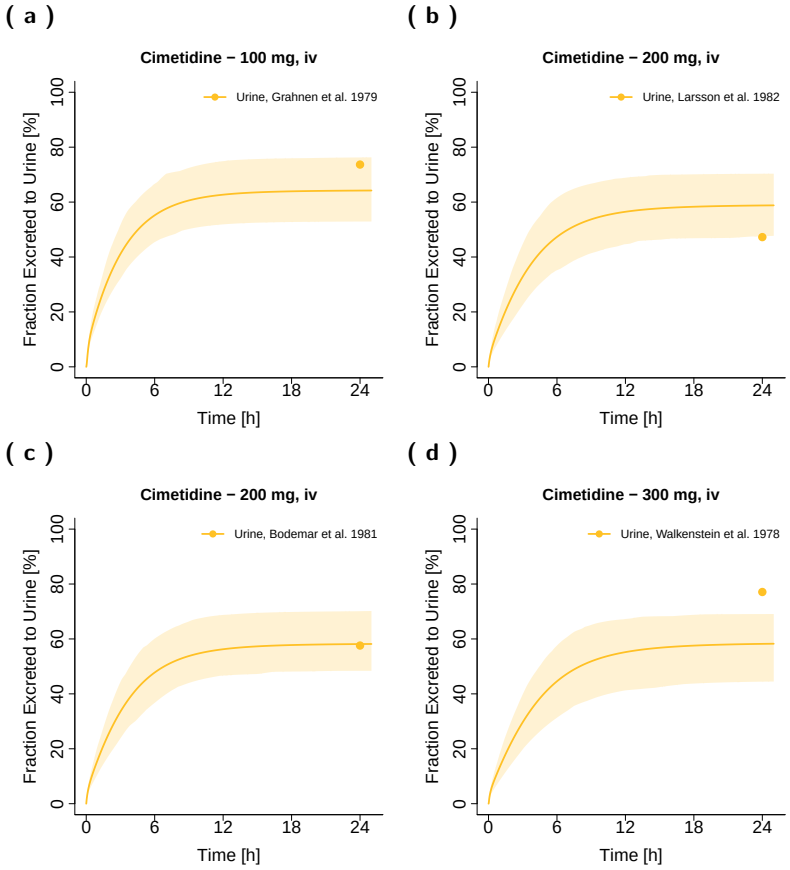

Figure S4.4.5: Cimetidine fraction excreted to urine (•, –) profiles (linear) following intravenous administration of cimetidine. Observed data are shown as dots. Population simulation arithmetic means are shown as lines; the shaded areas represent the predicted population variation (Q_{16} – Q_{84}).

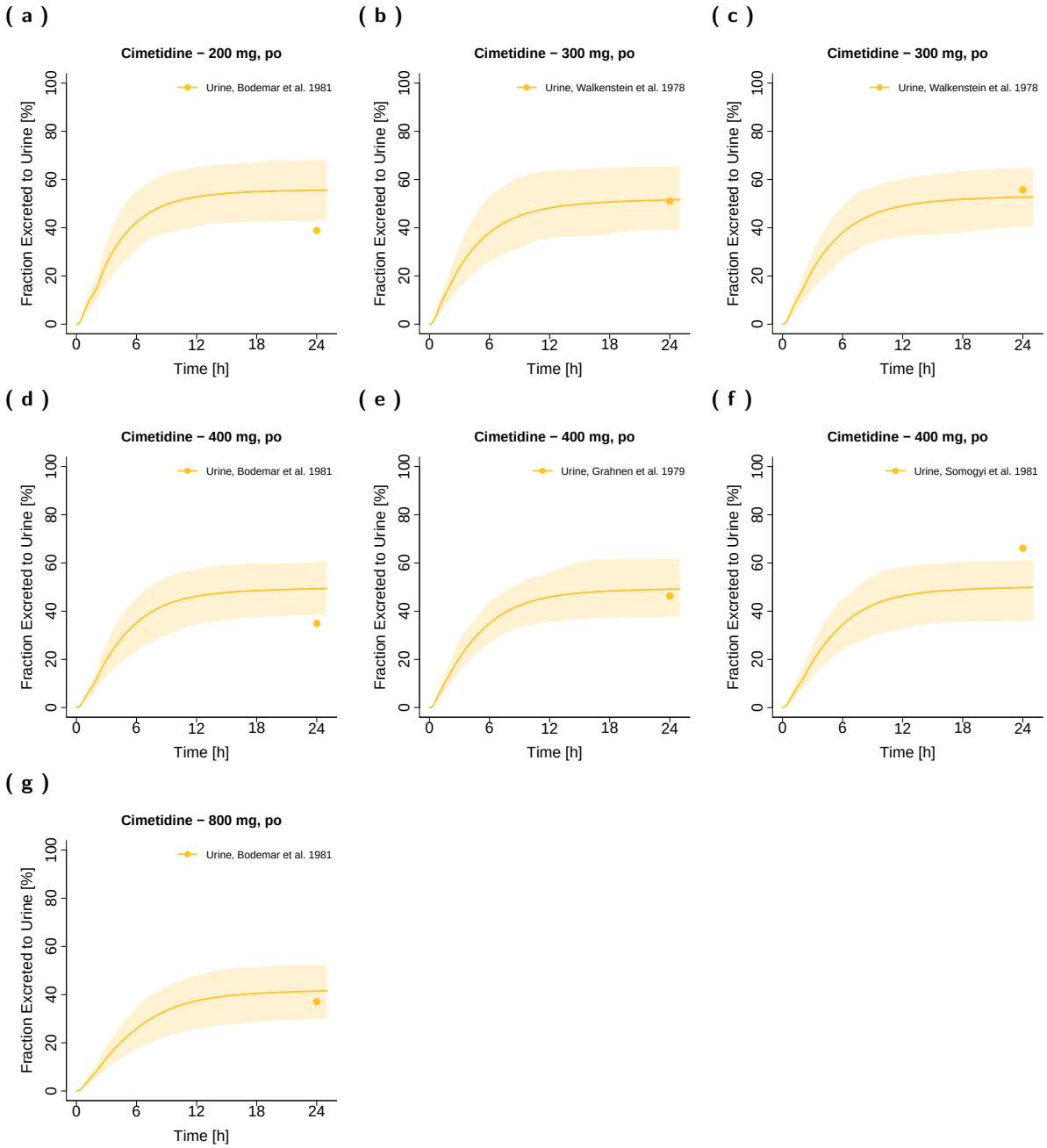

Figure S4.4.6: Cimetidine fraction excreted to urine (●, –) profiles (linear) following oral administration of cimetidine. Observed data are shown as dots. Population simulation arithmetic means are shown as lines; the shaded areas represent the predicted population variation (Q_{16} – Q_{84}).

4.5 Model evaluation

4.5.1 Predicted concentrations versus observed concentrations goodness-of-fit plot

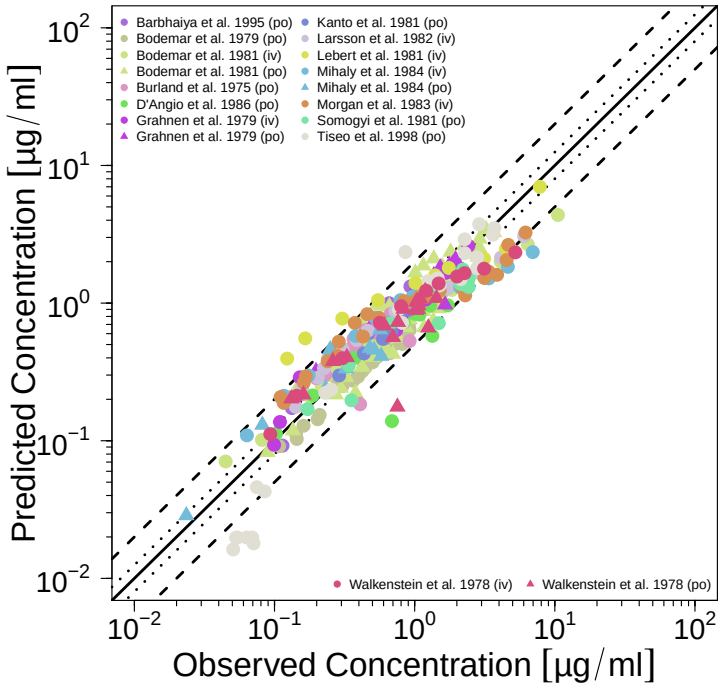

Figure S4.5.1: Predicted versus observed cimetidine concentrations. The black solid line (——) marks the line of identity. Black dotted lines (·····) indicate 1.25-fold, black dashed lines (– –) indicate 2-fold deviation.

4.5.2 Mean relative deviation of plasma concentration predictions

Table S4.5.1: Mean relative deviation (MRD) values of cimetidine plasma concentration predictions

Route	Compartment	Dose	MRD	Reference
Intravenous				
iv, 5 min	Venous Blood Plasma	100 mg	1.32	Grahnen et al. 1979 [43]
iv, bolus	Venous Blood Plasma	200 mg	1.48	Bodemar et al. 1981 [46]
iv, -	Venous Blood Plasma	200 mg	1.85	Mihaly et al. 1984 [45]
iv, -	Venous Blood Plasma	200 mg	1.47	Larsson et al. 1982 [44]
iv, 5 min	Venous Blood Plasma	200 mg	1.62	Morgan et al. 1983 [47]
iv, 30 min	Venous Blood Plasma	200 mg	1.74	Morgan et al. 1983 [47]
iv, 2 min	Venous Whole Blood	300 mg	1.44	Walkenstein et al. 1978 [49]
iv, 2 min	Venous Blood Plasma	300 mg	1.99	Lebert et al. 1981 [48]
MRD			**1.61 (1.32–1.99)**	
			8/8 with MRD ≤ 2	
Oral				
oral, tablet	Venous Blood Plasma	200 mg	1.26	Bodemar et al. 1981 [46]
oral, solution	Venous Whole Blood	200 mg	1.39	Burland et al. 1975 [52]
oral, capsule	Venous Whole Blood	200 mg	1.31	Burland et al. 1975 [52]
oral, tablet	Venous Blood Plasma	200 mg	1.10	Kanto et al. 1981 [51]
oral, tablet	Venous Blood Plasma	200 mg	1.33	Mihaly et al. 1984 [45]
oral, tablet	Venous Whole Blood	200 mg	1.31	Bodemar et al. 1979 [53]
oral, tablet	Venous Whole Blood	200 mg	1.34	Bodemar et al. 1979 [53]
oral, tablet	Venous Whole Blood	200 mg	1.34	Bodemar et al. 1979 [53]
oral, tablet	Venous Whole Blood	300 mg	1.72	Walkenstein et al. 1978 [49]
oral, solution	Venous Whole Blood	300 mg	1.19	Walkenstein et al. 1978 [49]
oral, tablet	Venous Blood Plasma	300 mg	1.64	D'Angio et al. 1986 [54]
oral, tablet	Venous Blood Plasma	300 mg (qid)	1.45	Barbhaiya et al. 1995 [57]
oral, tablet	Venous Blood Plasma	400 mg	1.29	Bodemar et al. 1981 [46]
oral, tablet	Venous Whole Blood	400 mg	1.22	Bodemar et al. 1979 [53]
oral, tablet	Venous Blood Plasma	400 mg	1.32	Grahnen et al. 1979 [43]
oral, tablet	Venous Blood Plasma	400 mg	1.54	Somogyi et al. 1981 [58]
oral, tablet	Venous Blood Plasma	200/400 mg (qid)	1.30	Bodemar et al. 1981 [46]
oral, tablet	Venous Blood Plasma	800 mg	1.36	Bodemar et al. 1981 [46]
oral, tablet	Venous Blood Plasma	800 mg (qd)	1.93	Tiseo et al. 1998 [55]
MRD			**1.43 (1.10–1.93)**	
			19/19 with MRD ≤ 2	
Overall MRD			**1.48 (1.10–1.99)**	
			27/27 with MRD ≤ 2	

iv: intravenous, **MRD**: mean relative deviation, **qd**: once daily, **qid**: four times daily

4.5.3 AUC and C_{max} goodness-of-fit plots

(a) AUC

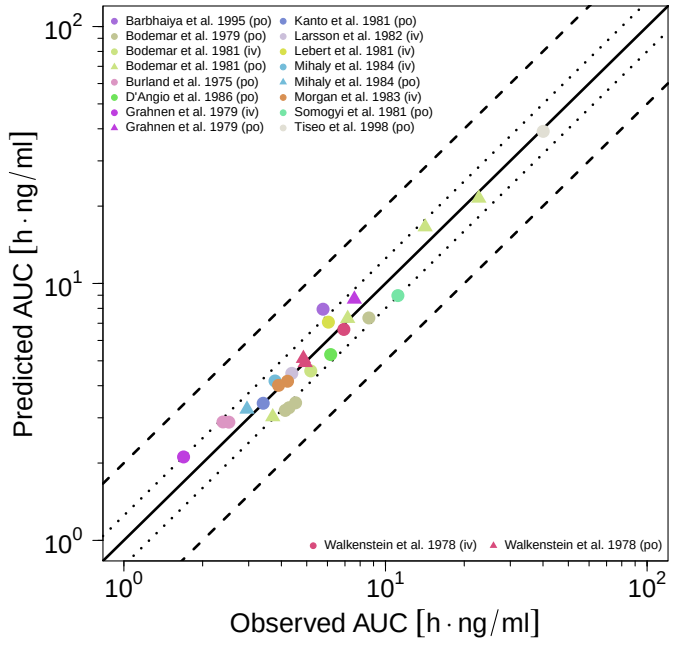

(b) C_{max}

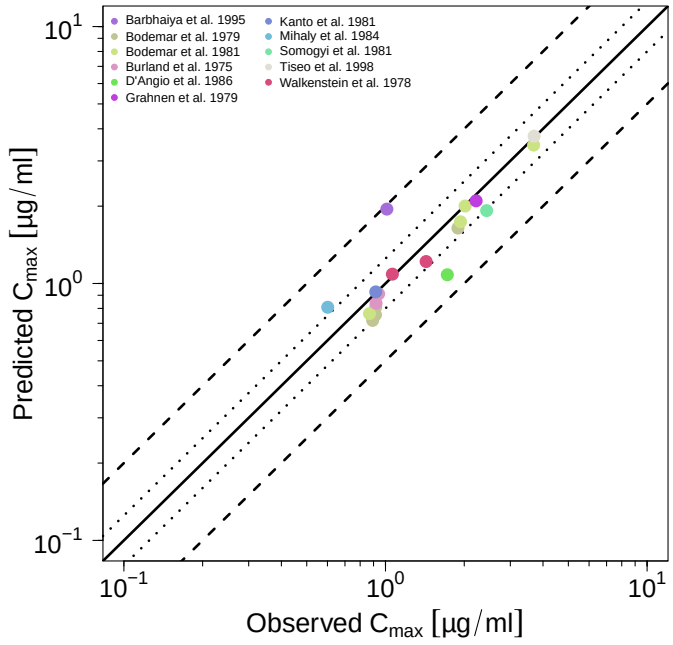

Figure S4.5.2: Predicted versus observed cimetidine AUC and C_{max} values. Each symbol represents the AUC or C_{max} of a different profile. The black solid line (——) marks the line of identity. Black dotted lines (·····) indicate 1.25-fold, black dashed lines (– –) indicate 2-fold deviation. **AUC**: area under the plasma concentration–time curve from the time of administration to the last data point, **C_{max}**: maximum plasma concentration

4.5.4 Geometric mean fold error of predicted AUC and C_{max} values

Table S4.5.2: Predicted and observed AUC and C_{max} values of cimetidine plasma concentrations

			AUC			C_{max}			
Route	Compartment	Dose	Pred [h·ng/ml]	Obs [h·ng/ml]	Pred/Obs	Pred [ng/ml]	Obs [ng/ml]	Pred/Obs	Reference
Intravenous									
iv, 5 min	Venous Blood Plasma	100 mg	2112.83	1691.08	1.25	-	-	-	Grahnen et al. 1979 [43]
iv, bolus	Venous Blood Plasma	200 mg	4567.49	5179.28	0.88	-	-	-	Bodemar et al. 1981 [46]
iv, -	Venous Blood Plasma	200 mg	4173.54	3781.58	1.10	-	-	-	Mihaly et al. 1984 [45]
iv, -	Venous Blood Plasma	200 mg	4468.99	4383.99	1.02	-	-	-	Larsson et al. 1982 [44]
iv, 5 min	Venous Blood Plasma	200 mg	4013.46	3902.27	1.03	-	-	-	Morgan et al. 1983 [47]
iv, 30 min	Venous Blood Plasma	200 mg	4163.49	4222.39	0.99	-	-	-	Morgan et al. 1983 [47]
iv, 2 min	Venous Whole Blood	300 mg	6624.29	6931.55	0.96	-	-	-	Walkenstein et al. 1978 [49]
iv, 2 min	Venous Blood Plasma	300 mg	7071.07	6049.42	1.17	-	-	-	Lebert et al. 1981 [48]
GMFE					**1.09 (1.01–1.25)**				
					8/8 with GMFE ≤ 2				
Oral									
oral, tablet	Venous Blood Plasma	200 mg	3026.33	3706.71	0.82	763.51	868.72	0.88	Bodemar et al. 1981 [46]
oral, solution	Venous Whole Blood	200 mg	2885.75	2518.87	1.15	837.85	920.18	0.91	Burland et al. 1975 [52]
oral, capsule	Venous Whole Blood	200 mg	2890.83	2392.58	1.21	911.24	941.39	0.97	Burland et al. 1975 [52]
oral, tablet	Venous Blood Plasma	200 mg	3418.44	3408.48	1.00	927.80	918.16	1.01	Kanto et al. 1981 [51]
oral, tablet	Venous Blood Plasma	200 mg	3239.75	2954.89	1.10	808.39	601.30	1.34	Mihaly et al. 1984 [45]
oral, tablet	Venous Whole Blood	200 mg	3284.10	4277.96	0.77	755.12	915.56	0.82	Bodemar et al. 1979 [53]
oral, tablet	Venous Whole Blood	200 mg	3205.96	4138.27	0.77	808.73	917.28	0.88	Bodemar et al. 1979 [53]
oral, tablet	Venous Whole Blood	200 mg	3431.94	4532.75	0.76	718.64	893.04	0.80	Bodemar et al. 1979 [53]
oral, tablet	Venous Whole Blood	300 mg	5105.12	4855.28	1.05	1217.67	1430.00	0.85	Walkenstein et al. 1978 [49]
oral, solution	Venous Whole Blood	300 mg	4919.28	4933.56	1.00	1087.48	1062.50	1.02	Walkenstein et al. 1978 [49]
oral, tablet	Venous Blood Plasma	300 mg	5288.20	6172.41	0.86	1081.49	1723.10	0.63	D'Angio et al. 1986 [54]
oral, tablet	Venous Blood Plasma	300 mg (qid)	7940.90	5770.98	1.38	1947.99	1012.06	1.92	Barbhaiya et al. 1995 [57]
oral, tablet	Venous Blood Plasma	400 mg	7306.11	7169.56	1.02	1739.37	1934.73	0.90	Bodemar et al. 1981 [46]
oral, tablet	Venous Whole Blood	400 mg	7343.54	8638.58	0.85	1643.51	1892.10	0.87	Bodemar et al. 1979 [53]
oral, tablet	Venous Blood Plasma	400 mg	8682.76	7603.51	1.14	2098.24	2220.10	0.95	Grahnen et al. 1979 [43]
oral, tablet	Venous Blood Plasma	400 mg	8971.83	11153.93	0.80	1921.68	2436.32	0.79	Somogyi et al. 1981 [58]
oral, tablet	Venous Blood Plasma	200/400 mg (qid)	21470.00	22736.61	0.94	2002.91	2015.41	0.99	Bodemar et al. 1981 [46]
oral, tablet	Venous Blood Plasma	800 mg	16600.10	14177.73	1.17	3458.87	3682.78	0.94	Bodemar et al. 1981 [46]
oral, tablet	Venous Blood Plasma	800 mg (qd)	39092.10	40070.83	0.98	3745.40	3700.33	1.01	Tiseo et al. 1998 [55]
GMFE					**1.15 (1.00–1.38)**			**1.17 (1.01–1.92)**	
					19/19 with GMFE ≤ 2			**19/19 with GMFE ≤ 2**	
Overall GMFE					**1.14 (1.00–1.38)**			**1.17 (1.01–1.92)**	
					27/27 with GMFE ≤ 2			**19/19 with GMFE ≤ 2**	

-: not calculated, **GMFE**: geometric mean fold error, **iv**: intravenous, **obs**: observed, **pred**: predicted, **qd**: once daily, **qid**: four times daily

4.5.5 Sensitivity analysis

Sensitivity of the final cimetidine model to single parameters (local sensitivity analysis) was calculated, measured as the relative change of the $AUC_{0\text{-}24}$ of a 400 mg single dose of cimetidine administered as tablet in the fasted state. Sensitivity analysis was carried out using a relative parameter perturbation of 1000 % (variation range 10.0, maximum number of 9 steps). Parameters were included into the analysis if they were optimized (OCT1 k_{cat}, OAT3 k_{cat}, MATE1 k_{cat}, total hepatic clearance, luminal intestinal permeability), if they are associated with optimized parameters (OCT1 K_m, OAT3 K_m, MATE1 K_m) or if they might have a strong impact due to calculation methods used in the model (solubility, lipophilicity, fraction unbound in plasma, blood/plasma concentration ratio, GFR fraction).

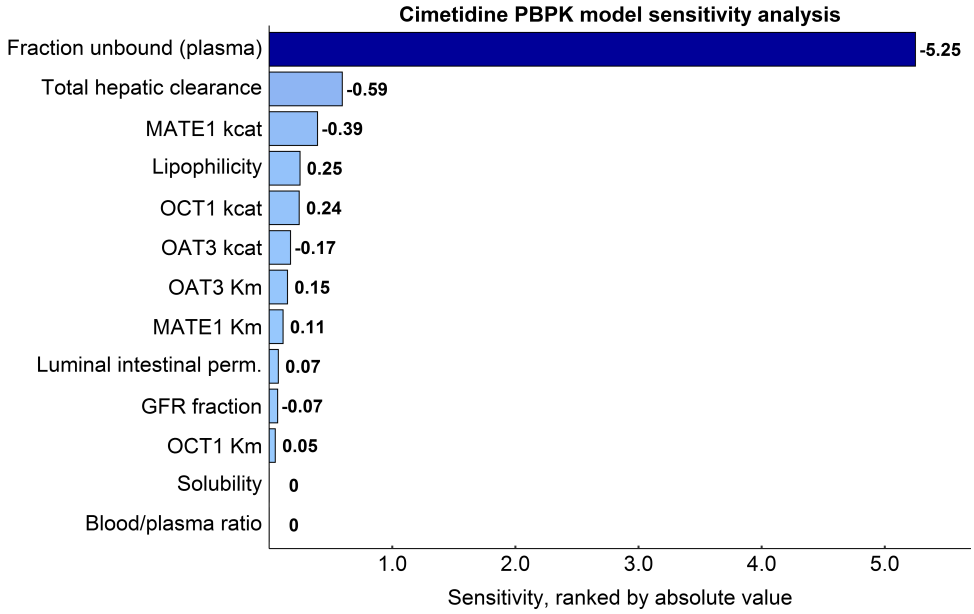

Figure S4.5.3: Cimetidine PBPK model sensitivity analysis. Sensitivity of the model to single parameters, measured as change of the simulated $AUC_{0\text{-}24}$ of a 400 mg single oral dose. **GFR**: glomerular filtration rate, **kcat**: transport rate constant (turnover number), **Km**: Michaelis-Menten constant, **perm**: permeability

5 Metformin drug-gene interaction (DGI)

5.1 PBPK model development

The most common polymorphism in the gene encoding for OCT2 is the *SLC22A2* 808G>T single-nucleotide polymorphism (SNP) [68], which results in an amino acid exchange from alanine to serine (A270S) and presumably increased function, leading to decreased metformin plasma exposure with ≈13-20 % decreased C_{max} [13, 27, 69]. The impact of the *SLC22A2* 808G>T SNP on metformin exposure was modeled using the same Michaelis-Menten constant for both isoforms [27, 68, 70], according to in vitro reports. The transport rate constant to describe the increased activity of the variant 808T OCT2 (2.67-fold higher turnover, see Table S2.3.1) was optimized based on the metformin plasma profile of the homozygous 808TT population studied by Christensen et al. [69] and Wang et al. [13]. The metformin plasma concentrations of all other 808TT and 808GT study populations were predicted.

Details on the modeled clinical studies investigating the metformin-*SLC22A2* 808G>T DGI are given in Table S5.2.1. Population predictions of metformin plasma concentration-time profiles and fraction excreted to urine in study populations expressing the variant OCT2, compared to observed data, are shown in Figures S5.3.1 to S5.3.3. The correlation of predicted to observed DGI AUC ratios and DGI C_{max} ratios is shown in Figure S5.4.1. Table S5.4.1 lists the corresponding predicted and observed DGI AUC ratios, DGI C_{max} ratios as well as model GMFE values.

5.2 Clinical studies

The clinical studies used for metformin DGI model building and evaluation are summarized in Table S5.2.1.

Table S5.2.1: Metformin-*SLC22A2* 808G>T DGI study table

Dose [mg]	Route	n	Men [%]	Age [years]	Weight [kg]	Height [cm]	BMI [kg/m^2]	Genotype	Dataset	Reference
500	po, -, fast	24	-	23 (20–49)	-	-	23 (20–34)	*SLC22A2*-808GG	test	Christensen et al. 2013 [69]
500	po, -, fast	20	-	23 (20–49)	-	-	23 (20–34)	*SLC22A2*-808GT	test	Christensen et al. 2013 [69]
500	po, -, fast	5	-	23 (20–49)	-	-	23 (20–34)	*SLC22A2*-808TT	training	Christensen et al. 2013 [69]
500	po, -, fast	9	78	25 ± 3	66 ± 12	170 ± 7	22 ± 3	*SLC22A2*-808GG	test	Song et al. 2008 [70]
500	po, -, fast	6	67	25 ± 3	66 ± 12	170 ± 7	22 ± 3	*SLC22A2*-808GT	test	Song et al. 2008 [70]
500	po, -, fast	6	67	25 ± 3	66 ± 12	170 ± 7	22 ± 3	*SLC22A2*-808TT	test	Song et al. 2008 [70]
500	po, -, fast	6	100	(21–32)	(53–73)	-	-	*SLC22A2*-808GG	test	Wang et al. 2008 [13]
500	po, -, fast	5	100	(21–32)	(53–73)	-	-	*SLC22A2*-808GT	test	Wang et al. 2008 [13]
500	po, -, fast	4	100	(21–32)	(53–73)	-	-	*SLC22A2*-808TT	training	Wang et al. 2008 [13]
850	po, tab, fast	14	36	27 ± 7	-	-	-	*SLC22A2*-808GG	test	Chen et al. 2009 [27]
850	po, tab, fast	9	56	31 ± 6	-	-	-	*SLC22A2*-808GT	test	Chen et al. 2009 [27]

-: not given, **BMI**: body mass index, **n**: number of individuals studied, **po**: oral, **tab**: tablet,
test: test dataset (model evaluation), **training**: training dataset (model development and parameter optimization)

5.3 Profiles

5.3.1 Semilogarithmic plots – Plasma

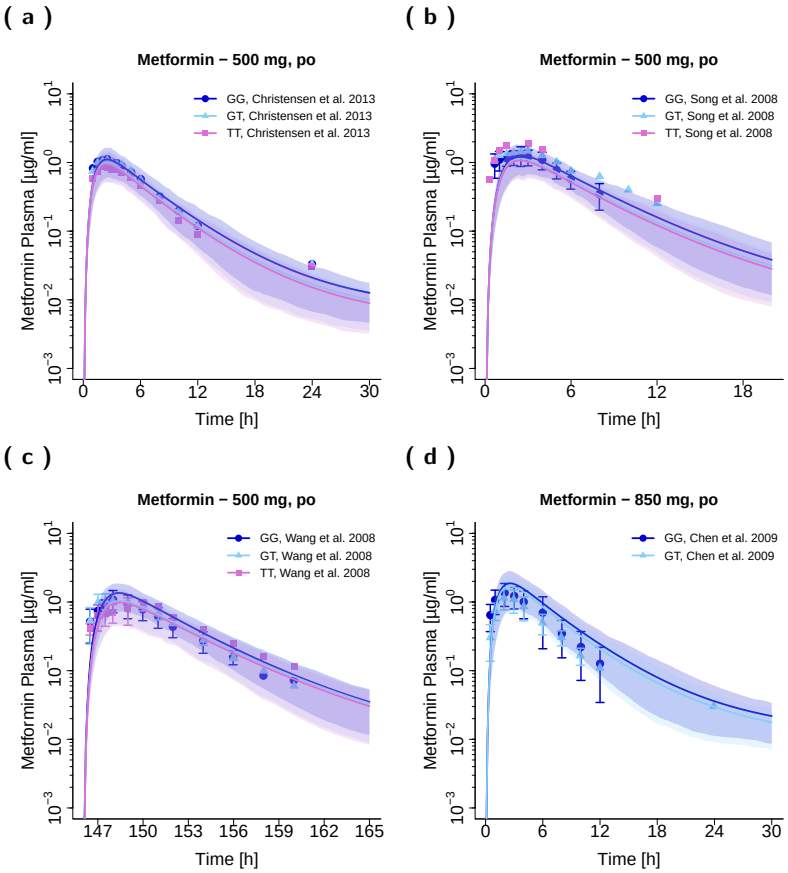

Figure S5.3.1: Metformin plasma concentration-time profiles (semilogarithmic) in different *SLC22A2* genotypes. Observed data are shown as symbols, if available ± standard deviation (SD). Population simulation arithmetic means are shown as lines; the shaded areas represent the predicted population variation (Q_{16} – Q_{84}). The reference genotype *SLC22A2* 808GG is shown as – and dots (GG), *SLC22A2* 808GT as – and triangles (GT) and *SLC22A2* 808TT as – and squares (TT).

5.3.2 Linear plots – Plasma

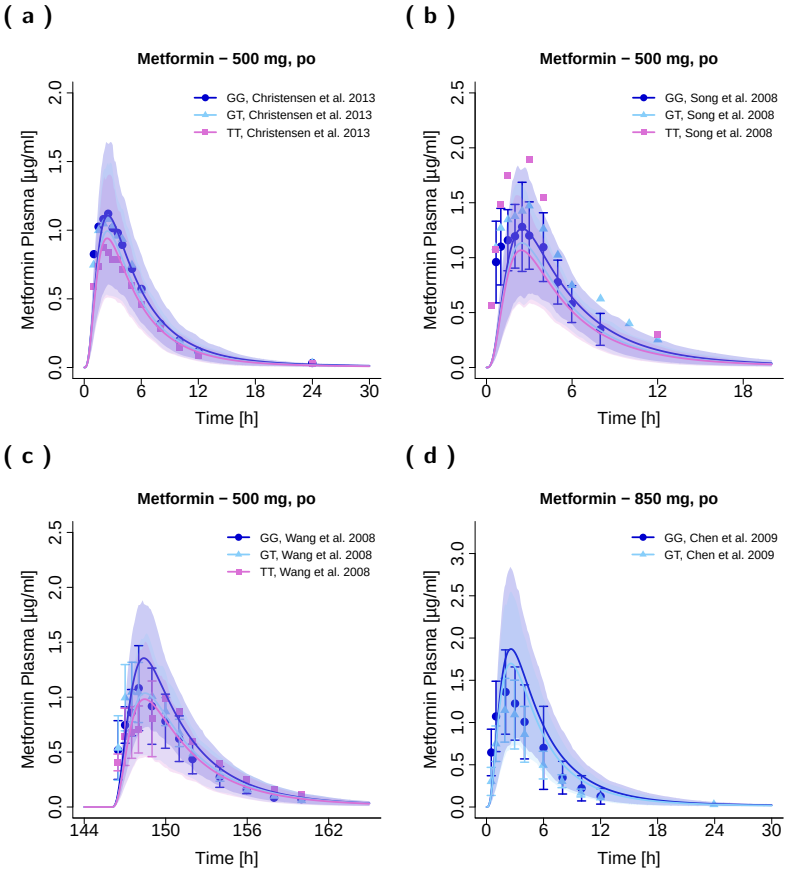

Figure S5.3.2: Metformin plasma concentration-time profiles (linear) in different *SLC22A2* genotypes. Observed data are shown as symbols, if available ± standard deviation (SD). Population simulation arithmetic means are shown as lines; the shaded areas represent the predicted population variation (Q_{16} – Q_{84}). The reference genotype *SLC22A2* 808GG is shown as – and dots (GG), *SLC22A2* 808GT as – and triangles (GT) and *SLC22A2* 808TT as – and squares (TT).

5.3.3 Linear plots - Fraction excreted to urine

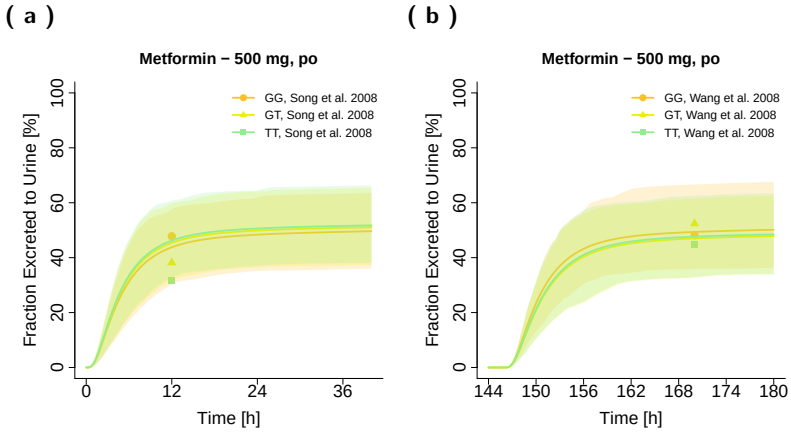

Figure S5.3.3: Metformin fraction excreted to urine profiles (linear) in different *SLC22A2* genotypes. Observed data are shown as symbols. Population simulation arithmetic means are shown as lines; the shaded areas represent the predicted population variation (Q_{16} – Q_{84}). The reference genotype *SLC22A2* 808GG is shown as – and dots (GG), *SLC22A2* 808GT as – and triangles (GT) and *SLC22A2* 808TT as – and squares (TT).

5.4 Model evaluation

5.4.1 DGI AUC and C_{max} ratio goodness-of-fit plots

(a) DGI AUC ratios

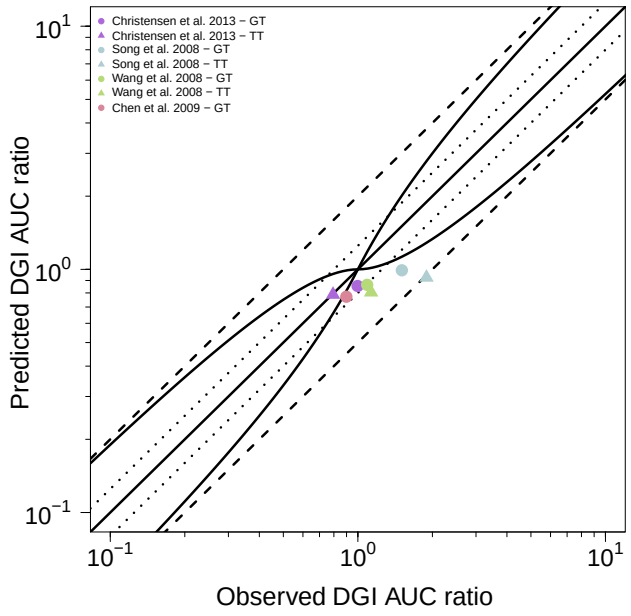

(b) DGI C_{max} ratios

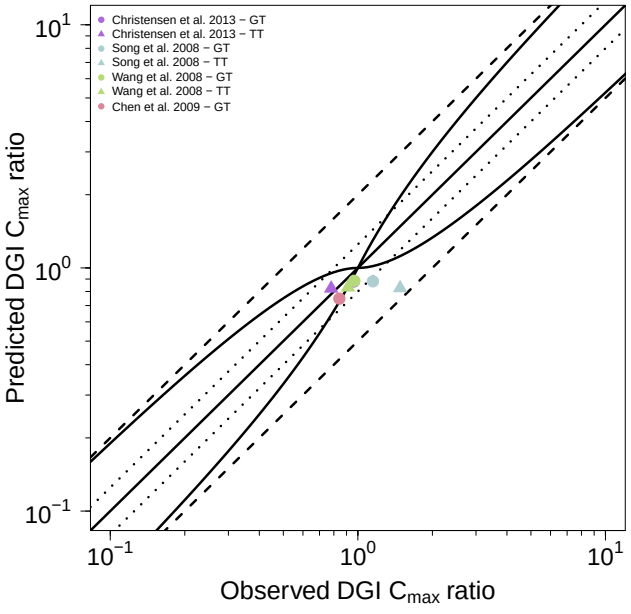

Figure S5.4.1: Predicted versus observed metformin DGI AUC ratios and DGI C_{max} ratios. Each symbol represents the DGI AUC or C_{max} ratio of a different study profile. The black solid line (——) marks the line of identity. Black dotted lines (·····) indicate 1.25-fold, black dashed lines (– –) indicate 2-fold deviation. The curved black lines show the prediction success limits suggested by Guest et al. [71]. **AUC**: area under the plasma concentration–time curve from the time of administration to the last data point, **C_{max}**: maximum plasma concentration, **GG**: *SLC22A2* 808GG reference genotype, **GT**: *SLC22A2* 808GT genotype, **TT**: *SLC22A2* 808TT genotype

5.4.2 Geometric mean fold error of predicted DGI AUC and C_{max} ratios

Table S5.4.1: Predicted and observed DGI AUC ratios and DGI C_{max} ratios of metformin plasma concentrations

			DGI AUC ratio			DGI C_{max} ratio			
Route	Genotype	Dose	Pred	Obs	Pred/Obs	Pred	Obs	Pred/Obs	Reference
oral, -	*SLC22A2*-808GT	500 mg	0.85	1.00	0.86	0.88	0.96	0.91	Christensen et al. 2013 [69]
oral, -	*SLC22A2*-808TT	500 mg	0.79	0.79	0.99	0.82	0.78	1.06	Christensen et al. 2013 [69]
oral, -	*SLC22A2*-808GT	500 mg	0.99	1.51	0.66	0.88	1.15	0.77	Song et al. 2008 [70]
oral, -	*SLC22A2*-808TT	500 mg	0.93	1.89	0.49	0.83	1.48	0.56	Song et al. 2008 [70]
oral, -	*SLC22A2*-808GT	500 mg	0.86	1.09	0.79	0.89	0.97	0.92	Wang et al. 2008 [13]
oral, -	*SLC22A2*-808TT	500 mg	0.80	1.13	0.71	0.83	0.91	0.91	Wang et al. 2008 [13]
oral, tablet	*SLC22A2*-808GT	850 mg	0.77	0.90	0.86	0.75	0.84	0.89	Chen et al. 2009 [27]
Overall GMFE					**1.36 (1.01–2.04)**			**1.20 (1.06–1.79)**	
					6/7 with GMFE ≤ 2			**7/7 with GMFE ≤ 2**	

GMFE: geometric mean fold error, **obs**: observed, **pred**: predicted

6 Cimetidine-metformin drug-drug(-gene) interaction (DDI/DDGI)

6.1 PBPK model development

To describe the competitive inhibition of OCT1, OCT2 and MATE1 by cimetidine, values for OCT1 K_i = 104.0 µmol/l, OCT2 K_i = 124.0 µmol/l and MATE1 K_i = 3.8 µmol/l were applied, measured using HEK293 cells overexpressing hOCT1, hOCT2 or hMATE1 [64]. The transport inhibition assays were conducted in protein-free Krebs-Henseleit buffer and the measured K_i values were not corrected for cimetidine binding in vitro.

Details on the modeled clinical studies investigating the cimetidine-metformin DDI/DDGI are given in Table S6.2.1. Population predictions of metformin plasma concentration-time profiles before and during cimetidine co-administration, compared to observed data, are shown in Figures S6.3.1 and S6.3.2. Population predictions of metformin fraction excreted to urine profiles before and during cimetidine co-administration, compared to observed data, are shown in Figure S6.3.3. The correlation of predicted to observed DDI/DDGI AUC ratios and DDI/DDGI C_{max} ratios is shown in Figure S6.4.1. Table S6.4.1 lists the corresponding predicted and observed DDI/DDGI AUC ratios, DDI/DDGI C_{max} ratios as well as model GMFE values.

6.2 Clinical studies

The clinical studies used for cimetidine-metformin DDI/DDGI model building and evaluation are summarized in Table S6.2.1.

Table S6.2.1: Cimetidine-metformin DDI/DDGI study table

Perpetrator Cimetidine	**Victim** Metformin	**Dose gap [h]**	**n**	**Men [%]**	**Age [years]**	**Weight [kg]**	**Height [cm]**	**BMI [kg/m²]**	**Genotype**	**Dataset**	**Reference**
400 mg, po, tab, qid	10 mg, po, sol[a]	1	11	100	38 ± 10 (22–52)	83 ± 12 (64–108)	180 ± 7 (170–191)	26 ± 3 (21–30)	-	test	Boehringer 2018 [14]
400 mg, po, tab, qid	250 mg, po, tab, qd, fed	0	7	43	(19–23)	(55–78)	-	-	-	test	Somogyi et al. 1987 [12]
400 mg, po, tab, qid	500 mg, po, sol	1	13	100	38 ± 10 (22–52)	83 ± 11 (64–108)	181 ± 7 (170–191)	25 ± 3 (20–30)	-	training	Boehringer 2018 [14]
400 mg, po, -, bid	500 mg, po, -	2	6	100	(21–32)	(53–73)	-	-	*SLC22A2*-808GG	test	Wang et al. 2008 [13]
400 mg, po, -, bid	500 mg, po, -	2	5	100	(21–32)	(53–73)	-	-	*SLC22A2*-808GT	test	Wang et al. 2008 [13]
400 mg, po, -, bid	500 mg, po, -	2	4	100	(21–32)	(53–73)	-	-	*SLC22A2*-808TT	test	Wang et al. 2008 [13]

-: not given, **bid**: twice daily, **BMI**: body mass index, **n**: number of individuals studied, **po**: oral, **qd**: once daily, **qid**: four times daily,
sol: solution, **tab**: tablet, **test**: test dataset (model evaluation), **training**: training dataset (model development and parameter optimization)
[a] 10 mg metformin together with 0.25 mg digoxin, 1 mg furosemide and 10 mg rosuvastatin

6.3 Profiles

6.3.1 Semilogarithmic plots – Plasma

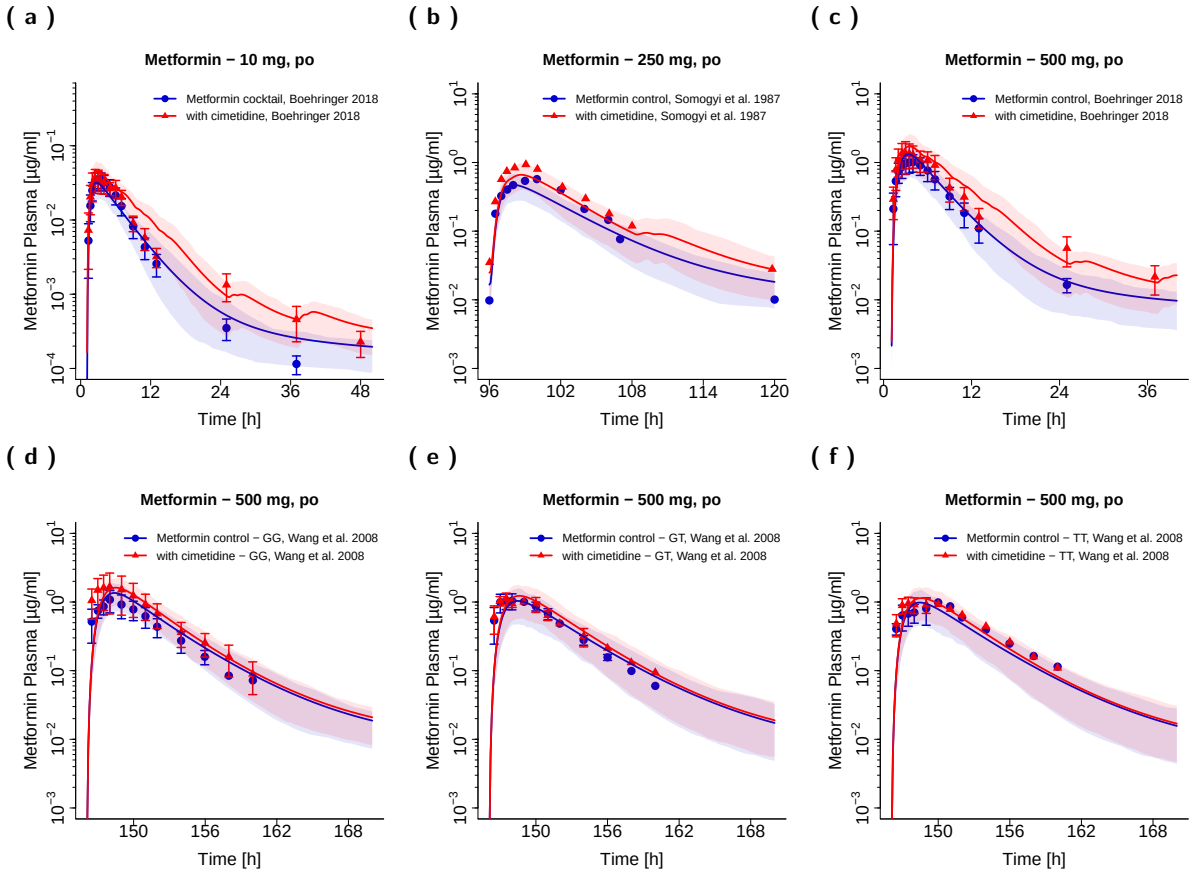

Figure S6.3.1: Metformin plasma concentration-time profiles (semilogarithmic) before and during cimetidine co-treatment of different *SLC22A2* genotypes. Observed data are shown as symbols (dots for control and triangles for co-treatment with cimetidine), if available ± standard deviation (SD). Population simulation arithmetic means are shown as lines (– for control and – for co-treatment with cimetidine); the shaded areas represent the predicted population variation (Q_{16} – Q_{84}). **GG**: *SLC22A2* 808GG genotype, **GT**: *SLC22A2* 808GT genotype, **TT**: *SLC22A2* 808TT genotype

6.3.2 Linear plots – Plasma

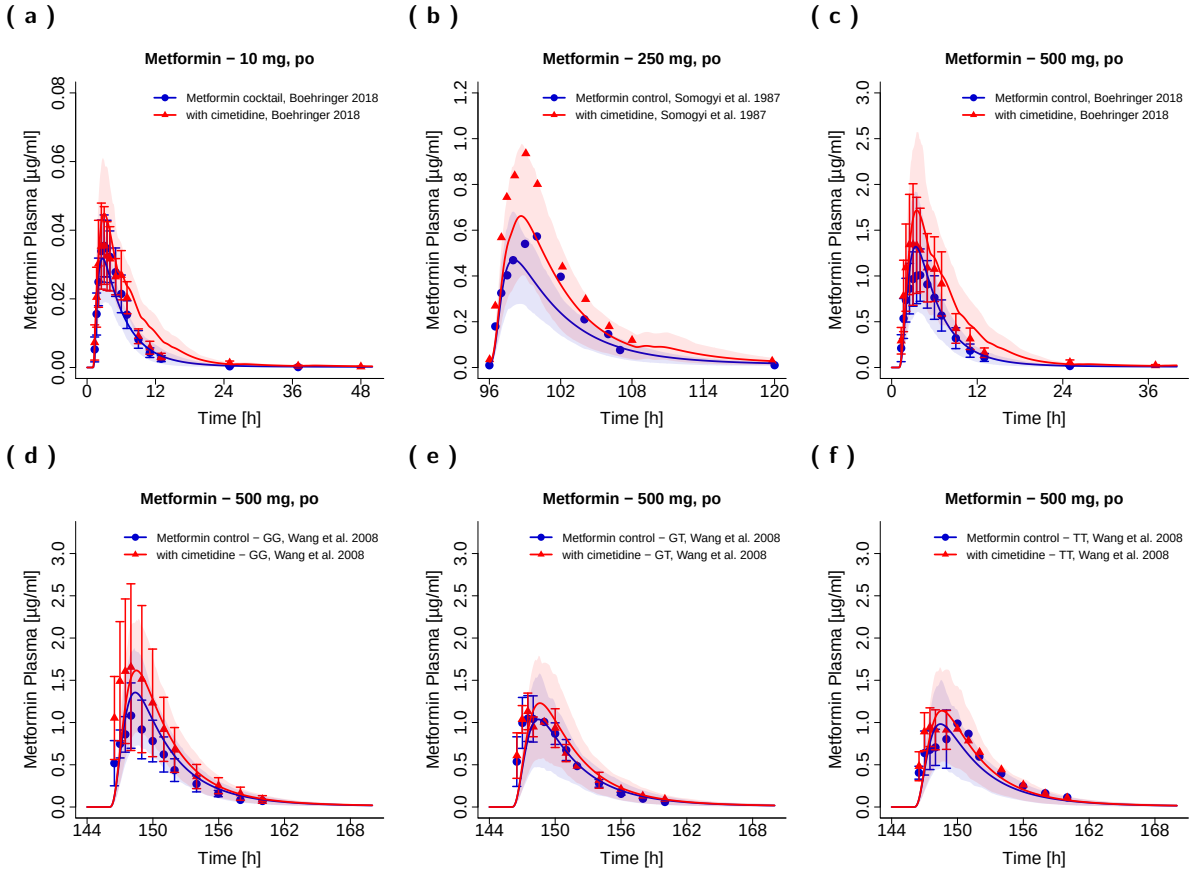

Figure S6.3.2: Metformin plasma concentration-time profiles (linear) before and during cimetidine co-treatment of different *SLC22A2* genotypes. Observed data are shown as symbols (dots for control and triangles for co-treatment with cimetidine), if available ± standard deviation (SD). Population simulation arithmetic means are shown as lines (– for control and – for co-treatment with cimetidine); the shaded areas represent the predicted population variation (Q_{16} – Q_{84}). **GG**: *SLC22A2* 808GG genotype, **GT**: *SLC22A2* 808GT genotype, **TT**: *SLC22A2* 808TT genotype

6.3.3 Linear plots - Fraction excreted to urine

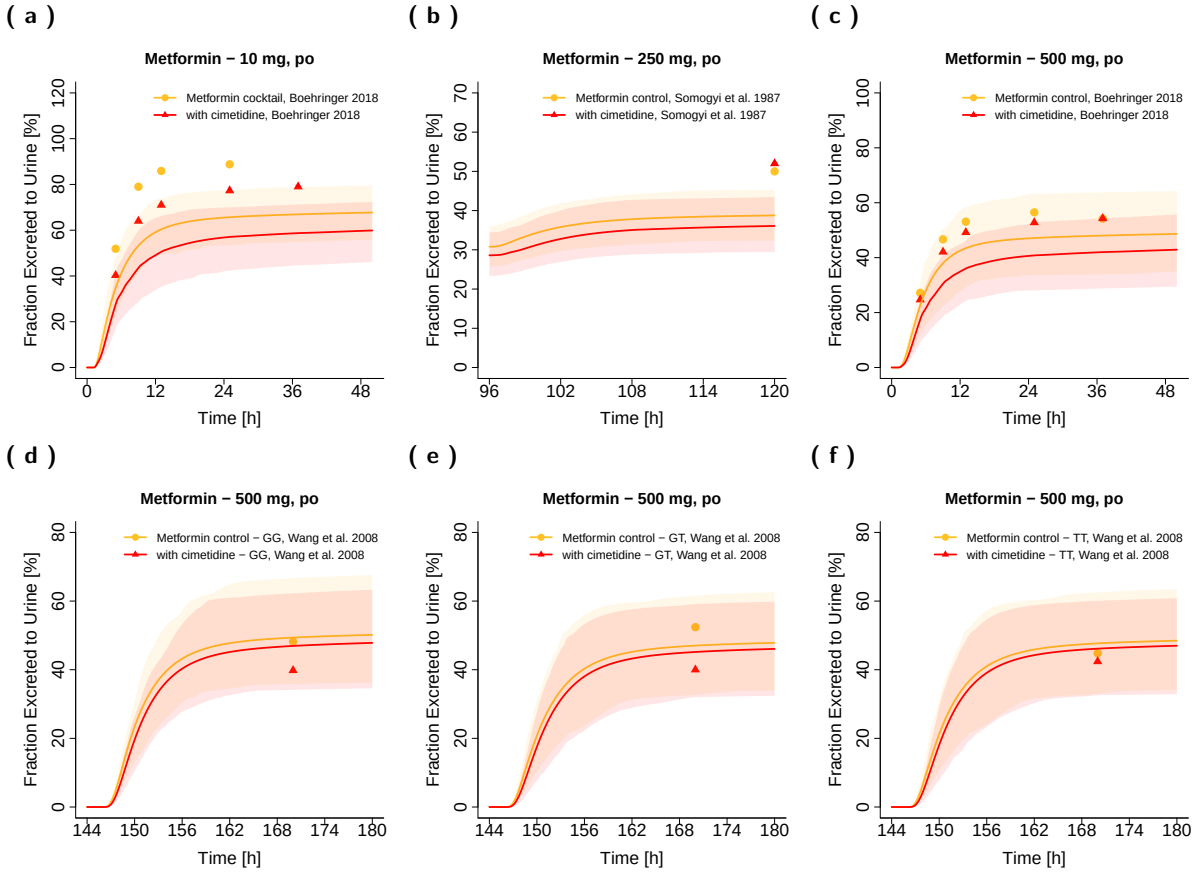

Figure S6.3.3: Metformin fraction excreted to urine profiles (linear) before and during cimetidine co-treatment of different *SLC22A2* genotypes. Observed data are shown as symbols (dots for control and triangles for co-treatment with cimetidine). Population simulation arithmetic means are shown as lines (– for control and – for co-treatment with cimetidine); the shaded areas represent the predicted population variation (Q_{16} – Q_{84}). **GG**: *SLC22A2* 808GG genotype, **GT**: *SLC22A2* 808GT genotype, **TT**: *SLC22A2* 808TT genotype

6.4 Model evaluation

6.4.1 DDI/DDGI AUC and C_{max} ratio goodness-of-fit plots

(a) DDI/DDGI AUC ratios

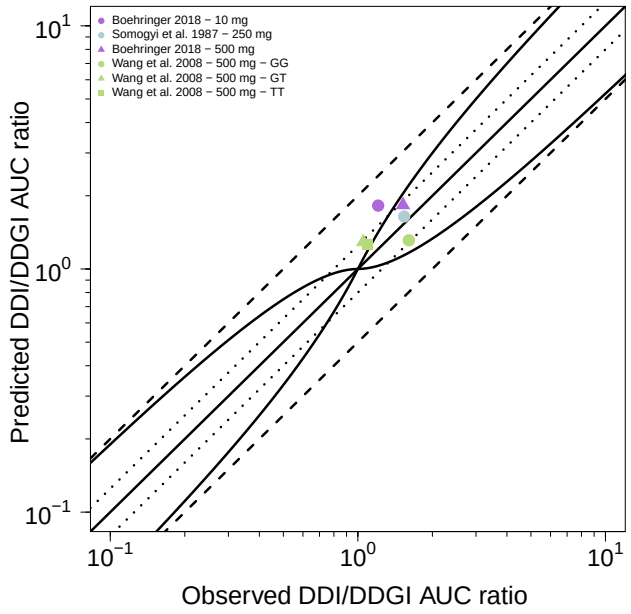

(b) DDI/DDGI C_{max} ratios

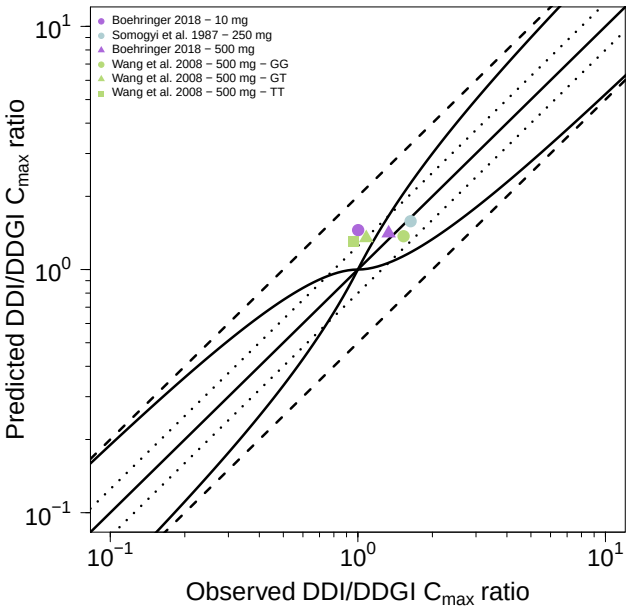

Figure S6.4.1: Predicted versus observed cimetidine-metformin DDI/DDGI AUC ratios and DDI/DDGI C_{max} ratios. Each symbol represents the DDI/DDGI AUC or C_{max} ratio of a different study profile. The black solid line (——) marks the line of identity. Black dotted lines (·····) indicate 1.25-fold, black dashed lines (– –) indicate 2-fold deviation. The curved black lines show the prediction success limits suggested by Guest et al. [71]. **AUC**: area under the plasma concentration–time curve from the time of administration to the last data point, **C_{max}**: maximum plasma concentration, **GG**: *SLC22A2* 808GG reference genotype, **GT**: *SLC22A2* 808GT genotype, **TT**: *SLC22A2* 808TT genotype

6.4.2 Geometric mean fold error of predicted DDI/DDGI AUC and C_{max} ratios

Table S6.4.1: Predicted and observed cimetidine-metformin DDI/DDGI AUC ratios and DDI/DDGI C_{max} ratios

Perpetrator	**Victim**			**DDI/DDGI AUC ratio**			**DDI/DDGI C_{max} ratio**			
Cimetidine	Metformin	Dose gap [h]	Genotype	Pred	Obs	Pred/Obs	Pred	Obs	Pred/Obs	Reference
400 mg, po, tab, qid	10 mg, po, sol[a]	1	-	1.82	1.21	1.51	1.45	1.00	1.45	Boehringer 2018 [14]
400 mg, po, tab, qid	250 mg, po, tab, qd, fed	0	-	1.64	1.54	1.07	1.58	1.63	0.97	Somogyi et al. 1987 [12]
400 mg, po, tab, qid	500 mg, po, sol	1	-	1.83	1.52	1.20	1.41	1.33	1.06	Boehringer 2018 [14]
400 mg, po, -, bid	500 mg, po, -	2	*SLC22A2*-808GG	1.31	1.61	0.82	1.37	1.53	0.90	Wang et al. 2008 [13]
400 mg, po, -, bid	500 mg, po, -	2	*SLC22A2*-808GT	1.29	1.05	1.23	1.35	1.08	1.25	Wang et al. 2008 [13]
400 mg, po, -, bid	500 mg, po, -	2	*SLC22A2*-808TT	1.26	1.09	1.15	1.30	0.96	1.36	Wang et al. 2008 [13]
Overall GMFE						**1.22 (1.07–1.51)**			**1.20 (1.03–1.45)**	
						6/6 with GMFE ≤ 2			**6/6 with GMFE ≤ 2**	

-: not given, **bid**: twice daily, **GMFE**: geometric mean fold error, **obs**: observed, **po**: oral, **pred**: predicted, **qd**: once daily, **qid**: four times daily, **sol**: solution, **tab**: tablet

[a] 10 mg metformin together with 0.25 mg digoxin, 1 mg furosemide and 10 mg rosuvastatin

7 Cimetidine-midazolam drug-drug interaction (DDI)

7.1 PBPK model development

The cimetidine-midazolam DDI was modeled using a previously established whole-body PBPK model of midazolam [72]. The drug-dependent parameters of this model are reproduced in Table S7.2.1. The competitive inhibition of CYP3A4 by cimetidine was implemented with K_i = 268.0 µmol/l, determined using human liver microsomes [65]. This value was not corrected for cimetidine binding in vitro, since no experimental values for cimetidine fraction unbound in microsomal incubations could be obtained and the prediction of $fu_{incubation}$ according to Austin et al. resulted in a theoretical $fu_{incubation}$ of 0.97 [73]. Applying this value to correct the cimetidine CYP3A4 K_i in the cimetidine-midazolam DDI predictions did not change the predicted DDI AUC or C_{max} ratios and was, therefore, not retained in the model.

Details on the modeled clinical studies investigating the cimetidine-midazolam DDI are given in Table S7.3.1. Population predictions of midazolam plasma concentration-time profiles before and during cimetidine co-administration, compared to observed data, are shown in Figures S7.4.1 and S7.4.2. The correlation of predicted to observed DDI AUC ratios and DDI C_{max} ratios is shown in Figure S7.5.1. Table S7.5.1 lists the corresponding predicted and observed DDI AUC ratios, DDI C_{max} ratios as well as model GMFE values.

7.2 Drug-dependent parameters

The drug-dependent parameters of the midazolam model are summarized in Table S7.2.1 below.

Table S7.2.1: Drug-dependent parameters of the midazolam PBPK model (adopted from [72])

Parameter	Value	Unit	Source	Literature	Reference	Description
MW	325.77	g/mol	Literature	325.77	[35]	Molecular weight
pKa (base)	6.15	-	Literature	6.15	[74]	Acid dissociation constant
Solubility (pH 6.8)	0.049	g/l	Literature	0.049	[75]	Solubility
logP	3.13	-	Optimized	2.9, 3.9	[76, 77]	Lipophilicity
fu	1.6	%	Literature	1.6, 2.4	[76, 78]	Fraction unbound
CYP3A4 K_m	2.73	µmol/l	Literature	2.73	[79]	CYP3A4 Michaelis-Menten constant
CYP3A4 k_{cat}	13.0	1/min	Optimized	-	-	CYP3A4 catalytic rate constant
GFR fraction	1.00	-	Assumed	-	-	Fraction of filtered drug in the urine
EHC continuous fraction	1.00	-	Assumed	-	-	Fraction of bile continually released
Partition coefficients	Diverse	-	Calculated	R&R	[66, 67]	Cell to plasma partition coefficients
Cellular permeability	6.98E-02	cm/min	Calculated	PK-Sim	[5]	Permeability into the cellular space
Luminal intestinal perm.	2.00E-05	cm/min	Optimized	1.88E-04	Calculated	Transcellular specific intestinal perm.
Formulation	Solution					

conc: concentration, **EHC**: enterohepatic circulation, **GFR**: glomerular filtration rate, **perm**: permeability, **PK-Sim**: PK-Sim standard calculation method, **R&R**: Rodgers and Rowland calculation method

7.3 Clinical studies

The clinical studies used for cimetidine-midazolam DDI model building and evaluation are summarized in Table S7.3.1.

Table S7.3.1: Cimetidine-midazolam DDI study table

Perpetrator Cimetidine	**Victim** Midazolam	**Dose gap [h]**	**n**	**Men [%]**	**Age [years]**	**Weight [kg]**	**Height [cm]**	**BMI [kg/m^2]**	**Dataset**	**Reference**
300 mg, po, -, qid	5 mg, iv, 1 min	0	8	63	(20–46)	-	-	-	test	Greenblatt et al. 1986 [80]
800 mg, po, -	7.5 mg, po, tab	0	8	100	(20–26)	(71–95)	-	-	test	Martinez et al. 1999 [81]
400 mg, po, -, bid	15 mg, po, -	0.5	8	88	(20–40)	-	-	-	training	Fee et al. 1987 [82]
400 mg, po, -	15 mg, po, -	2.0	6	-	(24–38)	(52–79)	(165–185)	-	test	Salonen et al. 1986 [83]
300 mg, po, -, qid	15 mg, po, tab	0	6	100	-	-	-	-	test	Greenblatt et al. 1986 [80]

-: not given, **bid**: twice daily, **BMI**: body mass index, **iv**: intravenous, **n**: number of individuals studied, **po**: oral, **qid**: four times daily, **tab**: tablet, **test**: test dataset (model evaluation), **training**: training dataset (model development and parameter optimization)

7.4 Profiles

7.4.1 Semilogarithmic plots – Plasma

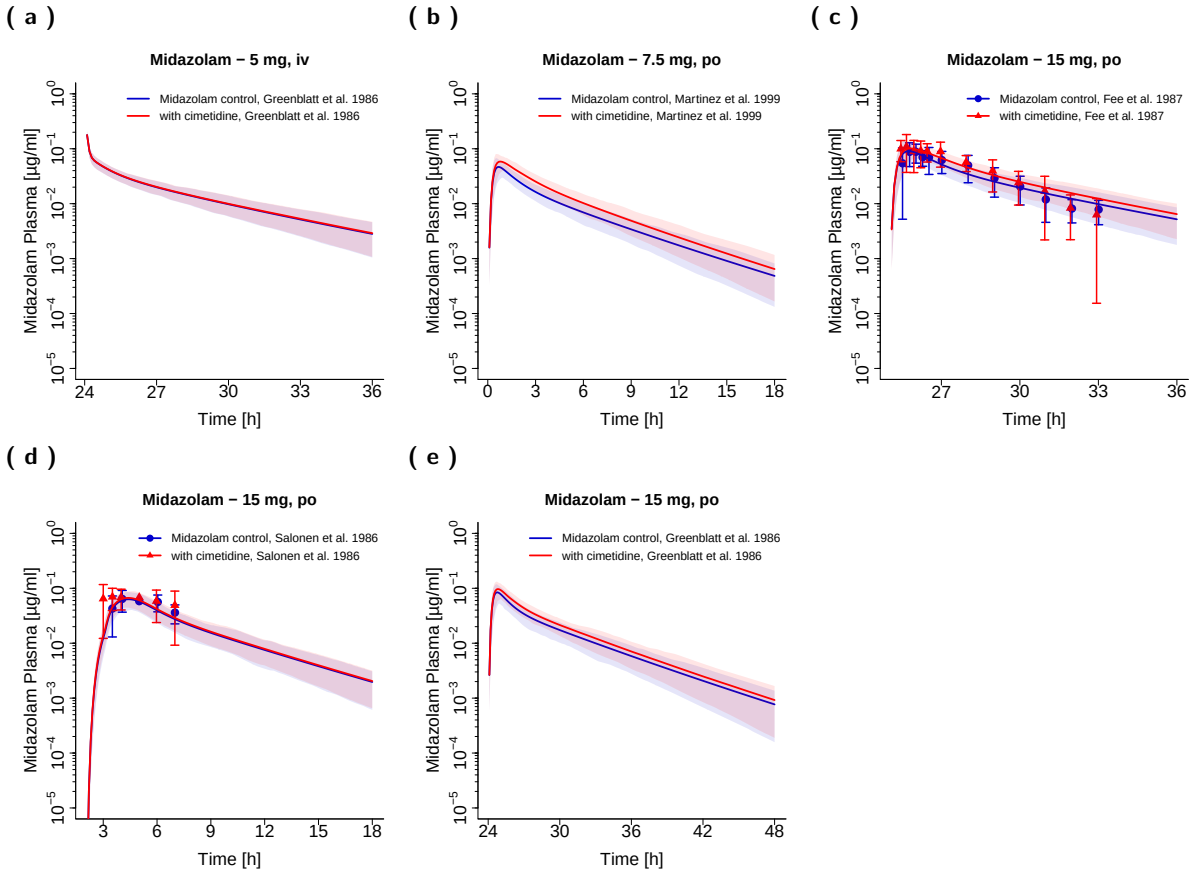

Figure S7.4.1: Midazolam plasma concentration-time profiles (semilogarithmic) before and during cimetidine co-treatment. Observed data are shown as symbols (dots for control and triangles for co-treatment with cimetidine), if available ± standard deviation (SD). Population simulation arithmetic means are shown as lines (– for control and – for co-treatment with cimetidine); the shaded areas represent the predicted population variation (Q_{16} – Q_{84}).

7.4.2 Linear plots – Plasma

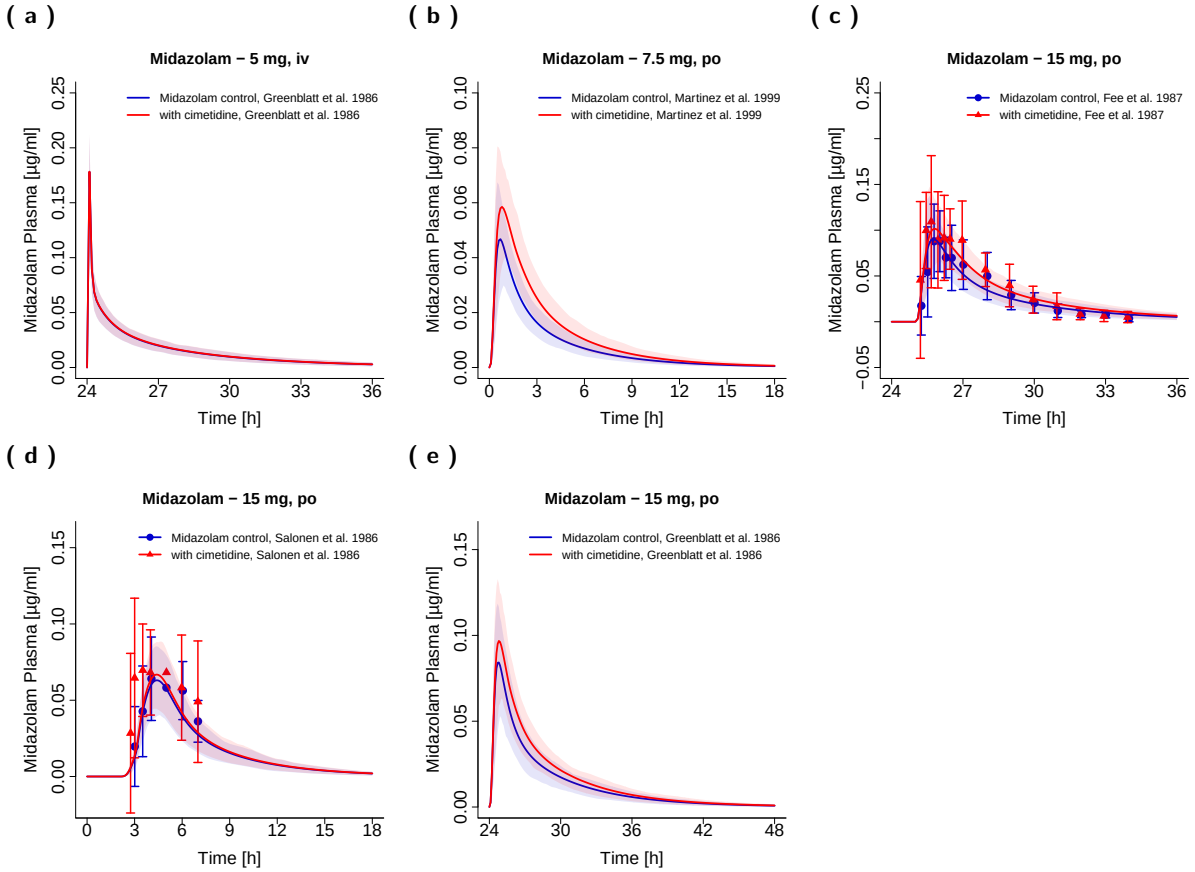

Figure S7.4.2: Midazolam plasma concentration-time profiles (linear) before and during cimetidine co-treatment. Observed data are shown as symbols (dots for control and triangles for co-treatment with cimetidine), if available ± standard deviation (SD). Population simulation arithmetic means are shown as lines (– for control and – for co-treatment with cimetidine); the shaded areas represent the predicted population variation (Q_{16} – Q_{84}).

7.5 Model evaluation

7.5.1 DDI AUC and C_{max} ratio goodness-of-fit plots

(a) DDI AUC ratios

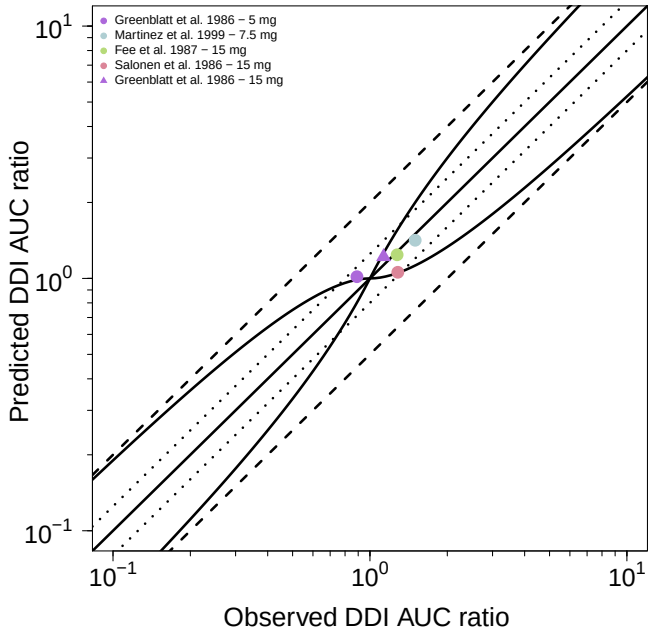

(b) DDI C_{max} ratios

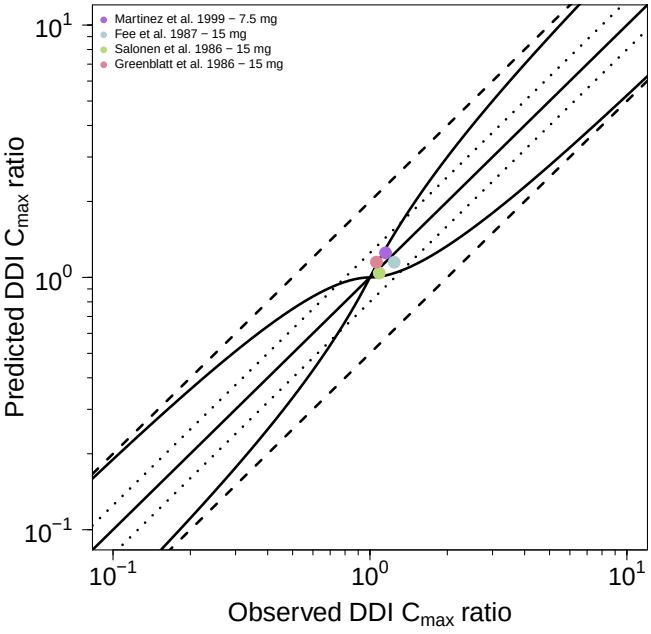

Figure S7.5.1: Predicted versus observed cimetidine-midazolam DDI AUC ratios and DDI C_{max} ratios. Each symbol represents the DDI AUC or C_{max} ratio of a different study profile. The black solid line (——) marks the line of identity. Black dotted lines (·····) indicate 1.25-fold, black dashed lines (- -) indicate 2-fold deviation. The curved black lines show the prediction success limits suggested by Guest et al. [71]. **AUC**: area under the plasma concentration–time curve from the time of administration to the last data point, **C_{max}**: maximum plasma concentration

7.5.2 Geometric mean fold error of predicted DDI AUC and C_{max} ratios

Table S7.5.1: Predicted and observed cimetidine-midazolam DDI AUC ratios and DDI C_{max} ratios

Perpetrator	**Victim**		**DDI AUC ratio**			**DDI C_{max} ratio**			
Cimetidine	Midazolam	Dose gap [h]	Pred	Obs	Pred/Obs	Pred	Obs	Pred/Obs	Reference
300 mg, po, -, qid	5 mg, iv, 1 min	0	1.02	0.89[a]	1.14	-	-	-	Greenblatt et al. 1986 [80]
800 mg, po, -	7.5 mg, po, tab	0	1.42	1.50[a]	0.94	1.25	1.15[a]	1.09	Martinez et al. 1999 [81]
400 mg, po, -, bid	15 mg, po, -	0.5	1.24	1.28	0.97	1.15	1.24	0.92	Fee et al. 1987 [82]
400 mg, po, -	15 mg, po, -	2.0	1.06	1.28	0.82	1.04	1.09	0.96	Salonen et al. 1986 [83]
300 mg, po, -, qid	15 mg, po, tab	0	1.22	1.13[a]	1.08	1.15	1.06[a]	1.08	Greenblatt et al. 1986 [80]
Overall GMFE					**1.10 (1.03–1.21)**			**1.08 (1.04–1.09)**	
					5/5 with GMFE ≤ 2			**4/4 with GMFE ≤ 2**	

-: not given, **bid**: twice daily, **GMFE**: geometric mean fold error, **iv**: intravenous, **obs**: observed, **po**: oral, **pred**: predicted, **qid**: four times daily, **tab**: tablet
[a] as stated in the literature

8 Renal impairment

8.1 PBPK model development

To model the impact of renal impairment on the pharmacokinetics of metformin, pathophysiological changes during chronic kidney disease (CKD) that are relevant for the pharmacokinetics of metformin, were identified. In a next step, these changes in anatomy and physiology were implemented, to create renally impaired individuals in PK-Sim® and to describe the published clinical studies of metformin in CKD3A–5 patients.

To model the metformin exposure in renal impairment, the actual individual GFR was used as reported. Second, renal secretion via OCT2 and MATE1 was decreased in proportion to the decrease in GFR, according to the «intact nephron hypothesis» [84–86]. Third, the hematocrit was gradually decreased with progressing stages of CKD [87]. As observed in previous PBPK analyses of drug pharmacokinetics in renal impairment [86, 88], these changes were not sufficient to describe the elevated metformin plasma concentrations in CKD patients, suggesting the inhibition of further elimination pathways by uremic solutes that accumulate during renal impairment. Therefore, inhibition of basolateral OCT1 (liver uptake) and PMAT (skeletal muscle uptake) was implemented, utilizing observed data of intravenously administered metformin in CKD3A–5 patients [10] to fit a linear correlation between the inhibition of these transporters and the GFR. Furthermore, to capture the broader shape of the plasma concentration-time profiles in CKD patients, the permeability at the basolateral side of the small intestinal mucosa cells was decreased. This permeability was already adjusted in the model for healthy individuals, to release metformin from the enterocytes into the blood. Because of the negligible passive permeability of metformin, there are probably transporters involved at this membrane barrier as well, but due to the current lack of information on the identity of such transporters, the local passive permeability was adjusted in the model. Decreasing the basolateral small intestinal permeability in CKD might well be a surrogate for the inhibition of these unknown transporters by accumulating uremic solutes, consistent with their inhibition of basolateral transporters of the liver. Finally, induction of OCT2 and MATE1, as observed in hyperuricemic rats [89], was assumed and incorporated for CKD4–5 patients, greatly improving the predictions in severe renal disease.

Details on the modeled clinical studies of metformin in renally impaired patients are given in Table S8.2.1. The system-dependent parameter changes to describe the diseased individuals are summarized in Table S8.3.1. Population predictions of metformin plasma and urine concentration-time profiles during CKD, compared to observed data, are shown in Figures S8.4.1 to S8.4.3. Furthermore, a metformin plasma concentration goodness-of-fit plot is presented (Figure S8.5.1) and MRD values for each study are given (see Table S8.5.1). The correlation of predicted to observed AUC and C_{max} values is shown in Figure S8.5.2, together with a summary of the respective PK parameters, including calculated model GMFE values (Table S8.5.2).

8.2 Clinical studies

The clinical studies used for renal impairment PBPK model building and evaluation are summarized in Table S8.2.1.

Table S8.2.1: Metformin study table – renal impairment

Dose [mg]	Route	n	Men [%]	Age [years]	Weight [kg]	Height	BMI	CKD	GFR	CLCR	Dataset	Reference
667	iv, bolus	1	100	72	53	-	-	3A		34[c]	training	Sirtori et al. 1978 [10]
667	iv, bolus	1	100	72	67	-	-	3A		45[c]	training	Sirtori et al. 1978 [10]
667	iv, bolus	1	0	40	70	-	-	3B		48[c]	training	Sirtori et al. 1978 [10]
667	iv, bolus	1	100	59	64	-	-	4		22[c]	training	Sirtori et al. 1978 [10]
667	iv, bolus	1	100	29	96	-	-	5		20[c]	training	Sirtori et al. 1978 [10]
250, qd	po, -, fast	6	67	64 (42–74)	118	-	44[b]	4	21[d]	29[c]	test	Dissayanake et al. 2017 [90]
500, qd	po, -, fast	6	100	64 (49–70)	111	-	37[b]	4	25[d]	33[c]	test	Dissayanake et al. 2017 [90]
1000, qd	po, -, fast	6	83	68 (61–72)	85	-	31[b]	4	20[d]	28[c]	test	Dissayanake et al. 2017 [90]
500, bid[a]	po, -	5	67	65 ± 6	-	-	34 ± 5[b]	3A	53 ± 6[c]		test	Lalau et al. 2018 [91]
500, bid[a]	po, -	5	63	66 ± 9	-	-	31 ± 4[b]	3B	36 ± 5[c]		test	Lalau et al. 2018 [91]
500, bid[a]	po, -	5	38	64 ± 7	-	-	33 ± 4[b]	4	23 ± 4[c]		test	Lalau et al. 2018 [91]
850	po, tab, fast	5	-	42 ± 11	-	-	-	2		73 ± 7[c]	test	Sambol et al. 1995 [30]
850	po, tab, fast	4	-	46 ± 6	-	-	-	3B		41 ± 9[c]	test	Sambol et al. 1995 [30]
850	po, tab, fast	6	-	38 ± 14	-	-	-	4		22 ± 6[c]	test	Sambol et al. 1995 [30]

-: not given, **bid**: twice daily, **BMI**: body mass index, **CKD**: stage of chronic kidney disease, **iv**: intravenous, **n**: number of individuals studied, **CLCR**: creatinine clearance, **GFR**: glomerular filtration rate, **po**: oral, **qd**: once daily, **tab**: tablet, **test**: test dataset (model evaluation), **training**: training dataset (model development and parameter optimization)

[a] morning dose 500 mg, evening dose dependent on CKD stage

[b] in kg/m^2

[c] in ml/min

[d] in $ml/min/1.73m^2$

8.3 System-dependent parameter changes

Changes in system-dependent parameters for the metformin renal impairment PBPK model are summarized in Table S8.3.1.

Table S8.3.1: System-dependent parameter changes of the metformin renal impairment PBPK model

CKD stage	**GFR** [ml/min]	**Individual GFR** [ml/min]	**Factor to reduce renal secretion via OCT2 and MATE1**[a] [84–86]	**Factor to reduce the hematocrit** [87]	**Factor to inhibit muscle PMAT and OCT1**[b]	**Factor to reduce the basolateral intestinal permeability**[c]	**Induction of OCT2** [fold] [89]	**Induction of MATE1** [fold] [89]
Healthy	≥ 90	116.6	1.00	1.00	1.000	1.00	-	-
3A	45–59	52.5	0.45	0.90	0.019	0.50	-	-
3B	30–44	37.5	0.32	0.90	0.026	0.50	-	-
4	15–29	22.5	0.19	0.82	0.045	0.50	1.33	2.99
5	< 15	7.5	0.06	0.63	0.144	0.50	1.33	2.99

CKD stage: stage of chronic kidney disease, **GFR**: glomerular filtration rate

[a] Factor = $\frac{\text{actual GFR}}{\text{age-based healthy GFR}}$

[b] Factor = $\frac{1}{1.027 \cdot \text{GFR} - 0.758}$

[c] Hypothesis

8.4 Profiles

8.4.1 Semilogarithmic plots – Plasma

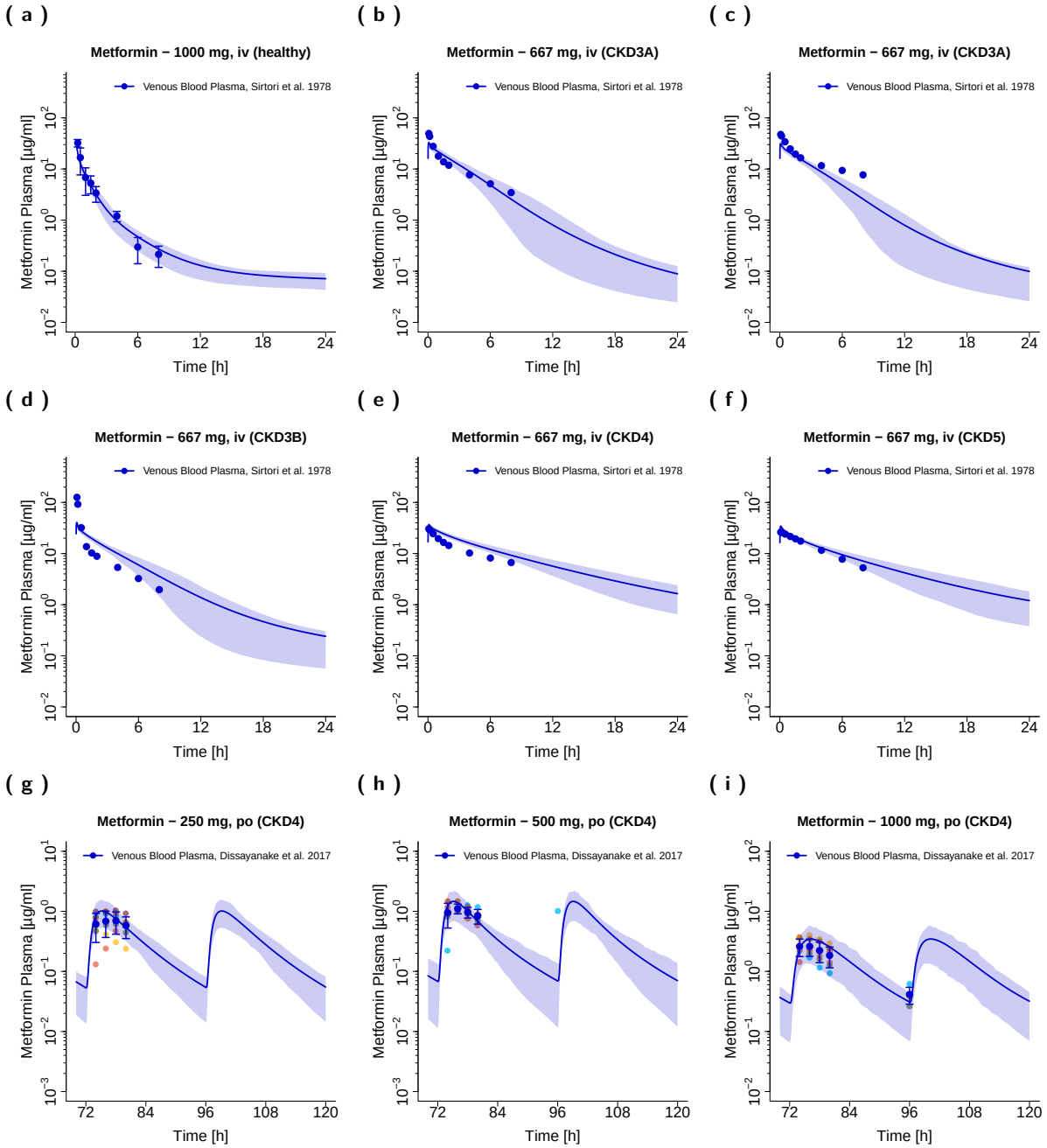

Figure S8.4.1: Metformin venous blood plasma (•, –) and venous whole blood (•, –) concentration-time profiles (semilogarithmic) following intravenous or oral administration of metformin to subjects with impaired renal function. Observed arithmetic means are shown as dark blue (•, blood plasma) or dark red (•, whole blood) dots, if available ± standard deviation (SD). Observed individual data are shown as light colored dots. Population simulation arithmetic means are shown as lines; the shaded areas represent the predicted population variation (Q_{16} – Q_{84}).

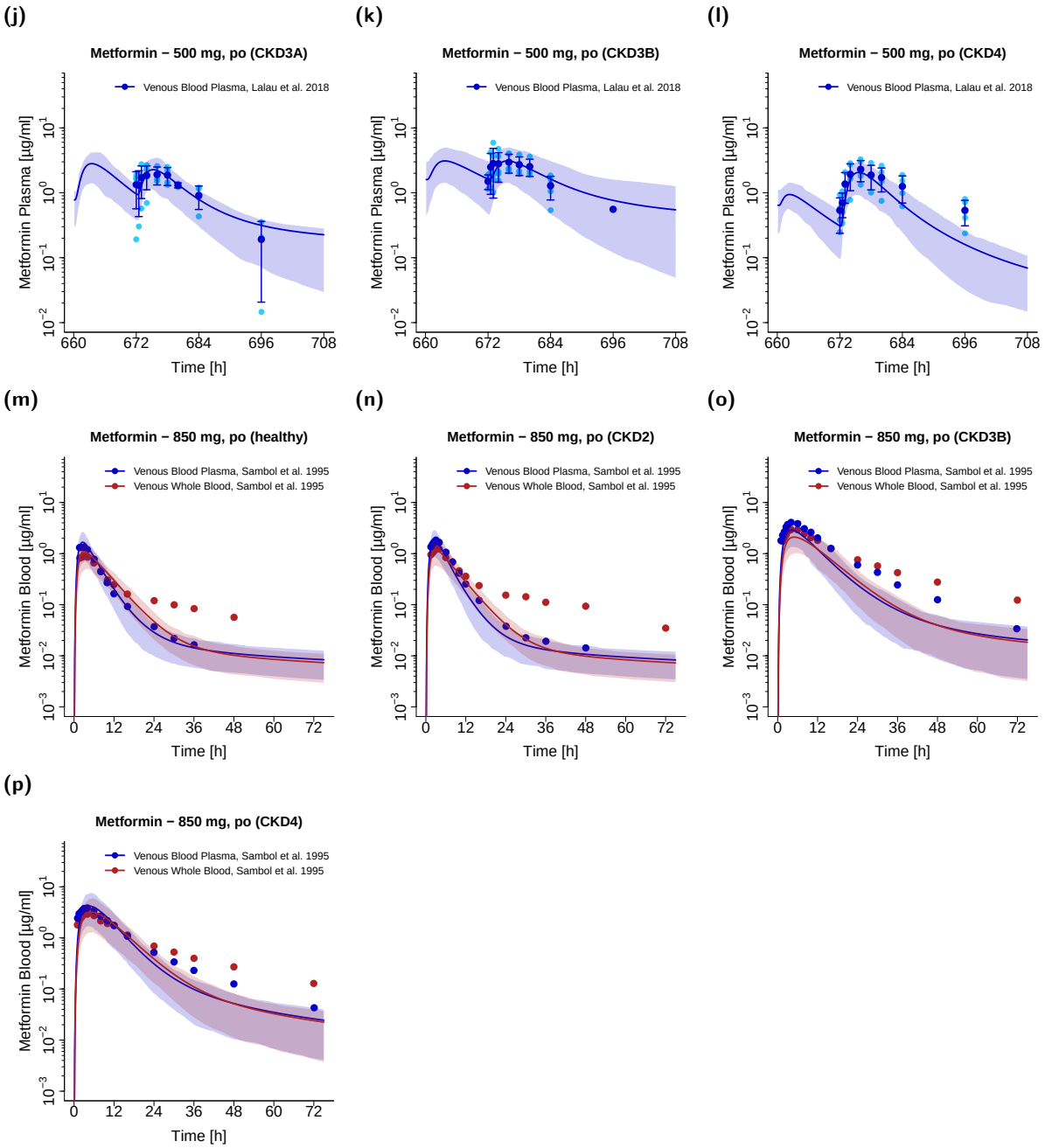

Figure S8.4.1: Metformin venous blood plasma (•, –) and venous whole blood (•, –) concentration-time profiles (semilogarithmic) following intravenous or oral administration of metformin to subjects with impaired renal function. Observed arithmetic means are shown as dark blue (•, blood plasma) or dark red (•, whole blood) dots, if available ± standard deviation (SD). Observed individual data are shown as light colored dots. Population simulation arithmetic means are shown as lines; the shaded areas represent the predicted population variation (Q_{16} – Q_{84}). (continued)

8.4.2 Linear plots – Plasma

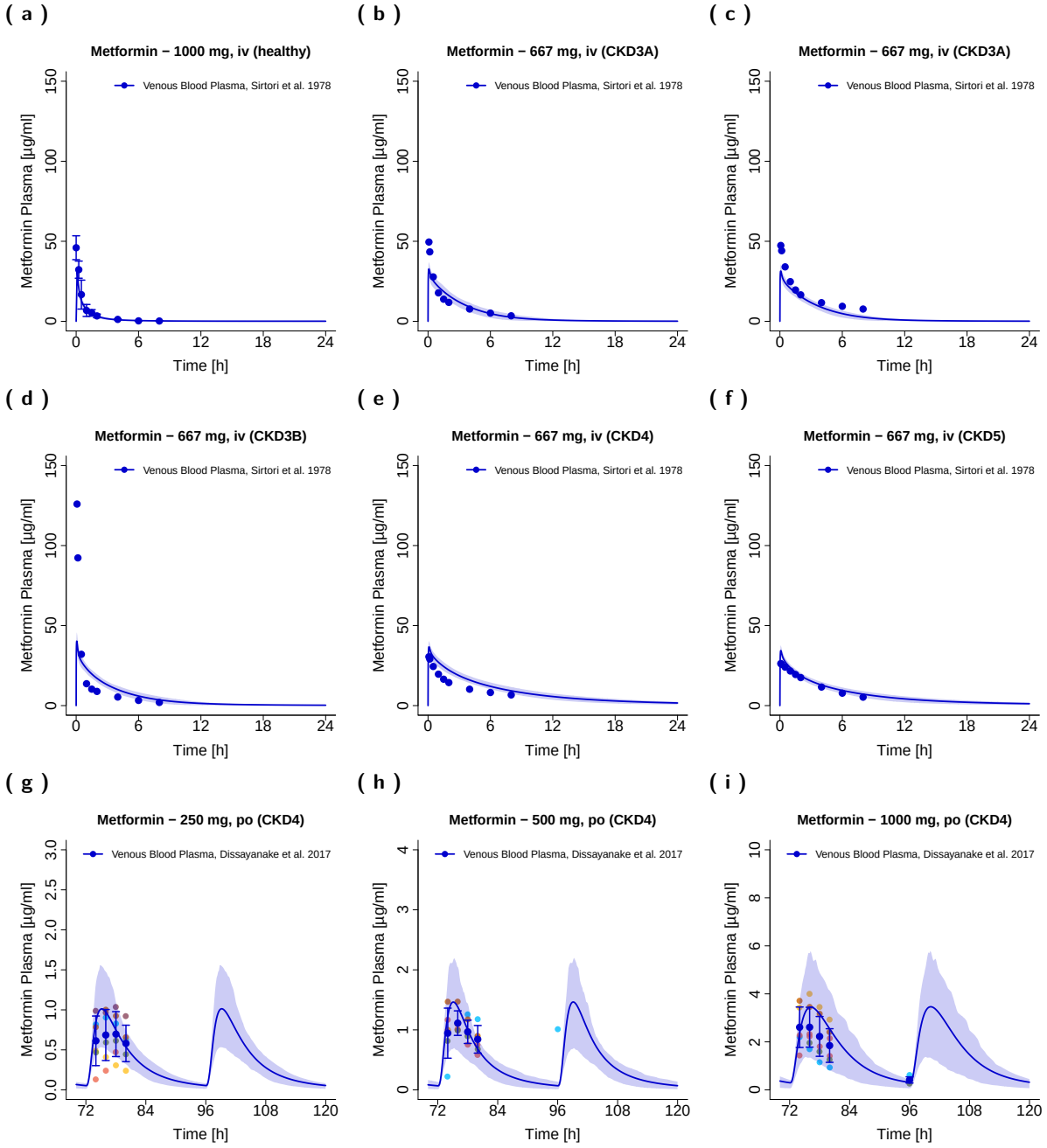

Figure S8.4.2: Metformin venous blood plasma (•, –) and venous whole blood (•, –) concentration-time profiles (linear) following intravenous or oral administration of metformin to subjects with impaired renal function. Observed arithmetic means are shown as dark blue (•, blood plasma) or dark red (•, whole blood) dots, if available ± standard deviation (SD). Observed individual data are shown as light colored dots. Population simulation arithmetic means are shown as lines; the shaded areas represent the predicted population variation (Q_{16} – Q_{84}).

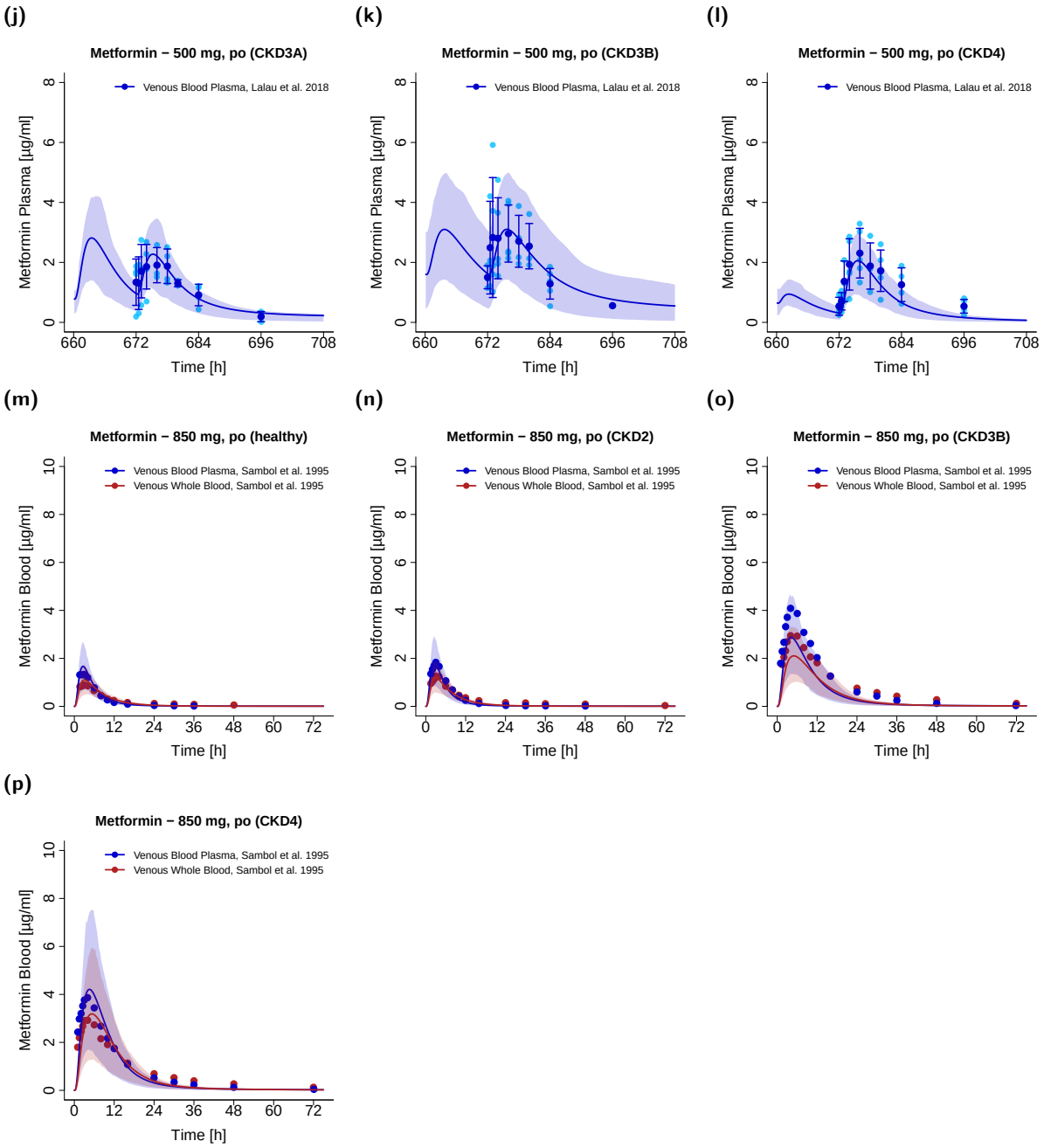

Figure S8.4.2: Metformin venous blood plasma (•, –) and venous whole blood (•, –) concentration-time profiles (linear) following intravenous or oral administration of metformin to subjects with impaired renal function. Observed arithmetic means are shown as dark blue (•, blood plasma) or dark red (•, whole blood) dots, if available ± standard deviation (SD). Observed individual data are shown as light colored dots. Population simulation arithmetic means are shown as lines; the shaded areas represent the predicted population variation (Q_{16} – Q_{84}). (continued)

8.4.3 Linear plots - Fraction excreted to urine

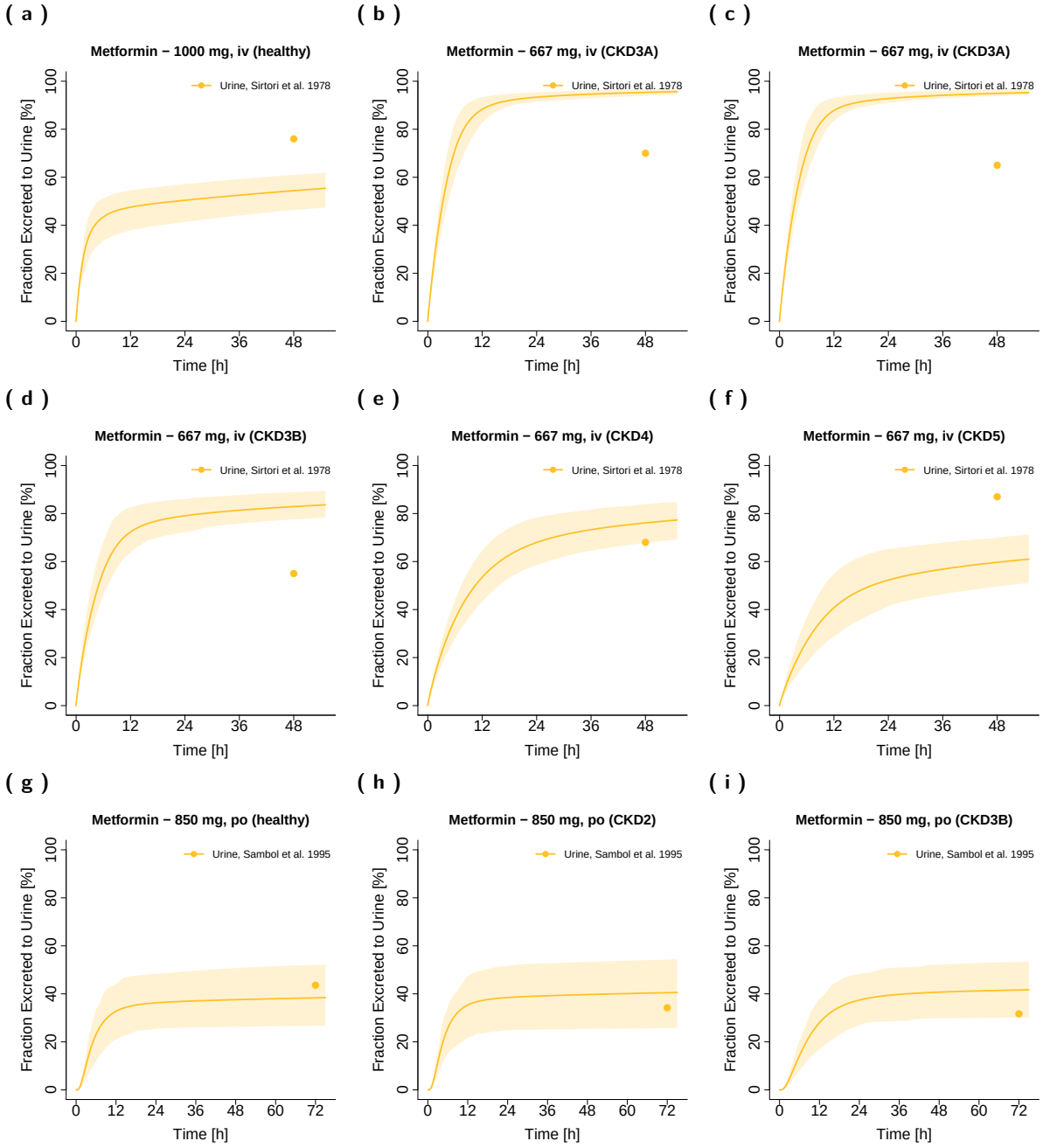

Figure S8.4.3: Metformin fraction excreted to urine (●, –) profiles (linear) following intravenous or oral administration of metformin to subjects with impaired renal function. Observed data are shown as dots. Population simulation arithmetic means are shown as lines; the shaded areas represent the predicted population variation (Q_{16} – Q_{84}).

(j)

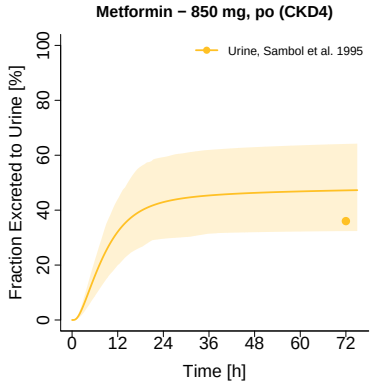

Figure S8.4.3: Metformin fraction excreted to urine (•, –) profiles (linear) following intravenous or oral administration of metformin to subjects with impaired renal function. Observed data are shown as dots. Population simulation arithmetic means are shown as lines; the shaded areas represent the predicted population variation (Q_{16} – Q_{84}). (continued)

8.5 Model evaluation

8.5.1 Predicted concentrations versus observed concentrations goodness-of-fit plot

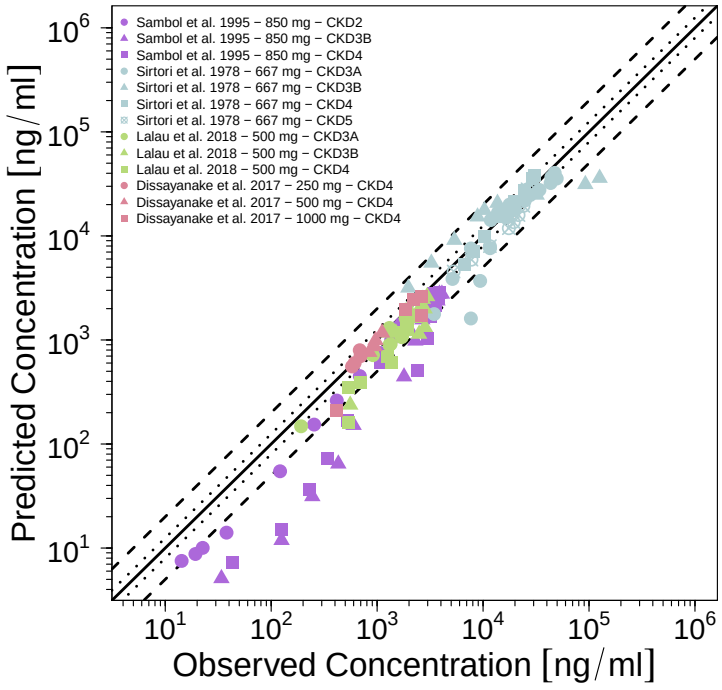

Figure S8.5.1: Predicted versus observed metformin concentrations in subjects with impaired renal function. The black solid line (——) marks the line of identity. Black dotted lines (·····) indicate 1.25-fold, black dashed lines (- -) indicate 2-fold deviation.

8.5.2 Mean relative deviation of plasma concentration predictions

Table S8.5.1: Mean relative deviation (MRD) values of metformin plasma concentration predictions for subjects with impaired renal function

Route	CKD	Compartment	Dose	MRD	Reference
Intravenous					
iv, bolus	CKD3A	Venous Blood Plasma	667 mg	1.35	Sirtori et al. 1978 [10]
iv, bolus	CKD3A	Venous Blood Plasma	667 mg	1.89	Sirtori et al. 1978 [10]
iv, bolus	CKD3B	Venous Blood Plasma	667 mg	2.00	Sirtori et al. 1978 [10]
iv, bolus	CKD4	Venous Blood Plasma	667 mg	1.16	Sirtori et al. 1978 [10]
iv, bolus	CKD5	Venous Blood Plasma	667 mg	1.31	Sirtori et al. 1978 [10]
MRD				**1.59 (1.16–2.00)**	
				5/5 with MRD ≤ 2	
Oral					
oral, tablet	CKD4	Venous Blood Plasma	250 mg	1.08	Dissayanake et al. 2017 [90]
oral, tablet	CKD3A	Venous Blood Plasma	500 mg	1.31	Lalau et al. 2018 [91]
oral, tablet	CKD3B	Venous Blood Plasma	500 mg	1.63	Lalau et al. 2018 [91]
oral, tablet	CKD4	Venous Blood Plasma	500 mg	1.87	Lalau et al. 2018 [91]
oral, tablet	CKD4	Venous Blood Plasma	500 mg	1.07	Dissayanake et al. 2017 [90]
oral, tablet	CKD2	Venous Blood Plasma	850 mg	1.75	Sambol et al. 1995 [30]
oral, tablet	CKD3B	Venous Blood Plasma	850 mg	3.36	Sambol et al. 1995 [30]
oral, tablet	CKD4	Venous Blood Plasma	850 mg	3.03	Sambol et al. 1995 [30]
oral, tablet	CKD4	Venous Blood Plasma	1000 mg	1.43	Dissayanake et al. 2017 [90]
MRD				**2.22 (1.07–3.36)**	
				7/9 with MRD ≤ 2	
Overall MRD				**2.01 (1.07–3.36)**	
				12/14 with MRD ≤ 2	

CKD: stage of chronic kidney disease, **iv**: intravenous, **MRD**: mean relative deviation

8.5.3 AUC and C_{max} goodness-of-fit plots

(a) AUC

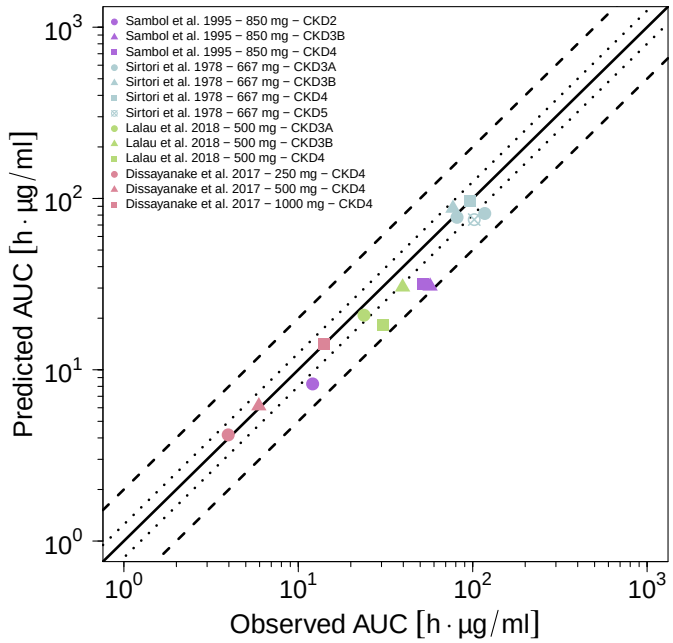

(b) C_{max}

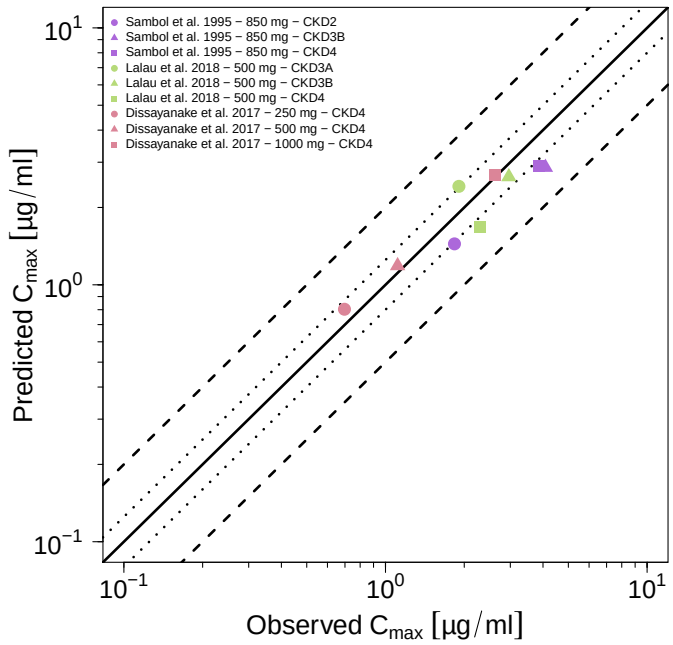

Figure S8.5.2: Predicted versus observed metformin AUC and C_{max} values in subjects with impaired renal function. Each symbol represents the AUC or C_{max} of a different plasma profile. The black solid line (——) marks the line of identity. Black dotted lines (·····) indicate 1.25-fold, black dashed lines (- -) indicate 2-fold deviation. **AUC**: area under the plasma concentration–time curve from the time of administration to the last data point, **C_{max}**: maximum plasma concentration

8.5.4 Geometric mean fold error of predicted AUC and C_{max} values

Table S8.5.2: Predicted and observed AUC and C_{max} values of metformin plasma concentrations in subjects with impaired renal function

				AUC			C_{max}			
Route	CKD	Compartment	Dose	Pred [h·µg/ml]	Obs [h·µg/ml]	Pred/Obs	Pred [µg/ml]	Obs [µg/ml]	Pred/Obs	Reference
Intravenous										
iv, bolus	CKD3A	Venous Blood Plasma	667 mg	77.62	81.33	0.95	-	-	-	Sirtori et al. 1978 [10]
iv, bolus	CKD3A	Venous Blood Plasma	667 mg	81.76	117.24	0.70	-	-	-	Sirtori et al. 1978 [10]
iv, bolus	CKD3B	Venous Blood Plasma	667 mg	87.60	77.05	1.14	-	-	-	Sirtori et al. 1978 [10]
iv, bolus	CKD4	Venous Blood Plasma	667 mg	96.86	96.63	1.00	-	-	-	Sirtori et al. 1978 [10]
iv, bolus	CKD5	Venous Blood Plasma	667 mg	75.29	102.05	0.74	-	-	-	Sirtori et al. 1978 [10]
GMFE						**1.18 (1.00–1.43)**				
						5/5 with GMFE ≤ 2				
Oral										
oral, tablet	CKD4	Venous Blood Plasma	250 mg	4.17	3.97	1.05	0.80	0.70	1.15	Dissayanake et al. 2017 [90]
oral, tablet	CKD3A	Venous Blood Plasma	500 mg	20.83	23.81	0.88	2.42	1.91	1.27	Lalau et al. 2018 [91]
oral, tablet	CKD3B	Venous Blood Plasma	500 mg	30.39	39.64	0.77	2.63	2.96	0.89	Lalau et al. 2018 [91]
oral, tablet	CKD4	Venous Blood Plasma	500 mg	18.24	30.56	0.60	1.67	2.31	0.73	Lalau et al. 2018 [91]
oral, tablet	CKD4	Venous Blood Plasma	500 mg	6.15	5.94	1.04	1.19	1.11	1.07	Dissayanake et al. 2017 [90]
oral, tablet	CKD2	Venous Blood Plasma	850 mg	8.27	12.08	0.68	1.44	1.84	0.79	Sambol et al. 1995 [30]
oral, tablet	CKD3B	Venous Blood Plasma	850 mg	30.77	56.99	0.54	2.86	4.09	0.70	Sambol et al. 1995 [30]
oral, tablet	CKD4	Venous Blood Plasma	850 mg	31.47	51.98	0.61	2.91	3.86	0.75	Sambol et al. 1995 [30]
oral, tablet	CKD4	Venous Blood Plasma	1000 mg	14.21	14.11	1.01	2.68	2.61	1.03	Dissayanake et al. 2017 [90]
GMFE						**1.32 (1.01–1.85)**			**1.22 (1.03–1.43)**	
						9/9 with GMFE ≤ 2			**9/9 with GMFE ≤ 2**	
Overall GMFE						**1.27 (1.00–1.85)**			**1.22 (1.03–1.43)**	
						14/14 with GMFE ≤ 2			**9/9 with GMFE ≤ 2**	

-: not calculated, **CKD**: stage of chronic kidney disease, **GMFE**: geometric mean fold error, **iv**: intravenous, **obs**: observed, **pred**: predicted

9 System-dependent parameters

Details on the expression of metabolic enzymes and drug transporters implemented to model the pharmacokinetics of metformin, cimetidine and midazolam are summarized in Table S9.0.1.

OCT2 is a basolateral uptake transporter that is predominantly expressed in the kidney [92] and forms a functional unit with the apical efflux transporter MATE1, to achieve a directed renal secretion of endogenous compounds and drugs from the blood into the urine. Although there are early reports of MATE2-K expression in the kidney [93, 94], a recent study that quantified the protein expression of renal transporters via LC-MS/MS found that the predominant transporters in the kidney are OCT2, MATE1, OAT1 and OAT3, with only negligible amounts of MATE2-K [95].

OCT1 is an uptake transporter that is strongly expressed in the liver [92, 96, 97], one of the major sites of metformin action. In addition, OCT1 seems to play a role in the uptake of metformin from the gut lumen. Although initially allocated to the basolateral membrane of intestinal epithelial cells, recent literature rather supports an apical localization and function of OCT1 in the gut [98, 99].

At the moment, there is no consensus on the most relevant transporters for metformin absorption from the gut lumen. PMAT was shown to be expressed in the villi of the human small intestinal mucosa and to transport metformin with an affinity similar to that of OCT1 [38]. Reduced expression of PMAT as well as reduced function variants of OCT1 have been associated with gastrointestinal intolerance to metformin caused by higher luminal metformin concentrations [100, 101]. Other transporters that might contribute to the absorption of metformin include THTR-2, SERT and OCT3 [98, 102, 103].

No active transport process to facilitate the efflux of metformin on the basolateral side of the enterocytes has been described so far, but this efflux was shown to be limited, causing 30–300-fold accumulation of metformin in the human jejunal mucosa compared to plasma, probably contributing to the extremely slow and elimination rate-limiting absorption of metformin [104–106].

Table S9.0.1: System-dependent parameters

	Reference concentration					Half-life [h]	
Enzyme/Transporter	**Mean**[a]	**GSD**[b]	**Relative expression**[c]	**Localization**	**Direction**	**Liver**	**Intestine**
CYP3A4	4.32 [110]	1.18 liver [1] 1.46 intestine [1]	RT-PCR [111]	Intracellular	-	36 [112]	23 [113]
MATE1	0.13[d] [95, 107]	1.53 [95]	Kidney [93, 94]	Apical	Efflux	36	-
OAT3	0.09[d] [95, 107]	1.53 [95]	RT-PCR [114]	Basolateral	Influx	36	-
OCT1	0.16[e] [108, 115]	1.50 [115]	Array [116], large intestinal mucosa → 0	Basolateral, in enterocytes apical	Influx	36	23
OCT2	0.19[d] [95, 107]	1.45 [95]	EST [117]	Basolateral	Influx	36	-
PMAT	1.00[f] [109]	1.40[g]	RT-PCR [114], large intestinal mucosa → 0	Basolateral, in enterocytes apical	Influx	36	23

CYP3A4: cytochrome P450 3A4, **MATE1**: multidrug and toxin extrusion 1, **OAT3**: organic anion transporter 3,
OCT1: organic cation transporter 1, **OCT2**: organic cation transporter 2, **PMAT**: plasma membrane monoamine transporter

[a] µmol protein/l in the tissue of highest expression

[b] Geometric standard deviation of the reference concentration

[c] In the different organs (PK-Sim® expression database profile)

[d] Calculated from transporter per mg membrane protein × 26.2 mg human kidney microsomal protein per g kidney [107]

[e] Calculated from transporter per mg membrane protein × 37.0 mg membrane protein per g liver [108]

[f] If no information was available, the mean reference concentration was set to 1.0 µmol/l and the catalytic rate constant (k_{cat}) was optimized according to [109]

[g] If no information was available, a moderate variability of 35 % CV was assumed (= 1.40 GSD)

References

[1] Open Systems Pharmacology Suite Community (2018) PK-Sim® Ontogeny Database Documentation, Version 7.3. https://github.com/Open-Systems-Pharmacology/OSPSuite.Documentation/blob/master/PK-SimOntogenyDatabaseVersion7.3.pdf, accessed: 2019-11-19

[2] Valentin J (2002) Basic anatomical and physiological data for use in radiological protection: reference values: ICRP Publication 89. Annals of the ICRP 32(3):1 – 277

[3] National Center for Health Statistics (1997) Third National Health and Nutrition Examination Survey (NHANES III). Tech. rep., Hyattsville, MD 20782

[4] US Food and Drug Administration (2017) Drug development and drug interactions: Table of substrates, inhibitors and inducers. https://www.fda.gov/drugs/drug-interactions-labeling/drug-development-and-drug-interactions-table-substrates-inhibitors-and-inducers, accessed: 2019-11-19

[5] Open Systems Pharmacology Suite Community (2018) Open Systems Pharmacology Suite Manual, Version 7.4. https://github.com/Open-Systems-Pharmacology/OSPSuite.Documentation/blob/master/OpenSystemsPharmacologySuite.pdf, accessed: 2019-11-19

[6] Vidon N, Chaussade S, Noel M, Franchisseur C, Huchet B, Bernier JJ (1988) Metformin in the digestive tract. Diabetes Research and Clinical Practice 4(3):223–229

[7] Gormsen LC, Sundelin EI, Jensen JB, Vendelbo MH, Jakobsen S, Munk OL, Hougaard Christensen MM, Brosen K, Frokiaer J, Jessen N (2016) In Vivo Imaging of Human 11C-Metformin in Peripheral Organs: Dosimetry, Biodistribution, and Kinetic Analyses. Journal of Nuclear Medicine 57(12):1920–1926

[8] Tucker GT, Casey C, Phillips PJ, Connor H, Ward JD, Woods HF (1981) Metformin kinetics in healthy subjects and in patients with diabetes mellitus. British Journal of Clinical Pharmacology 12(2):235–246

[9] Pentikäinen PJ, Neuvonen PJ, Penttilä A (1979) Pharmacokinetics of metformin after intravenous and oral administration to man. European Journal of Clinical Pharmacology 16(3):195–202

[10] Sirtori CR, Franceschini G, Galli-Kienle M, Cighetti G, Galli G, Bondioli A, Conti F (1978) Disposition of metformin (N,N-dimethylbiguanide) in man. Clinical Pharmacology & Therapeutics 24(6):683–693

[11] Stopfer P, Giessmann T, Hohl K, Sharma A, Ishiguro N, Taub ME, Zimdahl-Gelling H, Gansser D, Wein M, Ebner T, Müller F (2016) Pharmacokinetic Evaluation of a Drug Transporter Cocktail Consisting of Digoxin, Furosemide, Metformin, and Rosuvastatin. Clinical Pharmacology & Therapeutics 100(3):259–267

[12] Somogyi A, Stockley C, Keal J, Rolan P, Bochner F (1987) Reduction of metformin renal tubular secretion by cimetidine in man. British Journal of Clinical Pharmacology 23(5):545–551

[13] Wang ZJ, Yin OQP, Tomlinson B, Chow MSS (2008) OCT2 polymorphisms and in-vivo renal functional consequence: studies with metformin and cimetidine. Pharmacogenetics and Genomics 18(7):637–645

[14] Boehringer Ingelheim Pharma GmbH & Co KG (2018) The effect of potent inhibitors of drug transporters (verapamil, rifampin, cimetidine, probenecid) on pharmacokinetics of a transporter probe drug cocktail consisting of digoxin, furosemide, metformin and rosuvastatin. BI Trial No. 0352-2100. EudraCT 2017-001549-29

[15] Caillé G, Lacasse Y, Raymond M, Landriault H, Perrotta M, Picirilli G, Thiffault J, Spénard J (1993) Bioavailability of metformin in tablet form using a new high pressure liquid chromatography assay method. Biopharmaceutics & Drug Disposition 14(3):257–263

[16] Gusler G, Gorsline J, Levy G, Zhang SZ, Weston IE, Naret D, Berner B (2001) Pharmacokinetics of Metformin Gastric-Retentive Tablets in Healthy Volunteers. The Journal of Clinical Pharmacology 41(6):655–661

[17] Najib N, Idkaidek N, Beshtawi M, Bader M, Admour I, Alam SM, Zaman Q, Dham R (2002) Bioequivalence evaluation of two brands of metformin 500 mg tablets (Dialon® & Glucophage®) - in healthy human volunteers. Biopharmaceutics & Drug Disposition 23(7):301–306

[18] Sambol NC, Brookes LG, Chiang J, Goodman AM, Lin ET, Liu CY, Benet LZ (1996) Food intake and dosage level, but not tablet vs solution dosage form, affect the absorption of metformin HCl in man. British Journal of Clinical Pharmacology 42(4):510–512

[19] Di Cicco RA, Allen A, Carr A, Fowles S, Jorkasky DK, Freed MI (2000) Rosiglitazone does not alter the pharmacokinetics of metformin. Journal of clinical pharmacology 40(11):1280–1285

[20] Jang K, Chung H, Yoon Js, Moon SJ, Yoon SH, Yu KS, Kim K, Chung JY (2016) Pharmacokinetics, Safety, and Tolerability of Metformin in Healthy Elderly Subjects. The Journal of Clinical Pharmacology 56(9):1104–1110

[21] Kim A, Chung I, Yoon SH, Yu KS, Lim KS, Cho JY, Lee H, Jang IJ, Chung JY (2014) Effects of Proton Pump Inhibitors on Metformin Pharmacokinetics and Pharmacodynamics. Drug Metabolism and Disposition 42(7):1174–1179

[22] Manitpisitkul P, Curtin CR, Shalayda K, Wang SS, Ford L, Heald D (2014) Pharmacokinetic interactions between topiramate and pioglitazone and metformin. Epilepsy Research 108(9):1519–1532

[23] Oh J, Chung H, Park SI, Yi SJ, Jang K, Kim AH, Yoon J, Cho JY, Yoon SH, Jang IJ, Yu KS, Chung JY (2016) Inhibition of the multidrug and toxin extrusion (MATE) transporter by pyrimethamine increases the plasma concentration of metformin but does not increase antihyperglycaemic activity in humans. Diabetes, Obesity and Metabolism 18(1):104–108

[24] Cho SK, Yoon JS, Lee MG, Lee DH, Lim LA, Park K, Park MS, Chung JY (2011) Rifampin Enhances the Glucose-Lowering Effect of Metformin and Increases OCT1 mRNA Levels in Healthy Participants. Clinical Pharmacology & Therapeutics 89(3):416–421

[25] Cho SK, Kim CO, Park ES, Chung JY (2014) Verapamil decreases the glucose-lowering effect of metformin in healthy volunteers. British Journal of Clinical Pharmacology 78(6):1426–1432

[26] Ding Y, Jia Y, Song Y, Lu C, Li Y, Chen M, Wang M, Wen A (2014) The effect of lansoprazole, an OCT inhibitor, on metformin pharmacokinetics in healthy subjects. European Journal of Clinical Pharmacology 70(2):141–146

[27] Chen Y, Li S, Brown C, Cheatham S, Castro RA, Leabman MK, Urban TJ, Chen L, Yee SW, Choi JH, Huang Y, Brett CM, Burchard EG, Giacomini KM (2009) Effect of genetic variation

in the organic cation transporter 2 on the renal elimination of metformin. Pharmacogenetics and Genomics 19(7):497–504

[28] Morrissey KM, Stocker SL, Chen EC, Castro RA, Brett CM, Giacomini KM (2016) The Effect of Nizatidine, a MATE2K Selective Inhibitor, on the Pharmacokinetics and Pharmacodynamics of Metformin in Healthy Volunteers. Clinical Pharmacokinetics 55(4):495–506

[29] Robert F, Fendri S, Hary L, Lacroix C, Andréjak M, Lalau JD (2003) Kinetics of plasma and erythrocyte metformin after acute administration in healthy subjects. Diabetes & Metabolism 29(3):279–283

[30] Sambol NC, Chiang J, Lin ET, Goodman AM, Liu CY, Benet LZ, Cogan MG (1995) Kidney Function and Age Are Both Predictors of Pharmacokinetics of Metformin. The Journal of Clinical Pharmacology 35(11):1094–1102

[31] Sambol NC, Chiang J, O'Conner M, Liu CY, Lin ET, Goodman AM, Benet LZ, Karam JH (1996) Pharmacokinetics and Pharmacodynamics of Metformin in Healthy Subjects and Patients with Noninsulin-Dependent Diabetes Mellitus. The Journal of Clinical Pharmacology 36(11):1012–1021

[32] Hibma JE, Zur AA, Castro RA, Wittwer MB, Keizer RJ, Yee SW, Goswami S, Stocker SL, Zhang X, Huang Y, Brett CM, Savic RM, Giacomini KM (2016) The Effect of Famotidine, a MATE1-Selective Inhibitor, on the Pharmacokinetics and Pharmacodynamics of Metformin. Clinical Pharmacokinetics 55(6):711–721

[33] Johansson S, Read J, Oliver S, Steinberg M, Li Y, Lisbon E, Mathews D, Leese PT, Martin P (2014) Pharmacokinetic Evaluations of the Co-Administrations of Vandetanib and Metformin, Digoxin, Midazolam, Omeprazole or Ranitidine. Clinical Pharmacokinetics 53(9):837–847

[34] Gan L, Jiang X, Mendonza A, Swan T, Reynolds C, Nguyen J, Pal P, Neelakantham S, Dahlke M, Langenickel T, Rajman I, Akahori M, Zhou W, Rebello S, Sunkara G (2016) Pharmacokinetic drug-drug interaction assessment of LCZ696 (an angiotensin receptor neprilysin inhibitor) with omeprazole, metformin or levonorgestrel-ethinyl estradiol in healthy subjects. Clinical Pharmacology in Drug Development 5(1):27–39

[35] Wishart DS, Knox C, Guo AC, Shrivastava S, Hassanali M, Stothard P, Chang Z, Woolsey J (2006) DrugBank: a comprehensive resource for in silico drug discovery and exploration. Nucleic Acids Research 34(Supplement 1):D668–D672,

[36] Desai D, Wong B, Huang Y, Ye Q, Tang D, Guo H, Huang M, Timmins P (2014) Surfactant-Mediated Dissolution of Metformin Hydrochloride Tablets: Wetting Effects Versus Ion Pairs Diffusivity. Journal of Pharmaceutical Sciences 103(3):920–926

[37] Graham GG, Punt J, Arora M, Day RO, Doogue MP, Duong JK, Furlong TJ, Greenfield JR, Greenup LC, Kirkpatrick CM, Ray JE, Timmins P, Williams KM (2011) Clinical pharmacokinetics of metformin. Clinical Pharmacokinetics 50(2):81–98

[38] Zhou M, Xia L, Wang J (2007) Metformin Transport by a Newly Cloned Proton-Stimulated Organic Cation Transporter (Plasma Membrane Monoamine Transporter) Expressed in Human Intestine. Drug Metabolism and Disposition 35(10):1956–1962

[39] Yin J, Duan H, Wang J (2016) Impact of Substrate-Dependent Inhibition on Renal Organic Cation Transporters hOCT2 and hMATE1/2-K-Mediated Drug Transport and Intracellular Accumulation. Journal of Pharmacology and Experimental Therapeutics 359(3):401–410

[40] Willmann S, Lippert J, Schmitt W (2005) From physicochemistry to absorption and distribution: predictive mechanistic modelling and computational tools. Expert Opinion on Drug Metabolism & Toxicology 1(1):159–168

[41] Block LC, Schemling LO, Couto AG, Mourão SC, Bresolin TMB (2008) Pharmaceutical equivalence of metformin tablets with various binders. Revista de Ciências Farmacêuticas Básica e Aplicada 29(1):29–35

[42] Stopfer P, Giessmann T, Hohl K, Sharma A, Ishiguro N, Taub ME, Jungnik A, Gansser D, Ebner T, Müller F (2018) Effects of Metformin and Furosemide on Rosuvastatin Pharmacokinetics in Healthy Volunteers: Implications for Their Use as Probe Drugs in a Transporter Cocktail. European Journal of Drug Metabolism and Pharmacokinetics 43(1):69–80

[43] Grahnén A, von Bahr C, Lindström B, Rosén A (1979) Bioavailability and pharmacokinetics of cimetidine. European Journal of Clinical Pharmacology 16(5):335–340

[44] Larsson R, Erlanson P, Bodemar G, Walan A, Bertler A, Fransson L, Norlander B (1982) The pharmacokinetics of cimetidine and its sulphoxide metabolite in patients with normal and impaired renal function. British Journal of Clinical Pharmacology 13(2):163–170

[45] Mihaly GW, Jones DB, Anderson JA, Smallwood RA, Louis WJ (1984) Pharmacokinetic studies of cimetidine and ranitidine before and after treatment in peptic ulcer patients. British Journal of Clinical Pharmacology 17(1):109–111

[46] Bodemar G, Norlander B, Walan A (1981) Pharmacokinetics of Cimetidine after Single Doses and during Continuous Treatment. Clinical Pharmacokinetics 6(4):306–315

[47] Morgan DJ, Uccellini DA, Raymond K, Mihaly GW, Jones DB, Smallwood RA (1983) The influence of duration of intravenous infusion of an acute dose on plasma concentrations of cimetidine. European Journal of Clinical Pharmacology 25(1):29–34

[48] Lebert PA, Mahon WA, MacLeod SM, Soldin SJ, Fenje P, Vandenberghe HM (1981) Ranitidine kinetics and dynamics: II. Intravenous dose studies and comparison with cimetidine. Clinical Pharmacology & Therapeutics 30(4):545–550,

[49] Walkenstein SS, Dubb JW, Randolph WC, Westlake WJ, Stote RM, Intoccia AP (1978) Bioavailability of cimetidine in man. Gastroenterology 74(2):360–365

[50] Jönsson KA, Eriksson SE, Kagevi I, Norlander B, Bodemar G, Walan A (1982) Cimetidine, but not oxmetidine, penetrates into the cerebrospinal fluid after a single intravenous dose. British Journal of Clinical Pharmacology 14(6):815–819,

[51] Kanto J, Allonen H, Jalonen H, Mäntylä R (1981) The effect of metoclopramide and propantheline on the gastrointestinal absorption of cimetidine. British Journal of Clinical Pharmacology 11(6):629–631

[52] Burland WL, Duncan WA, Hesselbo T, Mills JG, Sharpe PC, Haggie SJ, Wyllie JH (1975) Pharmacological evaluation of cimetidine, a new histamine H2-receptor antagonist, in healthy man. British Journal of Clinical Pharmacology 2(6):481–486

[53] Bodemar G, Norlander B, Fransson L, Walan A (1979) The absorption of cimetidine before and during maintenance treatment with cimetidine and the influence of a meal on the absorption of cimetidine – studies in patients with peptic ulcer disease. British Journal of Clinical Pharmacology 7(1):23–31,

[54] D'Angio R, Mayersohn M, Conrad KA, Bliss M (1986) Cimetidine absorption in humans during sucralfate coadministration. British Journal of Clinical Pharmacology 21(5):515–520

[55] Tiseo PJ, Perdomo CA, Friedhoff LT (1998) Concurrent administration of donepezil HCl and cimetidine: assessment of pharmacokinetic changes following single and multiple doses. British Journal of Clinical Pharmacology 46(S1):25–29

[56] Somogyi A, Gugler R (1983) Clinical Pharmacokinetics of Cimetidine. Clinical Pharmacokinetics 8(6):463–495

[57] Barbhaiya RH, Shukla UA, Greene DS (1995) Lack of interaction between nefazodone and cimetidine: a steady state pharmacokinetic study in humans. British Journal of Clinical Pharmacology 40(2):161–165

[58] Somogyi A, Thielscher S, Gugler R (1981) Influence of phenobarbital treatment on cimetidine kinetics. European Journal of Clinical Pharmacology 19(5):343–347

[59] Avdeef A, Berger CM (2001) pH-metric solubility. 3. Dissolution titration template method for solubility determination. European Journal of Pharmaceutical Sciences 14(4):281–291

[60] Taylor DC, Cresswell PR, Bartlett DC (1978) The metabolism and elimination of cimetidine, a histamine H2-receptor antagonist, in the rat, dog, and man. Drug Metabolism and Disposition 6(1):21–30

[61] Umehara KI, Iwatsubo T, Noguchi K, Kamimura H (2007) Functional involvement of organic cation transporter1 (OCT1/Oct1) in the hepatic uptake of organic cations in humans and rats. Xenobiotica 37(8):818–831

[62] Tahara H, Kusuhara H, Endou H, Koepsell H, Imaoka T, Fuse E, Sugiyama Y (2005) A Species Difference in the Transport Activities of H2 Receptor Antagonists by Rat and Human Renal Organic Anion and Cation Transporters. Journal of Pharmacology and Experimental Therapeutics 315(1):337–345

[63] Ohta Ky, Inoue K, Yasujima T, Ishimaru M, Yuasa H (2010) Functional Characteristics of Two Human MATE Transporters: Kinetics of Cimetidine Transport and Profiles of Inhibition by Various Compounds. Journal of Pharmacy & Pharmaceutical Sciences 12(3):388–396

[64] Ito S, Kusuhara H, Yokochi M, Toyoshima J, Inoue K, Yuasa H, Sugiyama Y (2012) Competitive Inhibition of the Luminal Efflux by Multidrug and Toxin Extrusions, but Not Basolateral Uptake by Organic Cation Transporter 2, Is the Likely Mechanism Underlying the Pharmacokinetic Drug-Drug Interactions Caused by Cimetidine in the Kidney. Journal of Pharmacology and Experimental Therapeutics 340(2):393–403

[65] Wrighton SA, Ring BJ (1994) Inhibition of human CYP3A catalyzed 1'-hydroxy midazolam formation by ketoconazole, nifedipine, erythromycin, cimetidine, and nizatidine. Pharmaceutical Research 11(6):921–924

[66] Rodgers T, Leahy D, Rowland M (2005) Physiologically based pharmacokinetic modeling 1: Predicting the tissue distribution of moderate-to-strong bases. Journal of Pharmaceutical Sciences 94(6):1259–1276

[67] Rodgers T, Rowland M (2006) Physiologically based pharmacokinetic modelling 2: Predicting the tissue distribution of acids, very weak bases, neutrals and zwitterions. Journal of Pharmaceutical Sciences 95(6):1238 – 1257

[68] Zolk O, Solbach TF, König J, Fromm MF (2009) Functional characterization of the human organic cation transporter 2 variant p.270Ala>Ser. Drug Metabolism and Disposition 37(6):1312–1318,

[69] Christensen MMH, Pedersen RS, Stage TB, Brasch-Andersen C, Nielsen F, Damkier P, Beck-Nielsen H, Brøsen K (2013) A gene–gene interaction between polymorphisms in the OCT2 and MATE1 genes influences the renal clearance of metformin. Pharmacogenetics and Genomics 23(10):526–534

[70] Song IS, Shin HJ, Shim EJ, Jung IS, Kim WY, Shon JH, Shin JG (2008) Genetic Variants of the Organic Cation Transporter 2 Influence the Disposition of Metformin. Clinical Pharmacology & Therapeutics 84(5):559–562

[71] Guest EJ, Aarons L, Houston JB, Rostami-Hodjegan A, Galetin A (2011) Critique of the two-fold measure of prediction success for ratios: Application for the assessment of drug-drug interactions. Drug Metabolism and Disposition 39(2):170–173,

[72] Hanke N, Frechen S, Moj D, Britz H, Eissing T, Wendl T, Lehr T (2018) PBPK models for CYP3A4 and P-gp DDI prediction: A modeling network of rifampicin, itraconazole, clarithromycin, midazolam, alfentanil, and digoxin. CPT: Pharmacometrics & Systems Pharmacology 7(10):647–659,

[73] Austin RP, Barton P, Cockroft SL, Wenlock MC, Riley RJ (2002) The influence of nonspecific microsomal binding on apparent intrinsic clearance, and its prediction from physicochemical properties. Drug Metabolism and Disposition 30(12):1497–1503,

[74] Walser A, Benjamin LE, Flynn T, Mason C, Schwartz R, Fryer RI (1978) Quinazolines and 1,4-benzodiazepines. 84. Synthesis and reactions of imidazo[1,5-a][1,4]benzodiazepines. The Journal of Organic Chemistry 43(5):936–944

[75] Heikkinen AT, Baneyx G, Caruso A, Parrott N (2012) Application of PBPK modeling to predict human intestinal metabolism of CYP3A substrates – an evaluation and case study using GastroPlus® . European Journal of Pharmaceutical Sciences 47(2):375–386

[76] Vossen M, Sevestre M, Niederalt C, Jang IJ, Willmann S, Edginton AN (2007) Dynamically simulating the interaction of midazolam and the CYP3A4 inhibitor itraconazole using individual coupled whole-body physiologically-based pharmacokinetic (WB-PBPK) models. Theoretical Biology and Medical Modelling 4(1):13

[77] Lemaitre F, Hasni N, Leprince P, Corvol E, Belhabib G, Fillâtre P, Luyt CE, Leven C, Farinotti R, Fernandez C, Combes A (2015) Propofol, midazolam, vancomycin and cyclosporine therapeutic drug monitoring in extracorporeal membrane oxygenation circuits primed with whole human blood. Critical Care 19(1):40

[78] Björkman S, Wada D, Berling B, Benoni G (2001) Prediction of the disposition of midazolam in surgical patients by a physiologically based pharmacokinetic model. Journal of Pharmaceutical Sciences 90(9):1226–1241

[79] Patki KC, von Moltke LL, Greenblatt DJ (2003) In vitro metabolism of midazolam, triazolam, nifedipine, and testosterone by human liver microsomes and recombinant cytochromes P450: role of CYP3A4 and CYP3A5. Drug Metabolism and Disposition 31(7):938–944,

[80] Greenblatt DJ, Locniskar A, Scavone JM, Blyden GT, Ochs HR, Harmatz JS, Shader RI (1986) Absence of interaction of cimetidine and ranitidine with intravenous and oral midazolam. Anesthesia and Analgesia 65(2):176–180

[81] Martinez C, Albet C, Agúndez JA, Herrero E, Carrillo JA, Márquez M, Benítez J, Ortiz JA (1999) Comparative in vitro and in vivo inhibition of cytochrome P450 CYP1A2, CYP2D6, and CYP3A by H2-receptor antagonists. Clinical Pharmacology & Therapeutics 65(4):369–376

[82] Fee JPH, Collier PS, Howard PJ, Dundee JW (1987) Cimetidine and ranitidine increase midazolam bioavailability. Clinical Pharmacology & Therapeutics 41(1):80–84,

[83] Salonen M, Aantaa E, Aaltonen L, Kanto J (1986) Importance of the interaction of midazolam and cimetidine. Acta Pharmacologica et Toxicologica 58(2):91–95,

[84] Bricker NS, Morrin PA, Kime SW (1997) The pathologic physiology of chronic bright's disease. an exposition of the "intact nephron hypothesis". Journal of the American Society of Nephrology 8(9):1470–1476,

[85] Bricker NS (1969) On the meaning of the intact nephron hypothesis. The American Journal of Medicine 46(1):1–11

[86] Hsueh CH, Hsu V, Zhao P, Zhang L, Giacomini KM, Huang SM (2018) PBPK modeling of the effect of reduced kidney function on the pharmacokinetics of drugs excreted renally by organic anion transporters. Clinical Pharmacology & Therapeutics 103(3):485–492,

[87] Schmulenson E, Schlender JF, Frechen S, Jaehde U (2018) A physiologically-based pharmacokinetic modeling approach to assess the impact of chronic kidney disease. PAGE Abstr Annu Meet Popul Approach Gr Eur PAGE 27:Abstr 8630

[88] Zhao P, Vieira MdLT, Grillo JA, Song P, Wu TC, Zheng JH, Arya V, Berglund EG, Atkinson Jr AJ, Sugiyama Y, Pang KS, Reynolds KS, Abernethy DR, Zhang L, Lesko LJ, Huang SM (2012) Evaluation of exposure change of nonrenally eliminated drugs in patients with chronic kidney disease using physiologically based pharmacokinetic modeling and simulation. The Journal of Clinical Pharmacology 52(S1):91S–108S,

[89] Zhang G, Ma Y, Xi D, Rao Z, Sun X, Wu X (2019) Effect of high uric acid on the disposition of metformin: in vivo and in vitro studies. Biopharmaceutics & Drug Disposition 40(1):3–11

[90] Dissanayake AM, Wheldon MC, Ahmed J, Hood CJ (2017) Extending Metformin Use in Diabetic Kidney Disease: A Pharmacokinetic Study in Stage 4 Diabetic Nephropathy. Kidney International Reports 2(4):705–712

[91] Lalau JD, Kajbaf F, Bennis Y, Hurtel-Lemaire AS, Belpaire F, De Broe ME (2018) Metformin Treatment in Patients With Type 2 Diabetes and Chronic Kidney Disease Stages 3A, 3B, or 4. Diabetes Care 41(3):547–553

[92] Gorboulev V, Ulzheimer JC, Akhoundova A, Ulzheimer-Teuber I, Karbach U, Quester S, Baumann C, Lang F, Busch AE, Koepsell H (1997) Cloning and Characterization of Two Human Polyspecific Organic Cation Transporters. DNA and Cell Biology 16(7):871–881

[93] Otsuka M, Matsumoto T, Morimoto R, Arioka S, Omote H, Moriyama Y (2005) A human transporter protein that mediates the final excretion step for toxic organic cations. Proceedings of the National Academy of Sciences of the United States of America 102(50):17923–17928

[94] Masuda S, Terada T, Yonezawa A, Tanihara Y, Kishimoto K, Katsura T, Ogawa O, Inui KI (2006) Identification and functional characterization of a new human kidney-specific H+/organic cation antiporter, kidney-specific multidrug and toxin extrusion 2. Journal of the American Society of Nephrology 17(8):2127–2135

[95] Prasad B, Johnson K, Billington S, Lee C, Chung GW, Brown CDA, Kelly EJ, Himmelfarb J, Unadkat JD (2016) Abundance of drug transporters in the human kidney cortex as quantified by quantitative targeted proteomics. Drug Metabolism and Disposition 44(12):1920–1924,

[96] Nies AT, Koepsell H, Winter S, Burk O, Klein K, Kerb R, Zanger UM, Keppler D, Schwab M, Schaeffeler E (2009) Expression of organic cation transporters OCT1 (SLC22A1) and OCT3 (SLC22A3) is affected by genetic factors and cholestasis in human liver. Hepatology 50(4):1227–1240

[97] Prasad B, Gaedigk A, Vrana M, Gaedigk R, Leeder JS, Salphati L, Chu X, Xiao G, Hop C, Evers R, Gan L, Unadkat JD (2016) Ontogeny of hepatic drug transporters as quantified by LC-MS/MS proteomics. Clinical Pharmacology & Therapeutics 100(4):362–370,

[98] Han TK, Everett RS, Proctor WR, Ng CM, Costales CL, Brouwer KLR, Thakker DR (2013) Organic Cation Transporter 1 (OCT1/mOct1) Is Localized in the Apical Membrane of Caco-2 Cell Monolayers and Enterocytes. Molecular Pharmacology 84(2):182–189

[99] Han TK, Proctor WR, Costales CL, Cai H, Everett RS, Thakker DR (2015) Four cation-selective transporters contribute to apical uptake and accumulation of metformin in caco-2 cell monolayers. Journal of Pharmacology and Experimental Therapeutics 352(3):519–528,

[100] Dawed AY, Zhou K, van Leeuwen N, Mahajan A, Robertson N, Koivula R, Elders PJM, Rauh SP, Jones AG, Holl RW, Stingl JC, Franks PW, McCarthy MI, 't Hart LM, Pearson ER (2019) Variation in the plasma membrane monoamine transporter (PMAT) (encoded by SLC29A4) and organic cation transporter 1 (OCT1) (encoded by SLC22A1) and gastrointestinal intolerance to metformin in type 2 diabetes: An IMI DIRECT study. Diabetes Care 42(6):1027–1033,

[101] Dujic T, Zhou K, Donnelly LA, Tavendale R, Palmer CNA, Pearson ER (2015) Association of organic cation transporter 1 with intolerance to metformin in type 2 diabetes: A GoDARTS study. Diabetes 64(5):1786–1793,

[102] Liang X, Chien HC, Yee SW, Giacomini MM, Chen EC, Piao M, Hao J, Twelves J, Lepist EI, Ray AS, Giacomini KM (2015) Metformin Is a Substrate and Inhibitor of the Human Thiamine Transporter, THTR-2 (SLC19A3). Molecular Pharmaceutics 12(12):4301–4310

[103] Müller J, Lips KS, Metzner L, Neubert RHH, Koepsell H, Brandsch M (2005) Drug specificity and intestinal membrane localization of human organic cation transporters (OCT). Biochemical Pharmacology 70(12):1851–1860

[104] Proctor WR, Bourdet DL, Thakker DR (2008) Mechanisms underlying saturable intestinal absorption of metformin. Drug Metabolism and Disposition 36(8):1650–1658,

[105] Bailey CJ, Wilcock C, Scarpello JHB (2008) Metformin and the intestine. Diabetologia 51(8):1552–1553

[106] McCreight LJ, Bailey CJ, Pearson ER (2016) Metformin and the gastrointestinal tract. Diabetologia 59(3):426–435

[107] Scotcher D, Billington S, Brown J, Jones CR, Brown CDA, Rostami-Hodjegan A, Galetin A (2017) Microsomal and cytosolic scaling factors in dog and human kidney cortex and application for in vitro-in vivo extrapolation of renal metabolic clearance. Drug Metabolism and Disposition 45(5):556–568,

[108] Prasad B, Evers R, Gupta A, Hop CECA, Salphati L, Shukla S, Ambudkar SV, Unadkat JD (2014) Interindividual variability in hepatic organic anion-transporting polypeptides and P-Glycoprotein (ABCB1) protein expression: Quantification by liquid chromatography tandem mass spectroscopy and influence of genotype, age, and sex. Drug Metabolism and Disposition 42(1):78–88,

[109] Meyer M, Schneckener S, Ludewig B, Kuepfer L, Lippert J (2012) Using Expression Data for Quantification of Active Processes in Physiologically Based Pharmacokinetic Modeling. Drug Metabolism and Disposition 40(5):892–901

[110] Rodrigues AD (1999) Integrated cytochrome P450 reaction phenotyping: attempting to bridge the gap between cDNA-expressed cytochromes P450 and native human liver microsomes. Biochemical pharmacology 57(5):465—480

[111] Nishimura M, Yaguti H, Yoshitsugu H, Naito S, Satoh T (2003) Tissue distribution of mRNA expression of human cytochrome P450 isoforms assessed by high-sensitivity real-time reverse transcription PCR. Yakugaku Zasshi 123(5):369–375

[112] Yeo KR, Walsky RL, Jamei M, Rostami-Hodjegan A, Tucker GT (2011) Prediction of time-dependent CYP3A4 drug–drug interactions by physiologically based pharmacokinetic modelling: Impact of inactivation parameters and enzyme turnover. European Journal of Pharmaceutical Sciences 43(3):160–173

[113] Greenblatt DJ, von Moltke LL, Harmatz JS, Chen G, Weemhoff JL, Jen C, Kelley CJ, LeDuc BW, Zinny MA (2003) Time course of recovery of cytochrome p450 3a function after single doses of grapefruit juice. Clinical Pharmacology & Therapeutics 74(2):121–129

[114] Nishimura M, Naito S (2005) Tissue-specific mRNA expression profiles of human ATP-binding cassette and solute carrier transporter superfamilies. Drug Metabolism and Pharmacokinetics 20(6):452–477

[115] Wang L, Prasad B, Salphati L, Chu X, Gupta A, Hop CECA, Evers R, Unadkat JD (2015) Interspecies Variability in Expression of Hepatobiliary Transporters across Human, Dog, Monkey, and Rat as Determined by Quantitative Proteomics. Drug Metabolism and Disposition 43(3):367–374

[116] Kolesnikov N, Hastings E, Keays M, Melnichuk O, Tang YA, Williams E, Dylag M, Kurbatova N, Brandizi M, Burdett T, Megy K, Pilicheva E, Rustici G, Tikhonov A, Parkinson H, Petryszak R, Sarkans U, Brazma A (2015) ArrayExpress update—simplifying data submissions. Nucleic Acids Research 43(D1):D1113–D1116

[117] National Center for Biotechnology Information (NCBI) (2019) Expressed Sequence Tags (EST) from UniGene